If we knew what it was we were doing, it would not be called research, would it?

Albert Einstein

Jury

Chairman:	Prof. Dr. Ken Haenen
	Universiteit Hasselt
Promotor:	Prof. Dr. Patrick Wagner
	Universiteit Hasselt, IMO-IMOMEC
Co-Promotor:	Prof. Dr. Mat Daemen
	University of Amsterdam, department of pathology
Members of the Jury:	Prof. Dr. Ward De Ceuninck
	Universiteit Hasselt, IMO-IMOMEC
	Prof. Dr. Wilfred Germeraad
	Maastricht University Medical Center
	Prof. Dr. Jerome Hendriks
	Universiteit Hasselt, BIOMED
	Prof. Dr. Liesbet Lagae
	Katholieke Universiteit Leuven, IMEC
	Prof. Dr. Veerle Somers
	Universiteit Hasselt, BIOMED
	Dr. Christiane Püttmann
	RWTH Aachen, Institute of Applied Medical Engineering
	Dr. Bart van Grinsven
	Universiteit Hasselt

Table of contents

Acknowledgements

Mijn verhaal als doctoraatsstudent in de Biosensor groep begint niet bij de start van het project in november 2009 maar ergens in het voorjaar van 2005. Voor mijn bachelorproef kreeg ik het onderwerp "nierdialyse" toegewezen onder supervisie van een zekere professor Patrick Wagner. Volgens de site van de Uhasselt (toen nog het Limburgs Universitair Centrum) bleek het om een professor van de vakgroep fysica te gaan. Een beetje vreemd om als bachelorstudent in de Biomedische Wetenschappen een project toegewezen te krijgen dat zich meer in de wereld van de fysica bevindt, maar "onbekend is onbemind" en dus startte ik met goede moed aan het project. Na enkele gesprekken ging ik aan de slag met mijn literatuurstudie en werd mijn interesse in het multidisciplinaire grensgebied van de wetenschap gewekt. Het project zou uiterst succesvol verlopen en later dat jaar volgde het vak "bio-elektronica en nanotechnologie" dat werd gecoördineerd door diezelfde professor Wagner en een zekere professor Thomas Cleij, van de vakgroep organische chemie. Wist ik veel dat deze twee heren later zouden uitgroeien tot mijn mentoren tijdens zowel mijn master- als mijn doctoraatsthesis! Wat wel vast stond was dat ik in die periode evolueerde van een student biomedische wetenschappen tot een student die inzicht en interesse vertoonden in alle takken van de wetenschap. Beide heren brachten me bij dat chemie en fysica wel degelijk hand in hand gingen met biomedisch onderzoek en dat verschillende wetenschappelijke benaderingen nodig zijn om tot succesvol, modern wetenschappelijk onderzoek te komen.

In de jaren die volgden kwam ik tijdens mijn bachelor- en junior masterstage onder begeleiding van Ronald Thoelen en Jan Alenus, terecht in het onderzoek naar biosensoren gebaseerd op molecularly imprinted polymers, kortweg MIPs. Ik vond het thema mateloos interessant en besloot dan ook om me tijdens mijn senior masterstage verder te verdiepen in dit topic. Ik sloot me aan bij de MIP synthese groep binnen de vakgroep organische chemie die onder leiding stond van professor Cleij. Samen met mijn begeleider Frederik Horemans ontwikkelde ik verschillende soorten MIPs. Na een bijzonder leerrijk en succesvol masterjaar, kreeg ik de kans om een doctoraat aan te vatten binnen de vakgroep fysica, in

de onderzoeksgroep Biosensoren, die geleid werd door… diezelfde professor Wagner die ik vier jaar eerder ontmoette! Aangezien het onderwerp van dit onderzoek nauw aansloot bij het onderzoek dat ik tijdens mijn stages had uitgevoerd, begon ik met veel honger aan het project. Het project bleek in de eerste jaren echter aanzienlijk anders dan het onderzoek naar MIPs. Maar na een moeilijke start, kwam er in de laatste twee jaar van mijn onderzoek alsnog de doorbraak die zich vertaald ziet in deze thesis. Dit was echter nooit gelukt zonder de al dan niet professionele hulp en/of steun van heel wat mensen. Het is dan ook niet meer dan logisch dat ik deze mensen even wens te bedanken, vooraleer we met het wetenschappelijke deel van de thesis van start gaan.

Professor Patrick Wagner: Patrick, zoals ik hierboven al heb uitgelegd was jij diegene die mijn interesse in multidisciplinair onderzoek wekte. Daarnaast heb je gedurende de afgelopen jaren enorm bijgedragen aan de evolutie die ik hier doormaakte. Mijn PowerPoint presentaties en Paint skills zijn er sterk op vooruit gegaan door de door jou gevraagde (vaak met stokmannetjes in potlood getekende) animaties. Voorts maakte ik ook veel progressie op het gebied van het presenteren van resultaten, het geven van fysica lessen aan studenten die het niet altijd even goed snappen en het schrijven wetenschappelijke publicaties.

Vervolgens zou ik ook graag mijn twee Nederlandse co-promotoren bedanken. Omwille van omstandigheden, hebben we elkaar de laatste jaren niet zo vaak gesproken maar jullie input, vooral in het begin van mijn project, waren essentieel voor het tot stand komen van deze thesis.

Professor Thomas Cleij, bedankt voor de chemische ondersteuning van het project, voor het gebruik van uw laboratorium en voor de kans die u me gaf om mijn masterthesis af te ronden binnen uw groep. Graag zou ik dan ook Frederik Horemans bedanken die tijdens deze stage mijn dagelijkse begeleider was.

Professor Mat Daemen, bedankt voor uw feedback over het biologische aspect van dit project. Uw inzichten hebben er toe geleid dat we onze cel-imprinting projecten vanaf de start op een kritische manier hebben uitgevoerd.

Doctor Bart van Grinsven, bedankt om me te overtuigen om eens een sample te maken voor een R_{th} meting "gewoon om eens te proberen". Sindsdien hebben we een enorme weg afgelegd, uren samen gemeten in de kelder, samen een artikel gemaakt (en een tweede onderweg), ettelijke keren samen naar IMEC gereden voor de patent-aanvraag,... We evolueerden van twee hamsters die met de mond open de metingen volgden en wat zaten te knoeien met het manueel injecteren van sapjes naar een geoliede tandem die Rth-metingen op SIPs uitvoeren als ware het potjes Tetrinet ☺ Bedankt voor alles Bart!

Doctor Anitha Ethirajan, thank you for guiding me through a difficult period of my Phd. You helped me optimize the synthesis and imprinting protocol which was a crucial part of my research. Without a working receptor, our sensor set-up would not work at all!

Doctor Karolien Bers, je was niet lang lid van het wereldteam dat de Biosgroep toch wel is maar je impact op ons onderzoek is in die korte tijd wel enorm geweest. Het was een productief en aangenaam jaar, bedankt voor je bijdrage!

Silke Timmermans, Dr. Jeroen Bogie, Prof. Hendriks, Prof. Somers, Dr. Bouwmans, Christel Bocken, bedankt voor jullie hulp en suggesties in verband met het opstarten en onderhouden van de celculturen. Sathya en Kathia thank you for the AFM characterization! Thijs bedankt voor je ondersteuning met de PDMS, een klein maar cruciaal onderdeel van het onderzoek! Jan D'Haen en Bart Rutten, wil ik bedanken voor de ondersteuning met de SEM. Christel en Hilde bedankt voor de technische ondersteuning in het lab, zonder jullie was het onmogelijk geweest om alle experimenten uit te voeren! Een speciaal bedankje nog voor Johnny die uren in de weer was om me te helpen met de glovebox.

En dan natuurlijk iedereen van onze intelligente, uiterst bekwame, hulpvaardige en algemeen heersende BIOS-groep! Mijn integratie verliep vlotjes aangezien ik met Jan, Lars en Rob al jaren kende. De kennismaking met Bart en Bert verliep al even vlot, en binnen de week was ik al part of the group. Matthias, die voor mijn doctoraat al twee jaar lang mijn classmate was, en ik werden meteen ingeschakeld in de rubberband war. Marloes en Mohammed volgden al snel en het team stond er. We verloren gedurende de jaren enkele prominente leden maar in ruil werden we versterkt met toppers zoals Kathia, Andreas, Evelien,

Karolien en Patricia. Thijs, onze Xios-informant die zijn plaats op onze bureau afdwong (en terecht!). Ik wil jullie allemaal bedanken voor de geniale tijden die we beleefden op het werk (shooter Friday, TETRINET!!!, Bang!,…) en daarbuiten (uitjes in Hasselt, cinema, ENFI's, Matthi's winter- en zomerbbq's,…). Natuurlijk ook de rest van het Xios legioen niet vergeten: Stijn, Koen, Jeroen, Michaël, Ronald, Tim,… bedankt voor de fantastische lunchpauzes en het leren van een belangrijke levensles: het maakt echt niet uit of je wint of verliest met kaarten (en bij uitbreiding alle spellen die er bestaan), zo lang Clukers maar verliest!

Voorts wens ik ook even alle studenten die de afgelopen hun stage bij mij uitvoerden, bedanken voor hun inzet en toewijding. Jordy, Evelien, Donald, Christopher, Lien, Hannelore, Martijn, Mehran, Theophilus, Sander, Peter, Jeroen, Brendan, Cédric en Vitor thank you for contributing to the project, I wish you all the best for your future (PhD) projects!

Naast de mensen op het werk zijn er natuurlijk ook mensen uit mijn privéleven die een grote impact hebben gehad op dit project. Professionele prestaties kan je natuurlijk enkel leveren als het op privévlak ook allemaal in orde is. Vandaar dat ik al mijn vrienden en mijn familie wil bedanken. In het bijzonder natuurlijk mama, papa, Matthi en Gaëlle, bedankt om me al die jaren te steunen zowel tijdens als ver voor mijn doctoraat. Bruno, Annie, Stef, Eva bedankt om me welkom te heten in jullie familie! En natuurlijk als laatste de twee meest belangrijke personen in mijn leven. Elke, het is niet toevallig dat de resultaten van mijn doctoraat in stijgende lijn zijn blijven gaan sinds ik jou ken. Bedankt om er altijd voor me te zijn, ook als ik het moeilijk heb en niet te genieten ben door de stress op het werk! Ella, mijn oogappeltje, je kan nu nog niet lezen maar later als je het wel kan, wil ik dat je weet dat alle frustraties op het werk in het niets vervagen als ik thuis kom bij jou en mama en jullie hoor en zie lachen. Als ik jullie in mijn armen neem, dan worden alle andere dingen bijzaak!

Abstract

Novel detection platforms for the identification of disease-related cells in patient samples are of enormous interest for the medical community. These platforms could also be useful in environmental and food safety by monitoring the amount of pathogens in drinking water and/or food. Current state-of-the-art cell detection platforms are very sensitive and specific but these techniques are typically very expensive, complicated and require analysis by a professional in a lab environment. Biosensors could offer a fast, low-cost and user-friendly alternative for these platforms. However, biosensors usually make use of biological receptors such as antibodies or enzymes for the detection of biological compounds. While these natural receptors are very selective and sensitive, they have the drawback of being instable and expensive. Molecularly imprinted polymers (MIPs) are a classic alternative for these natural receptors but due to the size of the target cells, MIPs produced by classical imprinting techniques are not suitable for the detection of these compounds. Therefore, a novel approach was tested, creating synthetic receptors by surface imprinting of thin polyurethane layers. For the sake of simplicity these surface imprinted polymers will be referred to as SIPs from hereon.

The principle of SIPs seems deceivingly simple. In a first step, a polyurethane mixture is polymerized up to the gelling point. Subsequently, the polymer is diluted and spin-coated onto a transducer substrate, in our case a flat aluminum chip. In parallel a solution of the desired target cells in buffer medium is dropcasted onto the surface of a rubber-like stamp. After the cells are allowed to sediment to the surface of the stamp, the excess buffer fluid is removed by spin-coating, leaving behind a dense monolayer of cells on the surface of the stamp. This stamp is gently pressed onto the semi-cured polyurethane layer. After curing of the layer, the stamp and cells are removed from the surface of the SIP, leaving behind microcavities that are able to rebind the cells in a specific and selective manner.

In addition to a low-cost synthetic receptor for cells, rebinding of target cells to these receptors has to be detected in a fast, easy but still selective and sensitive manner. Therefore, the heat-transfer method (HTM), previously used for the

detection of single-nucleotide polymorphisms in DNA, was adjusted to fit the demands for cell detection measurements. The concept of the method is based on the analysis of the heat-transfer resistance at a solid-liquid interface, containing the SIP. Binding of cells will result in an increase in the thickness of the thermal insulating layer at this interface, thereby increasing the heat-transfer resistance. For reasons of control, non-imprinted polyurethane layers (NIPs) were synthesized in the same manner but without imprinting of the template cells and analyzed for their response to target cells. Any rise in thermal resistance encountered when exposing this NIP to a cell solution can be attributed to non-specific binding of cells to the layer.

After careful optimization of the polyurethane synthesis and the imprinting protocol, SIPs were characterized to examine the morphology and topography of these patterned polyurethane surfaces. These experiments revealed that the lateral dimensions of the template cells can be faithfully transferred to the polymer layer. Since the imprints are made on the surface of a very thin film (approximately 1 µm), they are very shallow as compared to the size of the target cells (having diameters in the range of 10-25 µm). This aspect appears to be crucial for the selectivity of the receptor. Cells that fit the imprints due to their morphology will only remain bound to the microcavity if this morphological fit is aided by weak chemical interactions. During the cross-linking of the polymer, proteins on the membrane of the template cells, albeit in a non-native conformation, were able to interact with the forming polymer in a non-covalent manner. After removal of the cells from their microcavities, a distribution of functional groups is left behind inside these imprints that are complementary to epitopes (binding motifs) on the proteins displayed on the surface of the template cells. This ensures that is possible for cells to rebind to the layer.

In order to test the concept of merging two previously tested techniques for the development of a working cell biosensor platform, SIPs were imprinted for mouse and rat macrophage cell lines. The specificity, selectivity and sensitivity of these layers was analyzed by HTM in order to achieve a proof-of-principle for the proposed platform. Comparing the time-dependent profile of the thermal resistance of a SIP and a NIP, it was shown that exposing these layers to a suspension of target cells in buffer, led to an increase in thermal resistance at

the SIP-covered solid-liquid interface, while this effect is absent for the NIP layer. Moreover, the sensor seemed to be able to differentiate between macrophage cell lines from a mouse and a rat. In this way, the concept of the sensor was demonstrated, successfully combining a specific and selective synthetic receptor with a fast, label-free, and low-cost read out platform.

Since differentiating between macrophage cell lines from different rodent species has little to no medical or biological relevance, a new series of experiments was conducted in order to test the device for future, medical applications. After optimizing and automating the sensor set up, the device was capable of distinguishing between two different lines of cancer cells (the breast cancer cell-line MCF-7 and the leukemic T-cell-line Jurkat). More importantly, the device was able to distinguish cancer cells from healthy cells with any cross-selectivity observed. These experiments demonstrated that the device might be used for commercial, medical applications in the future, for instance for the detection of circulating tumor cells in blood samples.

In a final series of experiments the limits of the device were assessed, clearly demonstrating the striking selectivity of the SIP receptor layer. The sensor platform seemed capable of distinguishing between cell lines differing only in the expression of a single protein (the MUC1 protein). Furthermore, it was even possible to differentiate between cells based on the presence/absence of glycosylation patterns on the surface of the MUC1 protein. Additionally the sensitivity of the device was analyzed using mixtures of various cell types, showing that the sensitivity of the device can be increased by exposing the sensor surface repeatedly to these cell mixtures. Finally, the functioning of the sensor platform was benchmarked by validating the results obtained during our experiments with state-of-the-art cell detection platforms such as fluorescence microscopy and fluorescence-activated cell sorting.

The work presented in this thesis clearly demonstrates that the combination of SIPs and HTM has led to the development of a very promising bio(mimetic)sensor platform for the detection of human cells. The straightforward, fast and low-cost nature of the platform has great benefits as compared to commercially available platforms. In order to compete with these techniques the sensitivity of the device has to be greatly improved in the future.

Further improvement in this area can be made by the development of a novel flow cell and a small adjustment of the HTM set up, in order to work under continuous flow in a close loop system. In this way trace amounts of cells can be detected as they can gradually bind to the layer when flowing over it while competitor cells will just move over the surface without sticking to it. Additionally, progress can be made by fine-tuning the set up in order to decrease the noise levels on the signal. Finally, increasing the density of imprints on the surface of the SIP will also have a positive influence on the sensitivity and the detection limit of the device.

Nederlandse samenvatting

De ontwikkeling van nieuwe methoden voor het detecteren van ziekte-gerelateerde cellen in bloedstalen van patiënten is enorm belangrijk vanuit medisch oogpunt. Dergelijke technieken kunnen ook erg nuttig zijn in het kader van pathogeendetectie in drinkwater of voedsel. De huidige state-of-the-art technieken mogen dan wel erg gevoelig en precies zijn, ze zijn enorm duur en kunnen enkel in een laboratorium gebruikt worden door medisch getraind personeel. Biosensoren kunnen in dit kader een goedkoop, snel en gebruiksvriendelijk alternatief bieden. Het probleem met dergelijke sensoren is dat ze vaak gebruik maken van natuurlijke receptoren zoals antilichamen of enzymen voor de detectie van biologisch materiaal. Deze biologische receptoren zijn welliswaar gevoelig en erg specifiek naar hun target toe maar zijn ook duur en onstabiel. Een klassiek alternatief voor deze receptoren is het gebruik van zogenaamde molecularly imprinted polymers (MIPs), maar omwille van de grote afmetingen van de te detecteren cellen, zijn klassieke MIPs niet bruikbaar voor deze toepassing. Daarom werden synthetische receptoren gemaakt door middel van surface imprinting op dunne polyurethaan coatings. Dit soort receptoren, worden naar analogie met MIPs voor het gemak SIPs genoemd in het verdere verloop van deze samenvatting.

Het principe dat schuil gaat achter het creëren van SIPs lijkt op het eerste zicht eenvoudig. In een eerste stap wordt een polyurethaan mengsel gepolymeriseerd tot een gel. Deze gel wordt vervolgens verder verdund een aangebracht op een transducer platform, in dit geval een aluminium chip, door middel van spin-coating. In parallel wordt een suspensie van target cellen aangebracht op een rubberen stempel. Na sedimentatie van de cellen naar het oppervlak van deze stempel, wordt de overtollige buffer vloeistof verwijderd door spin-coating. Hierdoor blijft er een monolaag van cellen achter op de stempel. De stempel wordt zachtjes op de half-zachte polymeerlaag gedrukt waarna de laag wordt uitgehard over nacht. Vervolgens worden de stempel en de cellen verwijderd van het SIP oppervlak, waardoor er microcaviteiten achterblijven in de polymeerlaag waaraan cellen op een specifieke en selectieve manier kunnen binden.

De ontwikkelde biosensor applicatie moet naast een low-cost cel-receptor ook nog bestaan uit een innovatieve uitleesmethode die in staat is het binden van cellen aan de SIP laag te detecteren op een snelle en eenvoudige manier. Hiervoor werd de zogenaamde heat-transfer method (HTM), initieel ontwikkeld voor de detectie van single-nucleotide polymorfismen in DNA, aangepast voor het gebruik in een cel detectie context. Het concept achter deze methode is gebaseerd op het analyseren van de thermische weerstand van een solid-liquid interface waar de SIP onderdeel van uitmaakt. Wanneer cellen binden aan de SIP, zal de thermische isolatie laag aan deze interface dikker worden, waardoor de thermische weerstand aan de interace zal toenemen. Ter controle werd ook de thermische weerstand van niet-geïmprinte polyurethaan lagen geanalyseerd in respons op blootstelling aan cellen. Deze lagen werden vervaardigd op dezelfde manier als de SIPs maar dan zonder het stempelen van de cellen. Elke toename in thermische weerstand die waargenomen wordt tijdens deze analyse valt dan ook toe te schrijven aan aspecifieke binding van cellen aan het polymeeroppervlak.

De morfologie en topografie van verschillende SIPs werd geanalyseerd na nauwgezette optimalisatie van het synthese en imprinting protocol voor deze polyurethaanlagen. Hierbij werd duidelijk dat de laterale dimensies van de cellen worden overgedragen naar de polymeerlaag. De diepte van de imprints in de polyurethaanlaag zijn vrij vlak ten op zichte van de dimensies van de cellen (ongeveer 20 µm), hetgeen valt te verklaren door het feit dat de polyurethaanlaag vrij dun is in vergelijking met de cellen (ongeveer 1 µm). Dit blijkt echter cruciaal te zijn voor de selectiviteit van de receptor. Cellen die morfologisch perfect in de imprints passen zullen hierdoor immers niet binden aan de laag, wanneer ze niet worden ondersteund door chemische interacties tussen de cellen en de imprints. Tijdens het cross-linken van het polymeer, zullen eiwitten op het membraan van de cellen kunnen interageren met de vormende polymeerlaag. Deze non-covalente interacties zorgen ervoor dat er, na het verwijderen van de cellen, functionele groepen achterblijven in de imprints die dienst doen als ankerpunten waaraan de cel kan binden door middel van interactie met bepaalde epitopen op eiwitten op hun membraanoppervlak.

Om na te gaan of het mogelijk was om tot een werkend biosensorplatform te komen voor de detectie van cellen, door twee bestaande concepten te combineren, werden SIPs gemaakt voor muis en rat macrofaag cellijnen. De specificiteit, selectiviteit en gevoeligheid van deze receptors werd geanalyseerd door middel van het HTM device om tot een proof-of-principle te komen. Uit een vergelijkend experiment met een SIP en een NIP bleek dat de thermale weerstand toenam na additie van cellen aan een SIPlaag. Dit effect bleef echter uit wanneer hetzelfde experiment werd herhaald met een NIPlaag. Voorts bleek de sensor ook in staat te differentiëren tussen macrofaag cellen afkomstig van rat dan wel muis. Deze experimenten bewezen dat het concept werkt en dat het ontwikkelde platform wel degelijk in staat was een specifieke en selectieve receptor te combineren met een snelle, label-vrije en goedkope uitleestechniek.

Aangezien het onderscheiden van rat- en muismacrofagen weinig relevantie heeft vanuit biologisch en medisch standpunt werd nagegaan of het device ook bruikbaar was in een meer medisch relevante setting. Na automatisering en optimalisering van de set-up bleek de bio(mimetische)sensor in staat een onderscheid te maken tussen twee verschillende soorten kankercellen (MCF-7 borstkankercellen en de leukemische T-cellijn Jurkat) en, belangrijker, tussen gezonde cellen en kankercellen. Hierbij werd geen noemenswaardige kruisgevoeligheid waargenomen. Deze experimenten toonden duidelijk aan dat dit platform in de toekomst wel degelijk kan leiden tot commerciële medische applicaties, zoals het detecteren van circulerende tumor cellen in bloedstalen van patiënten.

In een laatste fase van het onderzoek werden de limieten van de set-up blootgelegd. Hieruit bleek dat de SIP receptor bijzonder selectief is. Zo is het mogelijk om een onderscheid te maken tussen twee cellijnen die enkel verschillen in de expressie van één eiwit (het MUC1 proteïne). Meer zelfs, het bleek ook mogelijk te differentiëren tussen twee cellen op basis van de aan- of afwezigheid van glycosylatie patronen op het oppervlak van het MUC1 proteïne. Ook de gevoeligheid van de sensor na blootstelling aan mengsels van verschillende celtypen werd getest. Hieruit bleek dat de gevoeligheid toeneemt naarmate het sensoroppervlak vaker wordt blootgesteld aan deze mengsels. In

de laatste fase van het onderzoek werden de bekomen resultaten gevalideerd aan de hand van enkele state-of-the-art cel detectie technieken.

Het geleverde onderzoek dat samengevat wordt in deze thesis toont aan dat het combineren van SIPs met de HTM heeft geleid tot de ontwikkeling van een veelbelovend bio(mimetisch) sensorplatform voor de detectie van humane cellen. Het eenvoudige, snelle en goedkope karakter van deze toepassing biedt enorme voordelen ten aanzien van andere, commercieel beschikbare technieken. Om echt te kunnen wedijveren met deze technieken zal echter de gevoeligheid van de sensor nog sterk moeten verbeteren. Verdere verbeteringen kunnen gemaakt worden door de ontwikkeling van een nieuwe flow cel in een zogenaamd gesloten-lus systeem waarbij de laag continu wordt blootgesteld aan suspensies van cellen. Op deze manier kunnen kleine hoeveelheden aan cellen gedetecteerd worden. Targetcellen zullen binden aan de laag terwijl de mechanische frictie als gevolg van de continue vloeistofstroom er voor zorgt dat competitor cellen niet blijven hangen in de imprints. Tot slot kan de gevoeligheid nog toenemen door het aantal imprints op het oppervlak van de SIP te verhogen.

1. Introduction

Sensors are ubiquitous in everyday life. Motion sensors make sure that your driveway is lit when you pull up at night, when you want to wash your hands in a public restroom you can wash your hands or flush the toilet without having to touch the tap or the toilet valve. Thermostats measure the temperature in your living room and use this information to switch your central heating system on or off, in order to keep the room temperature at the desired set point. The fact that you are able to operate your mobile phone or your tablet computer using a touchscreen is based on technology using proximity sensors as well as ambient light detectors, making the device able to distinguish between intentional and unintentional touches. Accelerometers detect the physical movement of the device, making it possible for the touchscreen display to switch to either portrait or landscape mode when switching the orientation of the tablet.

In addition this wide range of technologic sensors that were developed in recent years, sensors also play a vital role inside the human body. They allow us to see, hear, feel, taste and smell. Various substances such as nutrients, toxins, neurotransmitters and hormones are monitored constantly to control the body's metabolism and homeostasis. The immune system makes use of antibodies to detect 'intruders' like bacteria or viruses that are killed upon identification. Without all these sensors our body would not be able to function properly. However, the body's detection systems are not fail-proof, leading to various diseases and conditions that eventually result in death. Therefore, the demand for reliable sensors, which are able to detect diseases such as cancer or atherosclerosis in the early stages of their development, is increasing in modern-day healthcare.

1.1. Biosensors

According to Anthony Turner, George Wilson and Isao Karube a biosensor can be defined as an analytical device that combines a biological element with a physicochemical detector [1]. Typically a biosensor consists of 3 major components as shown in **figure 1.1** The biological receptor layer is able to recognize and bind the analyte. Biosensor platforms profit from the high degree of specificity that a natural receptor has for its target to detect the analyte of interest in a very selective manner. This layer can consist of nucleic acids (DNA or RNA) [2-4], enzymes [5-7], cells [8-10] or antibodies [11, 12].

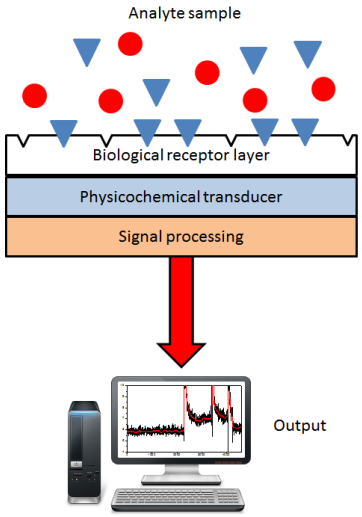

Figure 1.1: Schematic representation of a biosensor platform.

Binding of the analyte to the biological receptor layer will result in a physical or chemical change at the solid-liquid interface. The transducer makes sure that this change is transformed into a measurable signal. Depending on the analyte of interest and the biological receptor used, this transducer can be optical, thermal, electrochemical or piezoelectric. The connection between the transducer and the biological receptor layer is a key element in the development of a biosensor. It is possible to deposit the receptor layer directly onto the transducer element to ensure perfect coupling with the transducer layer. Alternatively the receptor layer can be deposited onto an immobilization platform. These platforms can include aluminium, gold, silicon, diamond, organic

polymers,… depending on the application. The signal processor will transform the signal into a readable output that can be displayed on a computer screen. In addition to the high degree of specificity, sensitivity and selectivity that are typical for biosensors, another benefit is that these devices can be miniaturized by micro-electronic techniques, making them perfectly suited for the real-time detection of medically relevant analytes.

One of the first "biosensors" known to man does not quite fit the schedule presented in figure 1. In coal mining, canaries were used as an early warning system for the presence of toxic gasses inside mining shafts. When exposed to gasses such as carbon monoxide, methane or carbon dioxide, the birds would die before the gasses were able to affect the miners. Conditions were considered unsafe when the bird would stop whistling.

1.1.1. Commercially available biosensor applications

In recent years, biosensors have evolved to more technological devices in comparison to the canary used by coal miners. A very crucial step in the process of developing commercially available biosensor applications is the transformation of a scientific prototype of a biosensor into a commercial device. A wide variety of biosensor applications has already been developed and is already commercially available. The most famous and widespread example of such a biosensor is the glucose sensor that helps patients suffering from diabetes mellitus control their blood glucose levels. In these patients, an auto-immune disorder causes the destruction of the insulin-producing beta cells of the islets of Langerhans in the pancreas, leading to elevated blood and urine glucose levels [14]. Failure to control the blood insulin levels can result in hyperglycaemia which puts patients at risk for ketoacidosis. These conditions cause fatigue, weight loss, poor wound healing and eventually even kidney failure, coma, blindness or seizures [15]. Patients can decrease the glucose concentration in blood by injecting themselves with insulin. However, if the injected dose of insulin is too high, blood glucose levels will be too low, a condition known as hypoglycaemia. This can result in unconsciousness, seizures and even permanent brain damage or death [16]. Therefore, a biosensor that can monitor the concentration of blood glucose in a reliable way is of great significance in handling diabetes.

In 1962 a first blood glucose meter was developed, combining a Clark electrode (measuring oxygen) with an oxygen-depended glucose-oxidase enzyme [17-18]. The oxidation of glucose to gluconalactone by the enzyme, consumes oxygen as shown in **figure 1.2**.

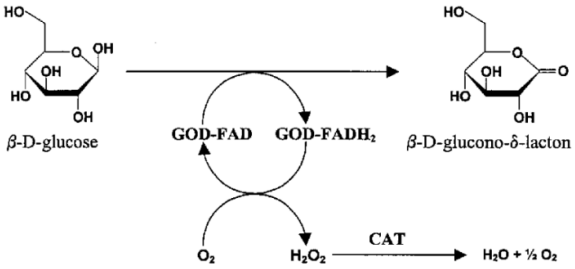

Figure 1.2: Enzymatic oxidation of glucose to gluconolactone.

This first generation glucose biosensor platform measured the glucose concentration in blood indirectly in function of the oxygen consumption. The enzyme was immobilized in a membrane spanning a platinum electrode (see **figure 1.3**). In absence of glucose, oxygen could freely diffuse towards the Clark electrode. The electrode measured the presence of oxygen amperometrically, a working voltage ensured that oxygen could take up electrons at the electrode, leading to a measurable current. In the presence of glucose however, the oxidation of glucose causes a decrease in oxygen concentration and hence a decrease in the current measured by the electrode.

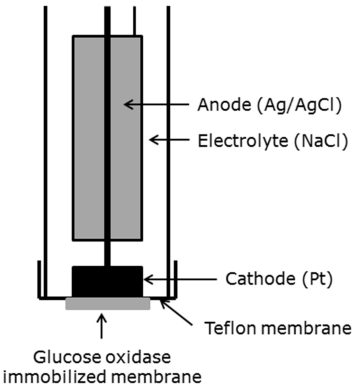

Figure 1.3: Glucose oxidase used in a Clark electrode-based glucose biosensor.

In recent years biosensors for the monitoring of blood glucose levels have become increasingly more sensitive. These sensors are able to detect the glucose in a more direct manner making the device faster and more sensitive. In the 1980s massive progress was made in the field of glucose sensing with the development of the Glucometer by Bayer and the Accu-Check by Roche. Patients could add a droplet of blood to a test strip and insert it into these devices, displaying the concentration minutes later. This way, patients were able to monitor the glucose concentration in their blood and adjust the rate of insulin injection accordingly. In the future sensors will be continuously monitoring the blood glucose concentration and insulin will be administered *in situ*. These sensors will make it possible to strictly regulate the blood glucose concentration.

Another example of a commercially available biosensor based on antigen-antibody binding, is so widespread that most people do not know it is a biosensor. Home test kits for pregnancy have been developed since 1968 and are an excellent example of what a biosensor should be: they are low-cost, fast and very user-friendly. Most pregnancy tests are based on the detection of the β-subunit of human chorionic gonadotropin (hCG) by anti-hCG antibodies (**figure 1.4**), binding results in a colour change that can be read out by the user in an easy manner. The drawback of the technique is that hCG can only be detected in blood or urine samples after implantation, six to twelve days after fertilization [19]. Alternative tests are based on the detection of the early pregnancy factor (EPF), which can be detected in blood within 48 hours after fertilization [20]. However, these tests are expensive and time-consuming.

Figure 1.4: BioAccu hCG Pregnancy test kit (www.okokchina.com).

1.1.2. Biosensors in scientific research

The demand for fast, reliable, low-cost and user-friendly biosensors in modern-day healthcare has driven the research and technologic development of these devices. Performing a search on Sciencedirect.com for the keyword 'biosensor' will result in over 40,000 articles. Especially in the last decade, the total amount of publications has risen enormously (**figure 1.5**), indicating the growing interest in and the rapid development of biosensors.

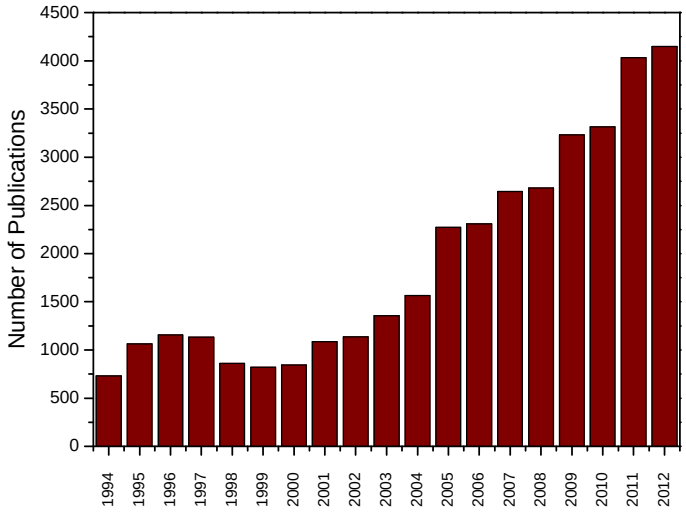

Figure 1.5: Number of publications involving biosensors per year. (statistics obtained *via* www.sciencedirect.com).

The use of biosensors in deoxyribonucleic acid (DNA) mutation analysis has been thoroughly investigated in recent years. According to the model proposed by James D. Watson and Francis Crick in 1953 DNA is shaped as a double helix as shown in **figure 1.6** [21]. According to their model the sugar phosphate backbones of both strands are connected to each other (hybridization) by means of complementary base pairs. Adenine can be paired to thymine by means of 2 hydrogen bonds, while cytosine and guanine form a more stable pair by means of 3 hydrogen bonds. This process results in the double-helical secondary structure of DNA. Both strands can be chemically or thermally separated from each other, a process that is known as denaturation.

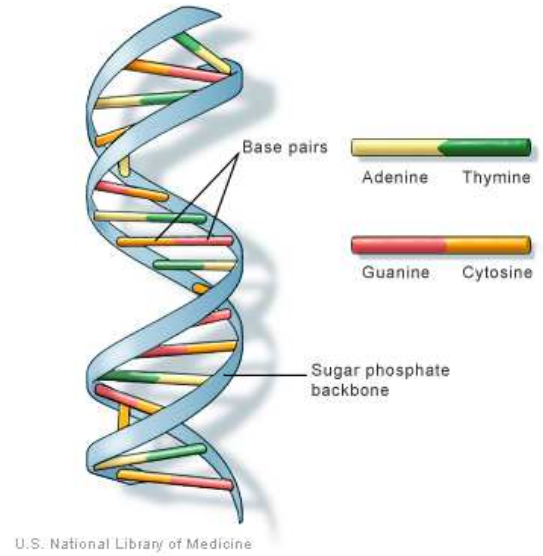

Figure 6: Schematic representation of the DNA double-helix structure (U.S. National Library of Medicine).

When considering the global gene pool it becomes apparent that there is a lot of variation in the genetic code (the sequence of base pairs in the DNA) of different human beings. These variations, called mutations, play a major role in the progression of various diseases and are therefore of great interest to the medical community. The smallest mutation possible is a single-nucleotide polymorphism (SNP), a variation in the DNA sequence consisting of one single nucleotide (adenine, cytosine, thymine or guanine) that differs between different members of the same biological species or between paired chromosomes within one single human. Many of these SNP's are harmless because they fall in non-coding regions, others do not change the protein they code for or cause harmless variations in phenotypic characteristics such as hair or eye colour. Some SNP's are even beneficial and natural selection fixates them in the gene pool as the most favorable genetic adaptation [22]. However, SNP's may also result in a wide variety of human diseases such as cystic fibrosis, sickle-cell anemia and various kinds of infectious diseases (hepatitis,…) and cancers [23-25]. There are many technological platforms available for the detection of these SNP's, including micro-arrays (based on hybridization) [26] and real-time

polymerase chain reaction with melting curve analysis [27]. However these techniques are typically very slow, with reaction times running up to 16 hours or more, are not suitable for high-throughput analysis, lack in dynamic information and they require a lab environment, fluorescent labeling and expensive equipment.

Therefore, van Grinsven *et al.* developed an electrochemical biosensor platform for the detection of SNP's [4]. The sensor platform is able to distinguish between different SNP's based on the analysis of denaturation time constants by impedance spectroscopy. Probe DNA is covalently attached to nanocrystalline diamond (NCD) electrodes, in a next step either full match DNA or DNA containing a SNP is hybridized to the probe DNA. The DNA is denatured by flushing the flow cell with sodium hydroxide causing the DNA to denature. This denaturation causes the impedance, monitored in real-time by the device, to decrease. The device is able to distinguish between two different types of DNA, each containing one SNP but at a different position (**figure 1.7**). The results are confirmed by a fluorescence-decay analysis using a confocal microscope.

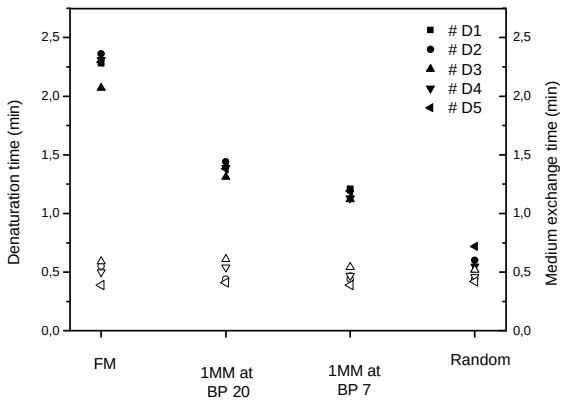

Figure 1.7: Denaturation time constant analysis of a SNP detection biosensor platform based on impedance analysis [4].

Apart from linear DNA, other nucleic acids structures such as DNA hairpins [29], aptamers [30] and RNA [31] have also been used as receptors in biosensor applications.

In addition to DNA sensors, considerable research efforts have been focused onto the development of biosensors based on antibody-antigen interactions in recent years. Antibodies, also called immunoglobulins, are very suitable to use as a receptor in a biosensor due to the specific interaction it can undergo with its antigen. These Y-shaped molecules are secreted by B-cells in the human blood and serve a crucial role in the human immune system. Antibodies are able to detect soluble antigens as well as those present on the membrane of 'intruders' such as viruses or bacteria. Each tip of the Y-shaped contains a paratope that interacts with an epitope on an antigen in a very specific manner (**figure 1.8**) [32]. The specificity of this interaction is a crucial element in the functioning of the human immune system and can readily be exploited for the development of biosensor platforms.

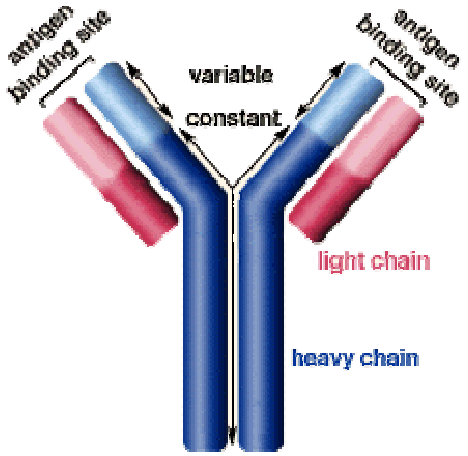

Figure 1.8: Schematic representation demonstrating the typical Y-shape of an antibody (www.biology.arizona.edu).

In 2011, Vermeeren *et al.* made use of the specificity of the antibody-antigen detection to construct a biosensor for the detection of C-reactive protein (CRP) [12]. CRP is considered an important marker for the development of cardiovascular diseases (CVD) such as atherosclerosis, myocardial infarction, coronary heart disease, angina and stroke [33]. Anti-CRP antibodies were immobilized onto NCD elecrodes by physical adsorption and binding of CRP to the sensor surface was analyzed by impedance spectroscopy. The sensor was able to detect CRP at concentrations as low as 10 nM. This indicates that the

prototype immunosensor proposed in this paper was able to detect CRP in the physiologically relevant concentration range, making it possible to discriminate between healthy controls (8-10 nM) and patients at risk for CVD (>10 nM). In addition, the sensor is able to discriminate between CRP and plasminogen with no apparent cross-selectivity observed. Preliminary serum measurements with spiked concentrations of CRP show that the sensor also functions in a more complex environment as compared to the measurements done in buffer solution (**figure 1.9**).

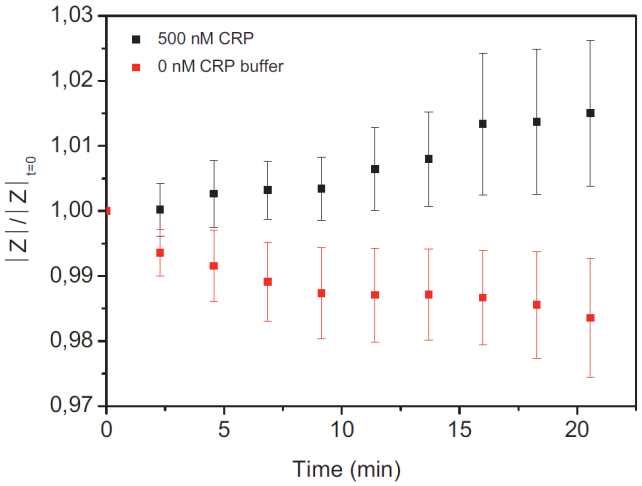

Figure 1.9: Response of the electrochemical immunosensor to serum samples spiked with CRP (black) and non-spiked serum samples (red) [12].

From these examples, it can be concluded that scientific research regarding biosensors has led to the development of applications that could be of medical and therefore commercial use. However, transforming these prototypes into a commercial device can prove to be a difficult task. The sensor set-up needs to be highly specific and selective in order to detect the analyte in a reliable manner. Quite often the physiologically relevant concentrations are very low, requiring the device to be highly sensitive. Furthermore, the device needs to be calibrated in order to transform the output into a value indicating the concentration of the analyte in the sample. Finally, the device has to be scaled down for practical reasons. These difficulties explain why up until know the number of commercially available biosensor applications is limited.

1.2. Biomimetic sensors

Biosensors based on biological recognition elements can be very sensitive and specific towards their target analyte but the use of biological receptors has many drawbacks. They are often unstable in changing physical and chemical environment, it is time consuming and expensive to obtain these receptors in sufficiently large quantities, display a limited shelf life and for certain analytes it is not possible to obtain a suitable biological receptor [34]. This makes them suitable for detection of analytes in buffer solution [35], but point-of-care diagnostics in biological samples proves more difficult.

1.2.1. Biomimetics

Whenever the use of biological systems in potentially valuable applications holds drawbacks, man attempts to create a synthetic system that works in a similar manner and has the same benefits but lacks the drawbacks. The development of these types of synthetic systems, mimicking the function of biological functions, has come to be known as biomimetics. The concept of biomimetics was introduced during the 1950s by Otto Schmitt, a biophysicist studying the nervous system in squids. During his PhD study, Schmitt acquired knowledge about the nerve propagation in the squid and he used this knowledge to engineer a device that replicated this biological system. Over the following years, Schmitt continued to study and mimic biologic systems and by 1957 he had established a new view field in the view of biophysics, which he would come to call biomimetics [36].

Although the concept of biomimetics was introduced by Schmitt, the approach of mimicking nature has existed for many hundreds of years. Leonardo da Vinci studied the mechanisms of flying in birds and swimming in fish and used this knowledge to design his flying and naval machines. In 1941 Swiss engineer George de Mestral took his dog for a walk. He noticed that his dog was covered by cockleburr seed casings. He analyzed the seeds under the microscope and discovered the surface of the burr seeds was covered by small hooks that were able to catch anything with a loop structure. This led de Mestral to the idea of using similar synthetic hook structures on patches or strips that could easily bind to similar structures covered in loose-looped weave or nylon. In this way de Mestral invented the Velcro strip (see **figure 1.10**) [37].

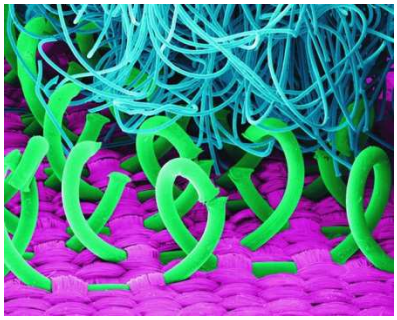

Figure 1.10: Scanning electron microscope image showing the detailed structure of two opposing Velcro strips (www.howitworksdaily.com).

Another well-known example of biomimetic applications are self-cleaning surfaces exploiting the lotus-effect, exhibited by the leaves of the of the *Nelumbo* lotus. These leaves display a distribution of small papillae protruding from the epidermis covered in wax, making the leaves of the lotus superhydrophobic [38]. This characteristic of the lotus plant has an interesting application, water droplets are easy removed from their leaves, dragging al long any dirt present on these leaves. In other words, the leaves are self-cleaning. This is based on a purely physicochemical effect that can be transferred to coatings or paints making it possible to design self-cleaning surfaces (**figure 1.11**) [39].

Figure 1.11: Schematic representation of the Mincor TX coating, developed by BASF. The coating exploits the lotus-effect in order to obtain self-cleaning textiles (www.BASF.com).

Analogous to the examples of biomimetics shown above, a lot of research has been aimed at creating biomimetic receptors. These synthetic receptors should display a similar specificity, sensitivity and selectivity towards their target in comparison to their natural counterparts. At the same time the use of these receptors should show improvement in the fields where biosensors fall short. Therefore, imprinting of polymers in order to create synthetic receptors has become an emerging field in biosensor research.

1.2.2. Molecular imprinting

Many of the drawbacks of working with biological receptors can be overcome by the use of so-called molecularly imprinted polymers (MIPs) [40-42]. These synthetic polymers can specifically rebind their target by means of nanocavities and display a specificity that is comparable to that of antibodies. MIPs are very robust and display a very high chemical and thermal stability which makes them usable in a wide temperature and pH range [43]. Furthermore, they can be regenerated easily and they display an extended shelf life [44]. After carefully optimizing of the synthesis protocol, they can be made in a low-cost and relatively straightforward manner, making use of conventional polymer chemistry. Especially the synthesis of bulk MIPs based on non-covalent interactions is simple and fits the scheme shown in **figure 1.12** [45].

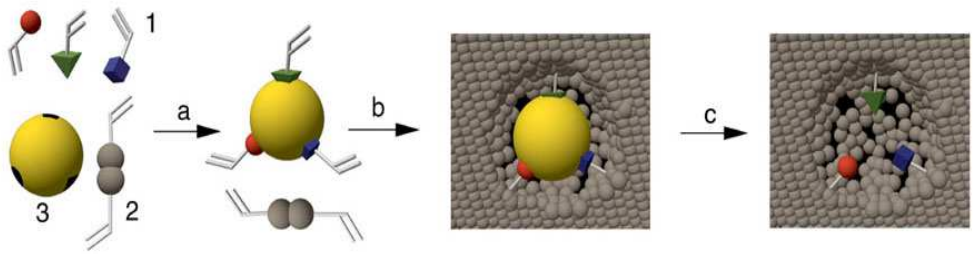

Figure 1.12: General scheme describing the synthesis of non-covalent MIPs. Functional monomers (1) are mixed together with cross-linking monomers (2) and the desired target analyte (3) in an appropriate porogen. (www.utc.fr).

The synthesis is initiated by dissolving the desired target analyte in an appropriate porogen. Functional monomers such as metacrylic acid (MAA) or acrylic amide (AA) [46] are added to the solvent and will form a pre-polymerisation around the template molecule due to non-covalent interactions

(a). The porogen will stabilize the complex. Polymerization is initiated by exposing the mixture to thermal activity or UV light; during this phase cross-linking monomers such as ethylene glycol dimethacrylate (EGDM) [46] interconnect the different polymer chains, creating a stable polymer matrix. Once polymerization is completed a bulk polymer is formed, trapping the analyte inside the polymer (b). After removal of the template, the MIP is ready to rebind the target in a specific manner through nanocavities spread over the polymer (c). These nanocavities are complementary to the target in size, shape and distribution of functional groups. Therefore the MIP system functions through the key-and-lock principle, with the target analyte and the nanocavities being analogous to the key and the lock respectively.

In addition to the bulk polymerization described above more homogenous MIP particles can be created by suspension, precipitation or emulsion polymerization [47-49]. Working with these types of MIPs in biomimetic sensors could be beneficial in terms of reproducibility.

MIPs can be packed into chromatographic columns and used for the analytical separation of target molecules [50] and can be used in environmental [51] and food analysis [52]. More recently, these MIPs were incorporated into universal biomimetic sensor set-ups. Various biosensor applications for bioanalytical detection of analytes have been developed based on impedance spectroscopy [53-55], microgravimetric detection [56, 57] and thermal transport measurements [58]. In these applications, MIPs are used for the detection of low-molecular weight compounds such as L-nicotine [53], serotonine [54] or histamine [55]. It is possible to synthesize MIPs for bigger structures such as viruses [59], DNA [60] and proteins [61]. However, the synthesis of synthetic receptors based on molecular imprinting is an extremely difficult task due to size limitations. Therefore, imprinting of micrometer-scaled objects has to be done in an alternative way.

1.2.3. Surface imprinting

In recent years, the concept of molecular imprinting has been extended to surface imprinting of thin polymer films, a technique that was perfected by Professor Franz L. Dickert at the University of Vienna. Research involving the implementation of these surface imprinted polymers (SIPs) into biosensor

platforms has led to the development of applications for the detection of proteins [62, 63], bacteria [64-66], viruses [63, 67], pollen grains [68], yeast [69], HeLa cells [70] and erythrocytes [63, 71]. The concept of surface imprinting is schematically presented in **figure 1.13.**

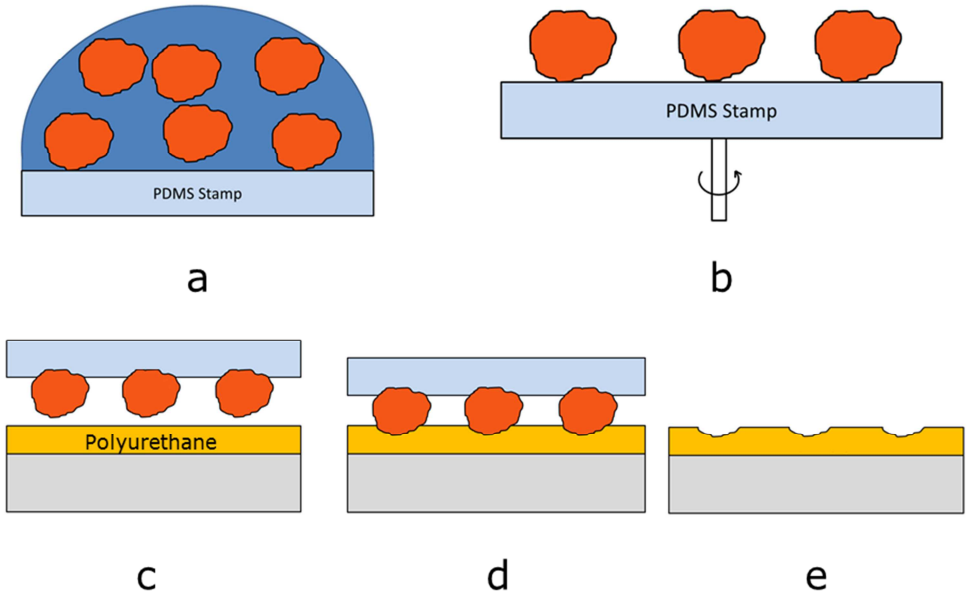

Figure 1.13: Schematic representation of the surface imprinting procedure. a) sedimentation of a suspension of target cells in buffer onto a home-made polydimethylsiloxane stamp b) excess buffer solution is removed by spin-coating c) a semi-cured polyurethane layer is applied to a sensor transducer such as a QCM crystal or a metallic substrate d) the cells are stamped into the polyurethane layer and the layer is cured overnight e) after curing of the layer, the stamp is removed and the cells are washed out of the polyurethane, leaving behind a surface imprinted polymer layer.

SIPs can be created in a relatively straightforward manner. The desired target cell type is dissolved in buffer solution and applied onto a stamp (a). The stamp can be composed of glass [71] or a more elastic material such as polydimethysiloxane (PDMS). The cells will sediment towards the surface of the stamp and after a short incubation time the excess buffer fluid is removed by spin-coating off the stamp (b). In parallel a pre-polymerization mixture is prepared containing functional monomers and cross-linkers in an appropriate

solvent. Polymerization of the mixture is initiated by heat and the mixture will gradually cross-link up to the gelling point. In order to deposit the semi-cured polymer onto an appropriate transducer the viscous gel is diluted using solvent, which makes it possible to spin-coat the mixture (c). This procedure ensures that a thin polymer layer (usually polyurethane) is left behind on the surface. The layer is not fully cross-linked and still displays enough elasticity to make an imprint of the cells while applying only moderate force on the stamp. The layer is cured overnight with the stamp lying on top of the sample, ensuring that the cells are residing inside the curing polyurethane layer (d). After curing of the layer, the stamp is removed from the surface and the cells are washed off by rinsing the layer with soap and buffer solution. This way, a surface imprinted polyurethane layer is left behind containing microcavities, complementary to the template cells in size, shape and the distribution of functional groups (e). The latter can be explained by the fact that the polymer mixture contains an excess of phenolic groups [69], making it possible for the cells to interact with the forming polymer by van der Waals forces, hydrophobic interaction, hydrogen bonding [44, 72] and CH-π interactions [73].

The concept of surface imprinting of polyurethane layers was demonstrated by O. Hayden and F. Dickert in 2001 in an attempt to detect *Saccharomyces cerevisiae* cells (*S. cerevisiae*) in buffer using a quart crystal microbalance (QCM) [69]. Polyurethane-coated QCM-electrodes (quartz) were imprinted with *S. cerevisiae* cells. Addition of a *S. cerevisiae* cell suspension in PBS buffer led to a decrease in resonance frequency of 700 Hz while this effect was absent at the non-imprinted reference electrode (**figure 1.14**). These experiments clearly constituted a proof-of-principle demonstrating that the concept of surface imprinting was indeed useful in terms of creating synthetic cell receptors.

More recently, the research was extended towards the detection of medically more relevant cell types. In 2006 Hayden, Dickert *et al.* reported on a biomimetic sensor platform for ABO blood-group typing [71]. Therefore, polyurethane-covered QCM electrodes were imprinted with erythrocytes of blood-group A and exposed to blood-groups A and B erythrocytes. The microgravimetric response of the sensor is shown in **figure 1.15**.

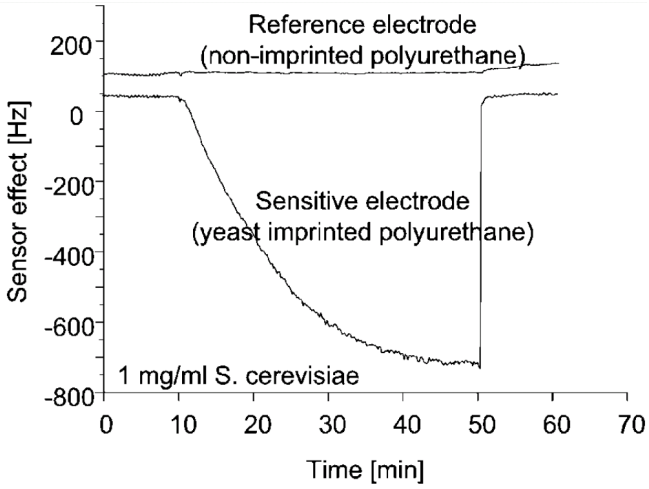

Figure 1.14: Response of a SIP-based microgravimetric biosensor platform to a suspension of target cells (S. cerevisiae). The response of a reference electrode covered by a NIP layer is also shown.

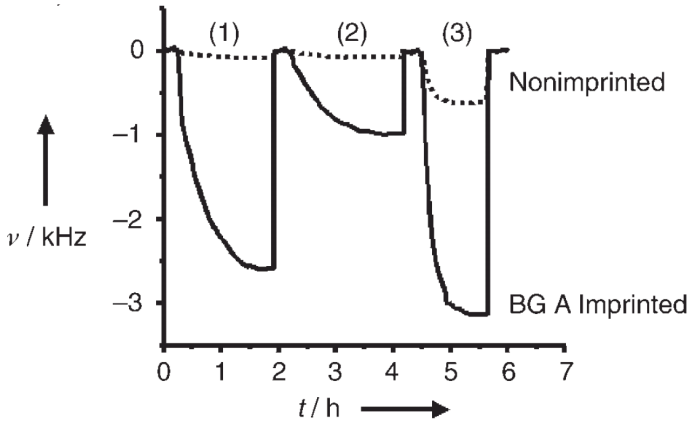

Figure 1.15: Microgravimetric response of a SIP-based biosensor platform for ABO blood-group typing. The solid line represents the response for an electrode covered by a SIP imprinted with blood-group A erythrocytes while the dashed line represents the response of an electrode covered with a NIP layer.

The results in figure 1.15 clearly demonstrate that the SIP-covered electrode is able to bind the blood-group A erythrocytes in a specific manner (step 1), the SIP-covered electrode (solid line) shows a response of 2.5 kHz upon addition of the cells. This effect is absent at the reference electrode (dashed line). Addition

of a suspension of analogue cells (blood-group B erythrocytes, step 2) only leads to a decrease 1 kHz, indicating that the sensor is capable of discriminating between both erythrocytes of blood-group A and B. For comparison the experiment was repeated without flow (step 3). In order to assess the full ABO blood-group typing capacity of the sensor, SIP's were made for all four blood-groups and tested for cross-selectivity against all possible blood types. The results are summarized in **figure 1.16**.

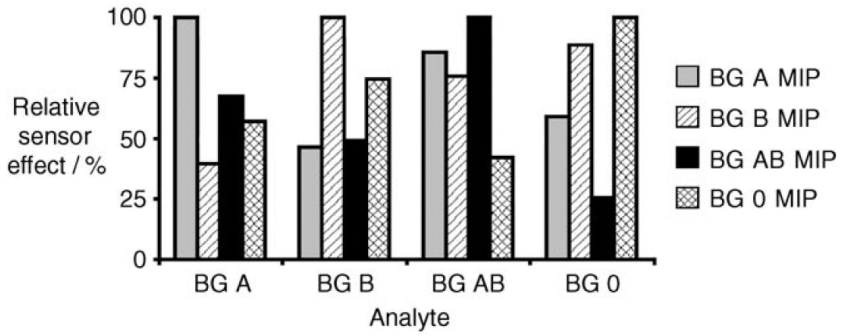

Figure 1.16: Selectivity of an ABO-specific SIP sensor based on microgravimetric detection. Polyurethane-electrodes were imprinted for four different types of erythrocytes (type A, B, AB and O) and tested for their response to all possible analytes.

The results in figure 1.16 clearly show that the sensor is a useful label-free tool for ABO phenotyping of erythrocytes. The best discrimination was found for AB-imprinted SIPs, showing a 25% response when exposed to O-type cells as compared to a 100% response upon binding of AB-type erythrocytes.

The platform proposed by Dickert *et al.* shows great promise for the development of similar platforms for the detection of medically more relevant cell species. However, all the proposed platforms use a QCM as read-out platform. Although it is a straightforward technique that requires little expertise, commercial QCM devices can be quite expensive. In addition, the piezoelectric electrodes are very delicate, consisting out of specialized AT-cut quartz crystal covered by evaporated gold electrodes on both sides. These electrodes will even increase the cost of the sensor platform. Therefore, a platform employing SIPs as synthetic receptors combined with an equally sensitive, fast and label-free but more low-cost read-out platform can be of great interest.

1.3. Aim of the thesis

The work done during this PhD project aimed at developing a novel detection format for the selective identification of human cells. Although it is hard to match up with the sensitivity associated with state-of-the-art cell detection techniques such as FACS or flow cytometry, the platform can be advantageous over these techniques by being low-cost, user-friendly, label-free and fast while displaying a comparable specificity and selectivity. In this way, the proposed platform could have a major impact on the medical community as a tool for monitoring serious diseases such as cancer or certain types of cardiovascular diseases (CVD) being prevalent causes of death in modern-day Western society.

1.3.1. Biomedical relevance of the platform

There are various examples that the precise shape of cells and the membrane structure correlate with certain physiological conditions or diseases: slight variations in the density of carbohydrate antigens of the ABO system on the glycocalyx of erythrocytes determine the blood group and Rhesus factor of mammals [74, 75]. Furthermore, the shape of the erythrocytes can also be characteristic for diseases such as sickle-cell anaemia [76], as can be seen in **figure 1.17**. In this disease the red blood cells assume an abnormal, sickle shape leading to a decreased flexibility of the cells which put the patients at risk of various complications such as decreased immune activity [77], chronic pain [78], pulmonary hypertension [79], chronic renal failure [80] or stroke [81].

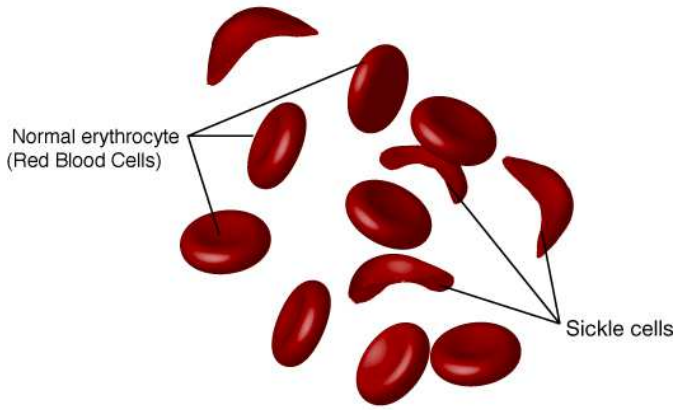

Figure 1.17: Comparison of the shape of a regular shaped erythrocyte and the distinct shape of red blood cells in people who suffer from sickle-cell anaemia.

White blood cells also deserve special attention because their shape and membrane groups can be related to cardiovascular disorders. For example, macrophages and monocytes in atherosclerosis patients display different antigens on their membranes as compared to macrophages of healthy individuals [82-84].

Atherosclerosis is an inflammatory disease of the vascular wall that can lead to serious conditions such as myocardial infarction, stroke and even sudden death [85]. Atherosclerosis is the most common form of CVD, accounting for the largest number of CVD-related deaths. Critical in the development of the disease is the formation and growth of the so-called atherosclerotic plaque. The migration of circulating monocytes to the plaque and their transformation into macrophages is a key element in the early stages of the disease (shown in **figure 1.18**). Phentoypical changes of monoctyes and macrophages play a major role in the formation of the plaque [82]. These phenotypically different blood cells can serve as a marker for atherosclerosis during the early stages of the disease. As the detection of atherosclerosis in these early stages is a difficult and expensive task [86], a sensitive, fast and low-cost biomimetic sensor platform that is able to identify these atherosclerotic macrophages or monocytes and distinguish them from healthy blood cells would therefore be of enormous interest to the biomedical community.

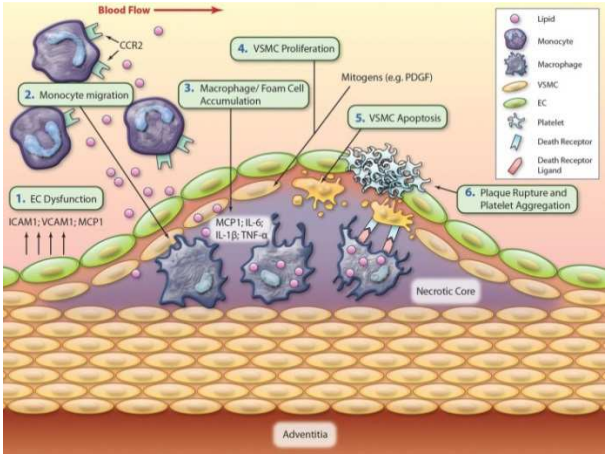

Figure 1.18: Schematic representation of the formation of an atherosclerotic plaque (www.circres.org).

Also, it is a well-established fact that overexpression of certain antigens on the membrane of human cells play a major role in the development of certain types of cancer [87]. These antigens can serve as markers for tumor formation. An important example is the Mucin-1 protein (MUC1). This transmembrane protein displays a high extent of *O*-linked glycosylation and is expressed on the apical surface of most secretory epithelia as well as on a variety of haematopoietic cells [88, 89]. Overexpression of MUC1 can lead to various types of cancer including most adenocarcinomas, colon-, lung-, pancreatic-, ovarian-, and breast cancers as well as blood cell lymphomas [89-92]. In addition, tumor cells display underglycosylation of the MUC1 protein (**figure 1.19**), due to premature termination of glycosylation, caused by upregulation of sialyltransferases and downregulation of glycosyltransferases [93, 94]. Altered MUC1 expression increases cancer cell-enothelial cell adhesion [95], cell proliferation [96] and cell survival leading to an increased tumorigenicity [97]. In addition, overexpression of MUC1 leads to a decreased intercellular adhesion due to steric hindrance. This allows tumor cells to escape recognition and removal by the immune system [98]. Detection of these changes in protein expression in an early state of the disease can therefore be considered valuable in cancer and follow-up therapy. State of the art tumor cell detection systems are very sensitive but expensive devices based on flow cytometry, while the platform proposed in this thesis offers a low-cost, user-friendly alternative for these devices.

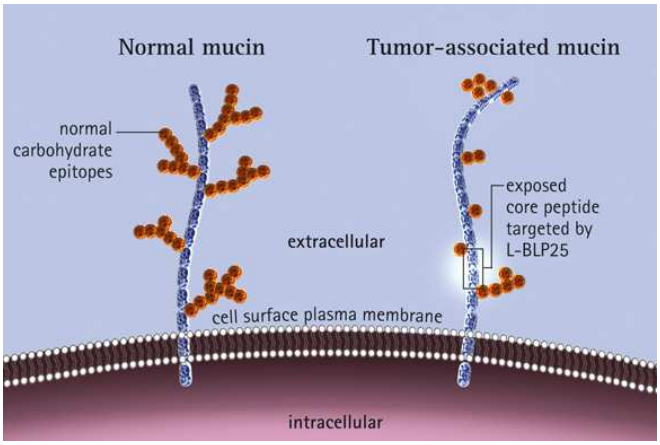

Figure 1.19: Underglycosylation of the MUC1 protein in tumor cells (magazine.merckgroup.com).

1.3.2. The need for a novel biomimetic platform

The identification of cells by sensor devices is commonly based on microbalances [71], electronic read-out [99, 100], or microfluidic techniques [101]. However the fact that the proposed synthetic receptor (SIP) is based on an electrical insulator (polyurethane) makes it difficult to combine SIP-based sensor platform with electronic read-out techniques. Microgravimteric detection with QCM-based detection platforms have shown to be an alternative but, as already mentioned previously, this technique requires expensive equipment. In addition, polyurethane layers can quench the piezoelectric vibrations making it difficult to achieve low detection limits. Therefore a fast, low-cost, label-free, automated sensor platform that overcomes these limitations while still allowing for sensitive cell detection and identification based on differences in size, shape or membrane functionalities is of great interest.

We will show that the heat-transfer method (HTM), developed recently in the context of DNA-mutation analysis [102], can indeed circumvent these limitations. Moreover, it can be readily combined with SIP-type synthetic cell receptors, selectivity is provided by the SIP layer and the read-out requires not more than a controlled heat source and two temperature sensors.

2. Development of the sensor set-up and surface characterization

2.1. Introduction

This section describes the materials and protocols, techniques and devices used for the creation of a selective biomimetic sensor platform for the detection of mammalian cells. Therefore, polyurethane layers are imprinted and coupled to an appropriate transducer, the so-called HTM. In addition the synthetic receptors are studied using various surface characterization techniques.

In order to optimize the polyurethane synthesis process and the imprinting procedure it is vital to study the surface morphology of the SIPs using different techniques. It also helps to understand the physical and chemical processes that take place during rebinding and provides insight into the functioning of the synthetic receptor. The protocol was optimized in a first phase of the research by imprinting polyurethane layers with silica beads (15 µm, Sigma-Aldrich N.V., Diegem, Belgium, **figure 2.1**). These spherical particles are used as a model for biological cells as they are comparable in size and shape to the cell types of interest in this study, but they have the benefit of being extremely robust, homogenous and low-cost. Furthermore, these beads do not require culturing and can be imprinted in the dry-state, avoiding that excess buffer fluid could interfere with the polymerization reaction.

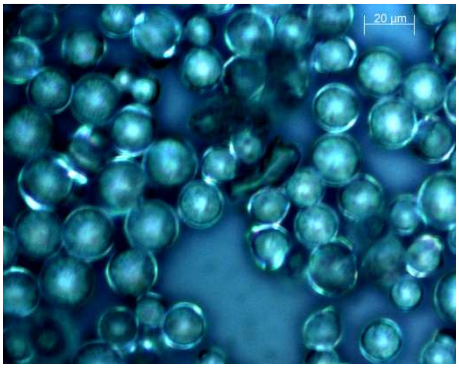

Figure 2.1: Optical microscopy image of silica beads deposited onto a microscope slide (Carl Zeiss Axiovert 40 microscope: 50x magnification).

After optimization of the SIP synthesis procedure with silica beads, SIP layers were synthesized with three cell types. NR8383 cells (rat alveolar macrophages) and RAW 264.7 cells (mouse leukemic monocyte macrophages) have both a spherical shape with diameters of ≈ 25 µm (NR8383) and ≈ 15 µm (RAW 264.7) and were chosen as model mammalian cell types for atherosclerotic monocytes as they are readily available and easy to culture in comparison to human cells. Additionally, imprints were made with yeast cells (*S. cerevisiae*) characterized by a diameter of only 5 µm. These are able to withstand the imprinting conditions better than mammalian cells and have been demonstrated in literature as a model cell type used for surface imprinting, leading to densely packed spherical imprints in polyurethane layers [69]. These three cell types were eventually used for a proof-of-principle experiment on the proposed biomimetic sensor platform. In a later phase of the research, polyurethane layers were imprinted for human cells including the breast-cancer cell line MCF-7, the immortalized T-lymphocyte cell line Jurkat, and peripheral blood mononuclear cells in order to demonstrate a proof-of-application.

2.2. Materials & Methods

In order to create an artificial receptor for the selective and specific rebinding of target cells surface imprinting was used as described in figure 1.13 in section 1.2.3. The following protocols were used in order to create the stamp and the polyurethane layer that is used as an artificial receptor for the detection of mammalian cells.

2.2.1. Synthesis of a polydimethylsiloxane (PDMS) stamp

PDMS stamps were made using the Sylgard 184 silicone elastomer kit (Malvom N.V., Schelle, Belgium). The kit consists of 2 components: a resin silicone solution and a curing agent. These components are mixed in a 10:1 ratio (silicon/curing agent) and the mixture is degassed using a desiccator, ensuring the complete removal of air bubbles from the mixture. The mixture is poured into a suitable mold ensuring that the stamp has the desired size and shape necessary for the stamping procedure. The mixture is heat-cured at 65°C in a dust-free environment, after curing and removal of the stamp from the mold, a firm, flexible stamp surface is created. Cell suspension in phosphate-buffered saline (PBS solution, 400 µl) was applied to the PDMS stamp. After

sedimentation of the cells, the excess fluid was removed by spinning at 3000 rpm for 60 seconds in order to create a dense monolayer of cells on the stamp surface.

2.2.2. Polyurethane synthesis and surface imprinting

Polyurethane layers were formed by dissolving 122 mg of 4,4'- diisocyanato-diphenylmethane, 222 mg of bisphenol A, and 25 mg of phloroglucinol in 500 µl of anhydrous tetrahydrofuran (THF). All reagents were used as received from Sigma-Aldrich N.V. (Diegem, Belgium) and had a purity of minimally 99.9%. The excess of phenolic groups used in the pre-polymerization mixture ensures excellent hydrogen bonding and CH-π interactions due to the carboxylic and mildly acidic hydroxyl groups of phloroglucinol and bisphenol A [68]. This mixture was stirred at 65°C for 200 minutes under inert nitrogen atmosphere until the polymer solution reached its gelling point. Then, the solution was diluted in a 1:5 ratio in THF and spin-coated during 60 seconds at 2000 rpm onto 1 cm^2 aluminium substrates.

In order to create an imprinted surface, the cell-covered stamp was gently pressed (pressure: 70 Pa) onto the polyurethane layer and cured for 18 hours at 65°C under nitrogen atmosphere. After curing, the stamp was removed from the surface. Rinsing the surface with 0.1% sodium dodecylsulfate (SDS) solution . Rinsing the layer with PBS, the template cells were lwashed off from the polymer layer, leaving behind selective binding cavities on the polyurethane surface. These cavities are complementary to the template cell type not only in size and shape but also in the distribution of functional groups due to the interaction of the forming polymer with proteins and carbohydrates on the membrane surface of the cells during cross-linking of the polymer. Non-imprinted polymer layers, used for assessing specificity, were made exactly in the same way as their imprinted counterparts, however without covering the PDMS stamp with template cells.

2.2.3. Cell culture protocol

Mouse leukemic monocyte macrophage RAW 264.7 cells (American-type culture collection ATCC: TIB-71), rat alveolar macrophage NR8383 cells (ATCC: CRL-2192), and human Jurkat cells (ATCC: TIB-152) were cultured in Roswell Park Memorial Institute medium (RPMI medium, Lonza Braine S.A., Braine-l'Alleud,

Belgium) supplemented with 10% Fetal Calf Serum (FCS) and 0.5% penicillin/streptomycin (P/S). Cells were passaged at a confluence of about 80%. Prior to imprinting and measurements, the RPMI medium was exchanged with phosphate buffered saline (PBS) in six washing steps in order to remove proteins of the culture medium. *S. cerevisiae* solutions were made by dissolving compressed baker's yeast from Dr. Oetker (Bielefeld, Germany) in PBS buffer solution. Cell counting to determine the cell concentration in buffer medium was done using a haemocytometer (VWR International, Leuven, Belgium). MCF-7 cells (ATCC: HTB-22) were cultured in Eagle's Minimum Essential Medium (EMEM medium, Lonza Braine S.A.). They were passaged and washed as described above for other cell types. Peripheral blood mononuclear cells (PBMC) were isolated from blood samples of a healthy, female subject using a Ficoll separation technique. In order to remove unwanted proteins from the medium, the cells were washed with PBS in three steps. All ATCC cell cultures were ordered at LGC Standards S.a.r.l., Molsheim Cedex, France.

2.2.4. Read-out platform: the heat-transfer method (HTM)

The sensor set-up shown in **figure 2.2** has been described in earlier work on the thermal denaturation of double-stranded DNA for the detection of single nucleotide polymorphisms [102]. The set-up was modified in order to be used for the detection of cells, to this extent the SIP-covered substrate was located at the bottom of the set-up instead of at the top set-up as was the case for DNA detection. This ensures a better transmission of heat from the copper to the liquid through the SIP layer by convection. In addition, it helps the cells to sediment towards the receptor layer.

2.2.5. Technical details of the HTM set-up

The polyurethane-covered aluminum substrates (10 x 10 x 1.0 mm^3) were horizontally mounted in a home-made flow cell of 110 µl (liquid-contact area of 28 mm^2, liquid height 4.0 mm). The substrates were fixed mechanically onto a copper backside contact of the device and heat-conductive paste was used to optimize the thermal contact between the copper and the aluminum chips. Liquids were exchanged either manually or automatically, using a syringe-driven flow system (ProSense, model NE-500, The Netherlands). All thermal resistance measurements were performed under static conditions without liquid flow. Two

miniaturized thermocouples (type K, diameter 500 µm, TC Direct, The Netherlands) were used for monitoring the temperature T_1 of the copper backside contact and the temperature T_2 of the solution in the center of the flow cell at a position 1.7 mm above the chip surface. Heat flow was generated with a power resistor (22 Ω, MPH20, Farnell, Belgium) attached to the copper block using heat-conductive paste and tightly fixed with a screw. The thermocouple signals were collected in a data acquisition unit (Picolog TC08, Picotech, United Kingdom) and further processed by a proportional-integral-derivative controller (PID controller parameters: P = 10, I = 5, D = 0.1) in order to regulate T_1 (in this case at 37.00 ± 0.1 °C). The output voltage calculated by the PID controller was fed back into the power resistor via a second controller (NI USB 9263, National Instruments, USA) and a power operal amplifier (LM675, Farnell, Belgium). The sampling rate of the T_1 and T_2 values was 1 measurement per second. All measurements were performed in a temperature-stabilized environment at an ambient temperature of 19.0°C.

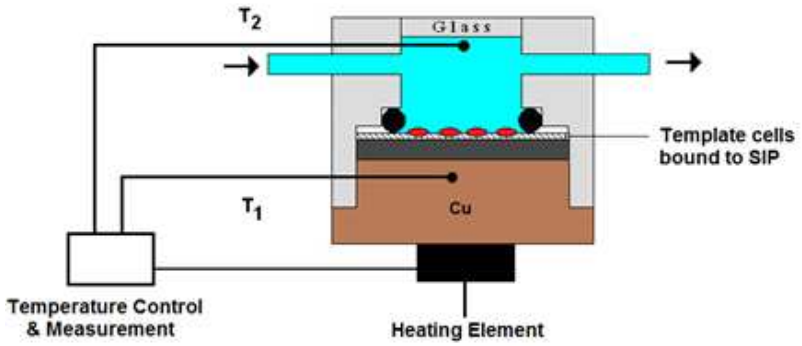

Figure 2.2: Schematics of the measuring set-up, not drawn to scale. The aluminum substrate covered with the SIP is attached to the copper block. The temperature of the copper block T_1 is kept constant at 37.0 °C and the temperature T_2 of the liquid and the heating power necessary to keep T_1 constant are monitored in time.

2.2.6. HTM concept for specific cell detection and identification

The central element of the platform consists of an adjustable heat source attached to a copper block that transfers a thermal current trough an aluminum chip (~ 1 by 1 cm^2) covered with a thin layer (~ 1.1 µm) of cell-imprinted

polyurethane. During measurements, the temperature underneath the aluminum chip, T_1, is stabilized at 37.00°C with a PID controller and the temperature T_2, in the liquid compartment above the polyurethane layer, is monitored. From the temperature difference $T_1 - T_2$ and the required heating power P to keep the copper block at 37.00°C, one can derive the heat-transfer resistance R_{th} by following equation [102, 103].

$$R_{th} = \frac{T_1 - T_2}{P}$$

The contact area between the chip and the liquid compartment was 28 mm^2. The imprinted cavities, where the PU film is thinner, form preferential heat transport channels as the Rth is directly proportional to the thickness of the insulating material. As it was recently shown that lipid bilayers have a higher thermal resistance than water [104], an increase in R_{th} at the solid-liquid interface should be encountered upon binding of cells into the cavities of the SIP-layer as schematically illustrated in **figure 2.3**.

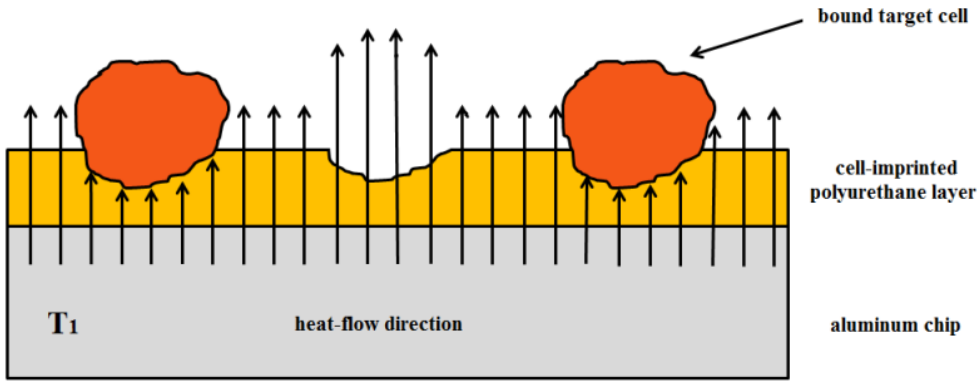

Figure 2.3: Schematic representation of cells binding to the SIP layer, blocking the heat-transfer from the copper to the liquid compartment.

2.2.7. Optical microscopy

The optical analysis of the imprinted polyurethane layers was performed with an Axiovert 40 inverted optical microscope (Carl Zeiss, Jena, Germany). Optical analysis of the morphology of the imprinted polyurethane layers provided a good insight into the size and shape of the imprints. In addition, the surface coverage of the polyurethane layers with cell imprints was determined on basis of the optical micrographs analyzed with the software package ImageJ 1.44P (National Institute of Health, Bethesda, USA).

2.2.8. Scanning electron microscopy (SEM)

In order to analyze the silica imprints in more detail the imprinted surface was analyzed using a FEI Quanta 200F scanning electron microscope (FEI co, Hillsboro, Oregon, USA). In addition, SEM analysis of non-imprinted polyurethane layers (NIPs) gives insight into the roughness of the polymer layer in relation to the morphology of the imprints.

2.2.9. Atomic force microscopy (AFM)

The topography of a surface-imprinted polymer imprinted with MCF-7 breast cancer cells as well as the depth of a typical imprint was analyzed by atomic force microscopy (AFM). AFM measurements were performed in non-contact mode (NCM) using a NX 10 AFM (Park Instruments, Suwon, South Korea). Standard, pyramidal-shaped silicon nitride (Si3N4) cantilever tips with a length of 125 µm and a nominal force constant of 40 N/m were employed (ST Instruments, Sliedrecht, The Netherlands). Topography, NCM-phase and NCM-amplitude were recorded across typical scanning areas of 45 x 45 μm^2. AFM imaging was performed in air at ambient temperature.

2.2.10. Profilometry

The thickness of NIP layers was analyzed by means of a profilometer (Dektak3ST, Sloan Instruments Corporation, Santa Barbara, USA). For this purpose, NIPs were synthesized in exactly the same manner as the imprinted polyurethane layers except no cells were deposited on the stamp that was pressed onto the polymer layer during cross-linking of the polymer. In order to measure the thickness of the layer, the center of the glass samples was covered with Scotch tape prior to spin-coating of the semi-cured polymer onto the sample surface. In this way a small region in the center of the sample is

shielded from the polyurethane. Removal of the tape after curing of the polymer resulted in two NIP-covered zones separated by a central region of bare glass. In order to avoid any anomalies, residual glue was removed from the central bare glass region by cleaning it with isopropanol. The layer thickness can be determined by measuring the difference in height between the NIP-covered surface and the bare glass region.

2.3. Results

2.3.1. Surface analysis of SIPs imprinted with silica beads

The morphology of SIPs imprinted for silica beads was analyzed in detail using SEM imaging. The SIPs were synthesized as described in section 2.2.2., using silica beads rather than cells as template. The silica beads were used as so-called model cells, in order to optimize the polyurethane synthesis protocol and the imprinting procedure. The resulting SIPs are shown in **figure 2.4.** The SIPs in this figure clearly show that a dense layer of polyurethane is formed around the beads and that removal of the beads leads to the formation of microcavities that appear to be complementary to the beads in size and shape.

However, the SIP in figure 2.4a clearly demonstrates that removing the stamp and gently rinsing the layer with warm water was insufficient to remove all the beads from the polyurethane layer. Applying a more stringent washing step with hot water caused all of the silica beads to be removed from the binding cavities, leaving behind a distinct pattern of closely-packed microcavities on the surface of the SIP. The morphology as well as the size of these microcavities matches the dimensions of the template beads precisely. In comparison, a non-imprinted polyurethane layer lacks this pattern and appears to be relatively smooth.

The results in this section clearly demonstrate that, although the silica beads do not functionally interact with the forming polymer, it is still hard to remove them physically from the polymer. Therefore, all SIPs should be properly washed in order to ensure full extraction from the template from the microcavities. Incomplete removal of the template cells from their binding cavities will lead to a decrease in the number of available binding sites for rebinding, thereby lowering the binding capacity of the SIP.

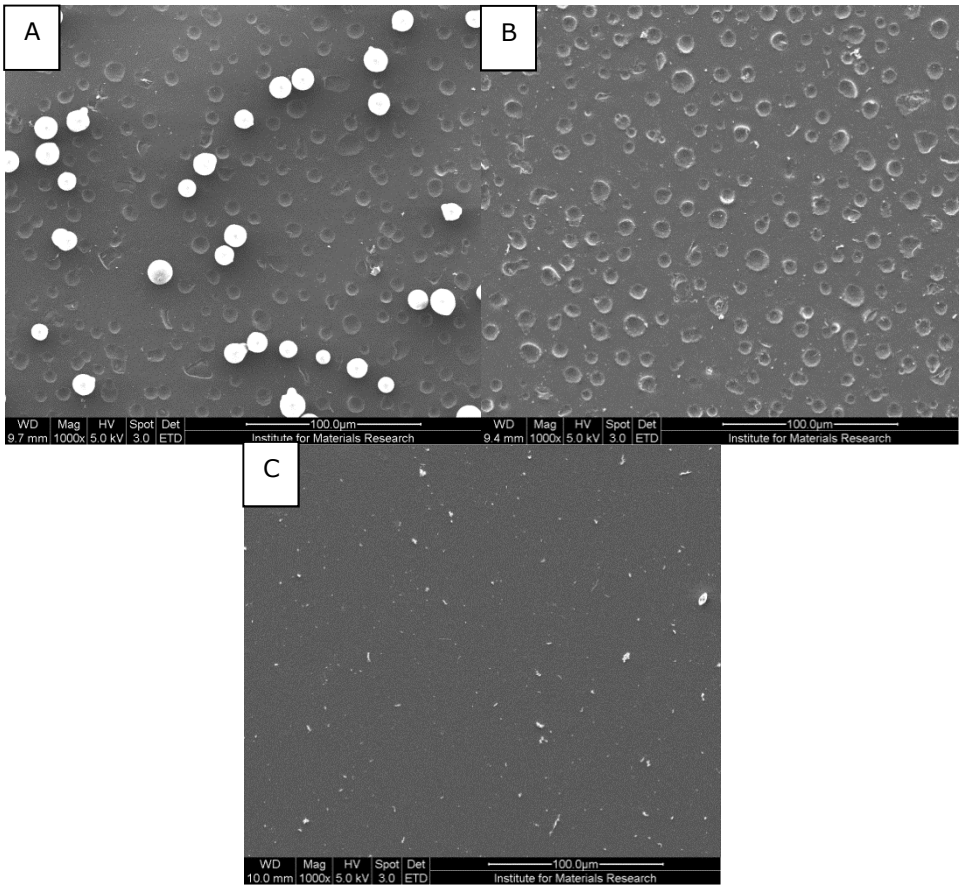

Figure 2.4: SEM analysis of polyurethane layers at 1000 times magnification. Removal of the stamp and mildly rinsing the layer with water results in incomplete removal of the silica beads from the microcavities (a). More thorough rinsing with hot water completely removes the beads, resulting in a patterned SIP surface (b). This patterning of the surface is not visible when analyzing a non-imprinted polyurethane layer (c).

2.3.2. Morphological analysis of cell-imprinted SIP layers

Polyurethane layers made for the different biological cells described in Chapter 2.2 are analyzed using an optical inverted microscope; the results are summarized in **figure 2.5**. It is clear that the size and shape of the template cells can be transferred to the SIP layer reliably. After removal of the stamp, the layer is rinsed with 0.1% sodiumdodecylsulphate (SDS) solution and PBS in order to ensure full removal off the cells [69, 70], leading to a pattern of densely packed microcavities on the surface of the SIP.

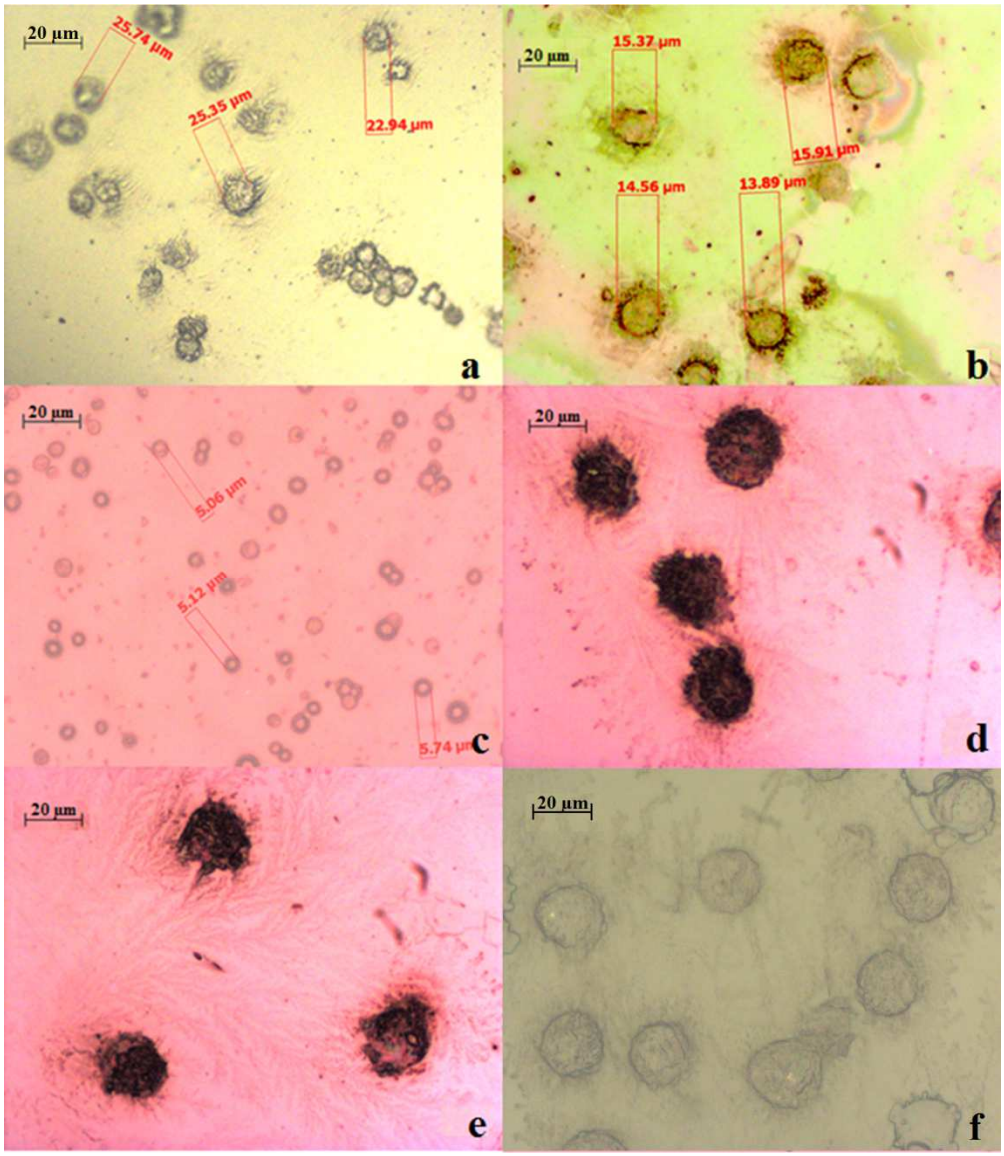

Figure 2.5: Optical analysis of polyurethane-covered substrates using an inverted microscope. SIPs are imprinted with NR8383 cells (a), RAW 264.7 cells (b), *S. cerevisiae* (c), Jurkat cells (d), peripheral blood mononuclear cells (PBMCs) (e) and the breast-cancer cell line MCF-7 (f).

2.3.3. Topographical analysis of a MCF-7 SIP

An atomic force microscopy analysis of a single imprint for an MCF-7 breast cancer cell is shown in **figure 2.6**. The 3D image shows the topography of the sample, the imprint displays a spherical shape, comparable to the dimensions of the template cell. The surrounding surface is relatively smooth as compared to the imprint. In addition a depth profile was made along the cross-section of the imprint (red line in figure 22). This profile clearly shows that the imprints are relatively shallow (depths up to 600 nm) in comparison to the dimensions of the template cell (20 µm). These values correspond well to the dimensions obtained in literature with other template cells [69, 70]. The relatively small depth of the imprint can be considered crucial to the selectivity of the synthetic receptor. It ensures that analogue cell types comparable in size and shape to the template cells do not rebind to the SIP. They might fall into the imprint but will easily diffuse out of the pit again. Only cells that display full complementarity to the imprint in size and shape as well as in the distribution of functional groups on their membrane will form a strong bond to the SIP (key-and-lock principle).

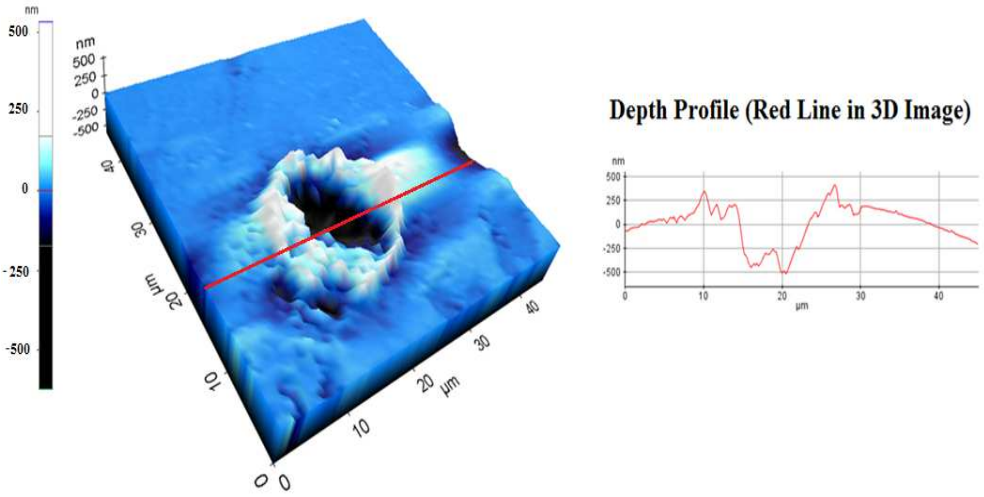

Figure 2.6: AFM-analysis on a single MCF-7 imprint shown as a 3D representation. The cross sectional depth profile of the same imprint shows the topography along the red line on the 3D figure.

2.3.4. Layer thickness analysis by profilometry

The layer thickness was analyzed by profilometry as described in section 2.10. Five different non-imprinted polyurethane-covered samples are analyzed on three different spots of the sample, an average layer thickness for each sample and a total average are calculated. All values are given in micrometer and the resulting average values are round to two decimal places. The results are summarized in **Table 2.1**.

Table 2.1: Measurement of the average layer thickness of NIP layers. The thickness is measured on three different spots of 5 different samples using a Dektak profilometer. These values are used to calculate the average layer thickness. All values are given in micrometer and rounded to two decimals.

	Spot 1	Spot 2	Spot 3	Average	Stdev
Sample 1	1.1	1.2	1.1	1.1	0.1
Sample 2	1.2	1.3	1.1	1.2	0.1
Sample 3	1.3	1.2	1	1.2	0.2
Sample 4	1.3	1.2	1.2	1.2	0.1
Sample 5	1.2	1.3	1.1	1.2	0.1
Total				1.2 µm	0.1 µm

2.3.5. Calculation of SIP surface coverage

The areal density of microcavities was analyzed for different SIPs. Optical microscopy images were analyzed using the image processing software ImageJ to determine the number of imprints per cm^2 on 5 different spots on a single sample, each spot had a surface area of 2.26 mm^2. These values were used to calculate the average areal density of imprints on each sample. For each template cell type, at least 3 samples were analyzed in this manner in order to calculate an average surface coverage for each SIP. The results of this analysis are summarized in **Table 2.2**. From these data it becomes apparent that there is some difference between SIPs made for different templates. These examples

can be explained by differences in size as well as in adherence behavior of different cell types.

Table 2.2: Areal density of microcavities on the surface of SIP layers imprinted for various cell types. For each target the average coverage was based on analysis of 5 different spots on at least 3 different samples.

Imprint	Average Coverage (cavities/cm^2)
NR8383	7900 ± 400
RAW 264.7	21700 ± 8800
S. cerevisiae	183200 ± 54200
MCF-7	24800 ± 3500
Jurkat	22600 ± 2800
PBMC	16400 ± 2900

2.4. Conclusion

Optimizing the synthesis protocol has led to firm, uniform polyurethane layers with an average thickness of 1.2 ± 0.1 µm. The results in this chapter show that it is possible to imprint these layers with silica beads as well as biological cells in order to create a pattern of microcavities on the surface of the polyurethane layer. The morphology of the cells is transferred to the imprints by stamping the cells into the semi-cured, flexible polyurethane layer. Additionally, during cross-linking of the polyurethane, functional groups on the membrane of the template cells interact with the forming polymer in a non-covalent manner. This process ensures a functional complementarity between target and imprint in addition to a morphological match [69]. Therefore, the shallowness of the cavities (600 nm) is a key element that ensures selectivity of the SIP, since only cells that are fully complementary to the SIP will rebind to the surface in a specific manner. This way, the surface-imprinted polyurethane will function as the biomimetic receptor layer ensuring that our sensor set-up is able to bind and identify cells in a specific and selective manner. This rebinding will be analyzed by means of a novel detection platform, the so-called heat-transfer method (HTM).

3. Selective detection of rodent macrophages: a proof-of-concept

3.1. Introduction

The rebinding of target cells to the SIP is detected by the set-up described in Chapter 2.3 of the thesis. In order to prove the concept SIP layers were synthesized with three cell types. NR8383 cells (rat alveolar macrophages), RAW 264.7 cells (mouse leukemic monocyte macrophages) and yeast cells (*S. cerevisiae*). Rebinding to these SIPs was tested in order to test the specificity, sensitivity and selectivity of the device. The rodent macrophage cells were used as a model for human macrophages, because they are more readily available, cheaper and easy to culture in comparison to their human counterparts. Macrophages play a major role in the development of atherosclerosis as explained previously [82-84]. However, elevated concentrations of blood macrophages and phenotypical changes of these macrophages are also correlated with other diseases. They also play a role in Human Immunodeficiency Virus (HIV) infection. Macrophages can become infected with the virus and become a reservoir for virus replication throughout the body [105]. Recently it was shown that this infection can change the phenotype of the residing macrophages [106]. Transfer of viral proteins such as Nef will influence the immune system in such a way that virus particles can escape detection and removal [107], this process is shown in **figure 3.1**.

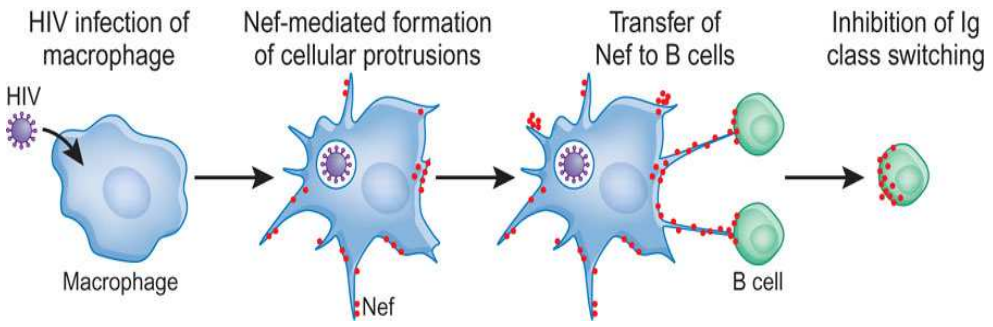

Figure 3.1: HIV infection of macrophage leads to inhibition of the immune system (www.nature.com)

Elevated levels of macrophages also contribute to tumor growth and progression by promoting chronic inflammation. Inflammatory compounds can increase the production of proteins that stop apoptosis by tumor cells, thereby helping these cells to escape from programmed cell death [108]. In addition these compounds can stimulate cell proliferation and angiogenesis contributing to further tumor growth [109]. An increase in the number of macrophages has shown to contribute to a poor prognosis in breast, cervix, bladder and brain cancer [110]. Furthermore, a change in phenotype (the so-called M2 phenotype) is observed in tumor-associated macrophages [111]. Therefore, a biosensor platform that is able to detect an elevated concentration and/or a phenotypical switch of blood macrophages will be of great interest to the medical community. Yeast cells were used for imprinting for historical reasons, as in previous work it was shown that these cells are easy to imprint [69].

3.2. Materials & Methods

3.2.1. General measurement scheme

In order to test the device and to achieve a proof-of-principle, SIPs were created for three different cell types (NR8383, RAW 264.7 and *S. cerevisiae*) as explained in Chapter 2.1.2. Details about the cell culture and imprinting procedures can be found in Chapters 2.1 and 2.2 of the thesis. The SIP covered aluminum chips were placed in the set-up as described in chapter 2.3. Throughout the whole measurement T_1 is kept at 37.00°C. In a first phase of the measurement the flow cell above the sensor surface is filled with PBS and T_2 is allowed to stabilize. Next, cell suspensions in PBS ($1\times10^6 \pm 2.10^5$ cells/ml, determined by cell counting) are manually injected into the flow cell. After the signal stabilizes again, the flow cell is flushed with 0.1% SDS solution and PBS in order to remove the cells from the imprints and re-establish the surface in its original state.

3.2.2. Derivation of time-dependent thermal resistance from time-dependent temperature data

The measurement protocol described in the previous chapter will result in a time-dependent data set for T_1 and T_2. However, since the solutions are injected at room temperature a dip in T_2 is encountered after every addition of liquid to

the flow cell. To avoid over-compensation by the device for this effect, it is more useful to analyze the time-dependence of the thermal resistance. As described earlier, the thermal resistance (R_{th}) can be calculated at any given moment in the time from the temperature data and the heating power P, needed to keep the copper block at 37°C, by the following formula: $R_{th} = (T_1 - T_2)/P$ [102, 103]. The heating power P, can be calculated via $P = V^2/R$ with V the voltage over and R the electrical resistance of the heating element (22 Ohm). The concept of the derivation of the time-dependence of the thermal resistance from the time-dependent temperature data and the power is illustrated in the example shown in **figure 3.2**.

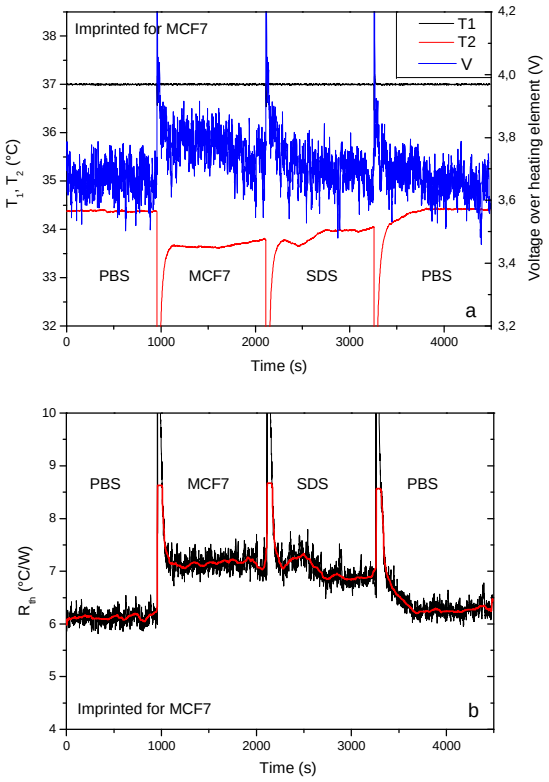

Figure 3.2: Raw data collected during the binding of MCF-7 cells to a MCF-7-imprinted polyurethane layer with subsequent rinsing steps with SDS and cell-free PBS buffer. T_1 (black line), T_2 (red line) and V (blue line) are shown (a). Time dependence of the heat-transfer resistance R_{th}, which is derived from the temperature difference and the heating power according to the formula $R_{th} = (T_1 - T_2)/P$. The red line was calculated with a percentile filter set at 50% with a window of 50 data points (b).

3.2.3. Specificity assessment and in-depth analysis of R_{th}

In a first phase of the research the theoretical model proposed in figure 2.3 is tested by some experiments involving NR8383 cells. In order to assess whether the rebinding of target cells to the SIP leads to a measurable change in T_2 and R_{th} an aluminum chip covered by a polyurethane layer, imprinted for NR8383 cells is exposed to a solution of target cells. The experiment is conducted following the general scheme as described in chapter 4.2.1 and T_2 and R_{th} are monitored in time. These data are compared to the data obtained by conducting the same experiment using a chip covered by a non-imprinted polyurethane layer. This way, one is able to distinguish effects arising from specific binding of cells to the SIP from effects caused by non-specific adsorption of cells onto the surface of the polymer. In addition, data sets of a yeast-addition experiment for a SIP and a NIP are compared to the data obtained when conducting the same experiment on a blank aluminum chip. This allows to further analyze the effect of imprinting on the thermal resistance and to support the model in figure 2.3 with a more in-depth theory supported by experimental evidence.

3.2.4. Cross-selectivity test

The platform is tested by conducting the experiments as described in chapter 4.2.1 for SIPs imprinted for NR8383 cells, RAW 264.7 and yeast cells (*S. Cerevisiae*) and by analyzing their response to each of the cell types. The cell types used differ in size with but all display a spherical shape and can therefore be used to assess selectivity of the platform. Additionally, NIPs were tested for their response to each target.

To ensure that recognition of cells is not only based on complementarity in size but is also assisted by weak chemical bonds, SIPs were imprinted with inorganic silica beads as described in chapter 2. These beads lack surface functionalities that are able to interact with the forming polymer. Therefore, any measurable change upon addition of these beads to the flow cell containing its SIP will be based on a full morphological complementarity without any chemical complementarity.

3.2.5. Sensitivity and reusability test

In order to test if it was possible to regenerate the sensor surface by flushing the flow cell with 0.1% SDS and PBS, a SIP imprinted for RAW cells was tested during two subsequent addition runs using a RAW cell solution in PBS (concentration 1×10^6 cells/ml). Each run was conducted as described in section 3.2.1 and the thermal resistance was analyzed in time.

The reusability of the system was further tested by a repeated sensitivity test. In this experiment a stock solution of NR8383 cells was diluted 100-, 50-, 20-, 10-, 5- and 2-times. In order to construct a dose-response curve, a SIP imprinted for NR8383 cells was exposed to each of the solutions in the dilution series. In between addition runs, the flow cell was flushed manually with SDS solution and PBS buffer to ensure full removal of the cells from the imprints. A detection limit, a saturation limit and a dynamic range could be determined from these experiments.

3.3. Results

3.3.1. Specificity assessment of the sensor

The results shows in **figure 3.3** were obtained by exposing a sample imprinted for NR8383 cells to a solution of target cells in PBS with a concentration of 1×10^6 cells/ml (3 ml liquid volume) after stabilization in PBS (pH 7.4). The cells were manually injected into the flow cell and after the stabilization of the signal the flow cell was manually flushed with 3ml of 0.1 % SDS. Finally, the flow cell was flushed with PBS buffer in order to re-establish the conditions prior to exposure of the sample to the target cells. The data shown are raw, unfiltered data and the noise level is induced by short-term fluctuations of the heating power P. The red line is a gentile percentile filter (50 data points), that was applied as a guide for the eye.

Looking at the time-dependence of the R_{th} it can be concluded that in the initial state, the thermal resistance is stable at R_{th} = 5.9 ± 0.2 °C/W. The R_{th} rises to a new equilibrium at 7.0 ± 0.2 °C/W upon addition of the target cells. This corresponds to an R_{th} increase by 20%, being substantially higher than the noise level on the signal (4%). The overshooting of the R_{th} signal upon flushing in the cell solution (originally at ambient temperature) is a temporary effect and

vanishes as soon as the temperature distribution is again under equilibrium conditions. After flushing the flow cell with 0.1% SDS, the R_{th} remains at an almost constant level as the damaged membrane fragments remain bound to the binding cavities. Finally, the R_{th} comes back to its initial value of 6 °C/W after rinsing the liquid compartment with PBS buffer.

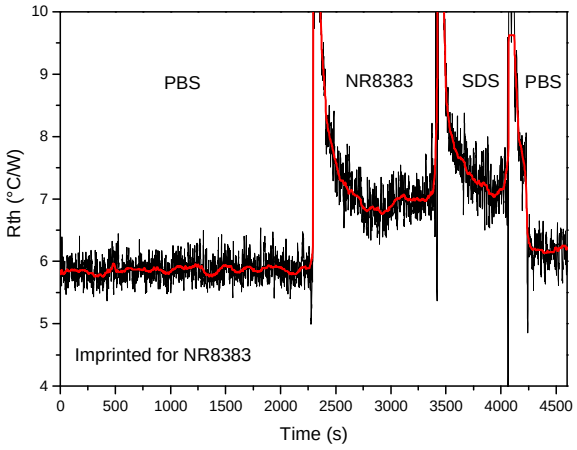

Figure 3.3: Time dependence of the thermal resistance (Rth) during an addition experiment with NR8383 cells on a SIP that was imprinted for these cells. The black line presents the raw data; the red line was obtained with a 50 data-points percentile filter.

In order to assess whether the rise in R_{th} shown in figure 3.3 was caused by specific binding of the cells to the microcavities of the SIP, the experiment was repeated on a chip coated with a non-imprinted polymer layer (**figure 3.4**). The increase in thermal resistance upon addition of the cells is not present in the data obtained from this experiment. This implies that the rise in thermal resistance seen in figure 3.3 is not caused by non-specific adsorption of the cells to the surface of the chip but can be attributed to the target cells binding to the microcavities on the SIP surface. Furthermore, the effect of an enhanced thermal conductivity as seen in 'nanofluids' [112] does not seem to play a role when exposing the surface to a fluid containing microparticles, as the R_{th} remains constant upon addition of the cell suspension to the flow cell. In addition, a medium change from PBS to SDS does not seem to have any effect on R_{th}.

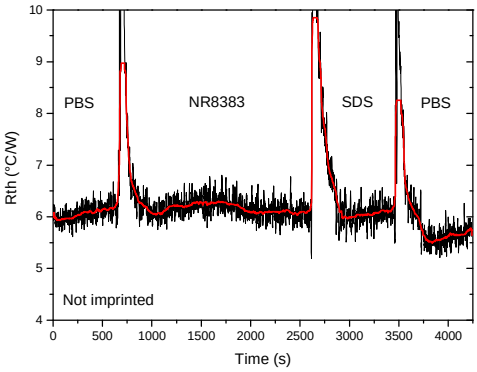

Figure 3.4: Time dependence of the thermal resistance (R_{th}) obtained by performing an addition experiment with NR8383 cells, on a non-imprinted polymer.

The model proposed in figure 2.3 seems to be valid according to these results. Binding of the cells blocks the heat-transfer through the microcavities, thereby increasing the thermal resistance of the SIP layer. The mechanical force of manually flushing the flow cell is insufficient to remove the cells from their binding cavities as can be concluded from the fact that R_{th} remains at an elvated level after rinsing with 0.1% SDS solution. However, incubation of the sample in SDS will cause the membranes of the bound cells to become permeable, making the cells more susceptible for removal by mechanical friction. This concept is proven by the fact that the thermal resistance returns back to the baseline value upon flushing of the liquid compartment with PBS (**figure 3.5**).

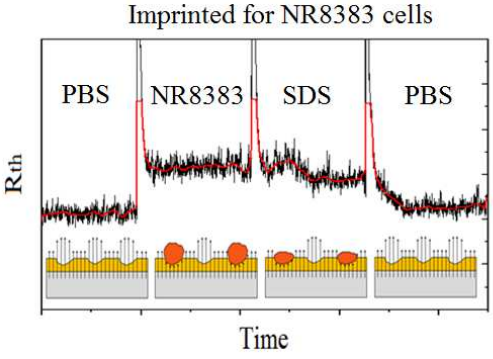

Figure 3.5: Schematic explanation of the effect of cell-rebinding on R_{th}. Initially the imprints form preferential heat channels due to the thinner thermal insulating layer. Binding of cells to the imprints increases the thermal insulating layer, thereby blocking the preferable heat channels and forcing the heat to transfer along the thicker membrane..

3.3.2. In-depth analysis of thermal resistance

In order to further explain the concept behind thermal resistance measurements for the specific detection of cells, an addition experiment was performed on a yeast-imprinted SIP analogous to the experiment described in section 4.3.1 for NR8383 cells. The filtered thermal resistance data of this experiment were compared to the data obtained when repeating the experiment for a non-imprinted polymer-coated chip and a blank aluminum chip as shown in **figure 3.6.**

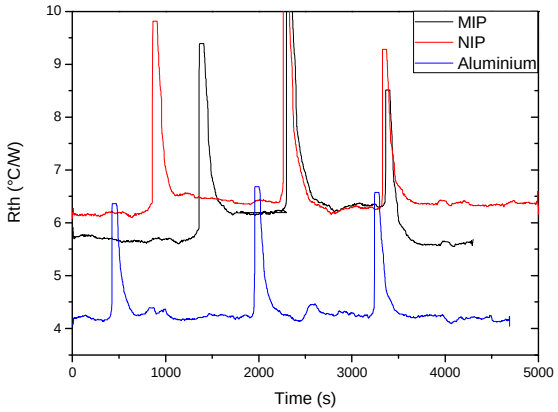

Figure 3.6: Comparison of filtered (50-points percentile filter) R_{th} data obtained with a blank aluminum substrate (blue curve), a non-imprinted polyurethane layer (red curve, 'NIP'), and a polyurethane layer with yeast-cell imprints (black curve, 'SIP'). The figure illustrates that the sensor base line is different for the three types of chips.

From the time-dependent thermal resistance data it can be obtained that a blank aluminum chip has a much lower baseline R_{th} (4.2 °C/W) in comparison to the same chip after coating with a 1 µm thick polyurethane layer (6.1 °C/W). Imprinting the SIP with yeast cells causes a slight decrease in the baseline thermal resistance (5.7 °C/W). The R_{th} contribution of the polyurethane depends on the precise layer thickness, but imprinted chips tend to have a slightly lower R_{th} as compared to their non-imprinted counterparts. This can partly be attributed to their larger surface area, an effect which is known *e.g.* from cooling fins. However, we will show now that imprinting causes an intrinsic decrease of R_{th}, irrespective of the enlargement of the surface. For these considerations we will focus strictly on heat flow along the vertical direction. Furthermore, we assume that polyurethane layers have a thickness d_0 = 1.00 µm and the

polymer layer underneath the imprints has a thickness d_2 = 500 nm (compare figure 22 to **figure 3.7** below). Due to the limited reproducibility of the spin-coating process, there might be deviations of ± 0.1 µm as compared to the idealized layer thickness of 1.00 µm, as described earlier.

First, the non-imprinted polyurethane layers cause an increase of R_{th} by ΔR_{th} = 1.90 °C/W as compared to the blank chips. The contact area between the chip and the liquid compartment has a size A_0 = 28 mm^2 and this allows calculating the thermal conductivity λ of the polyurethane layer:

$$\lambda = \frac{1}{\Delta R_{th}} \cdot \frac{d_0}{A_0} = 1.9 \cdot 10^{-2} \frac{W}{°C \cdot m}$$

Although our calculation is an approximation of λ due to small amounts of heat loss, the calculated numerical value of λ agrees well with literature data on polyurethane foam [113] and is roughly 25 times lower than values for high-density polymers. The areal density of yeast imprints is $2 \cdot 10^5$ cm^{-2} and, with a diameter of approximately 5 µm, each imprint occupies a surface area of $1.96 \cdot 10^{-11}$ m^2. Therefore, the total area of imprints within the contact area of 28 mm^2 corresponds to A_2 = 1.1 mm^2 while the remaining A_1 = 26.9 mm^2 is the non-imprinted surface fraction. For simplicity, we assume that the imprints have a muffin-tin shape with a uniform depth. During the imprinting process, the volume of the polyurethane layer has to be conserved, and this allows calculating the resulting layer thickness d_1 in the regions outside the imprinted cavities:

$$A_0 \cdot d_0 = A_1 \cdot d_1 + A_2 \cdot d_2 \quad \Rightarrow \quad d_1 = 1.02 \mu m$$

With this information, we can calculate the thermal conductance S_{th} of the imprinted polyurethane layer and the associated change of the thermal resistance Δ R_{th}:

$$S_{th} = \lambda \cdot \left\{ \frac{A_1}{d_1} + \frac{A_2}{d_2} \right\} = 0.543 \frac{W}{°C} \quad \Rightarrow \quad \Delta R_{th} = \frac{1}{S_{th}} = 1.84 °C/W$$

Hence, already a moderate coverage of the surface with imprints will decrease the heat-transfer resistance of the device as compared to the 1.90 °C/W obtained with the non-imprinted, blank polyurethane layer. Suppose now that half of the active surface would be covered with imprints: With A_1 = A_2 = 14 mm^2, d_1 = 500 nm and d_2 = 1,500 nm we fulfill the volume conservation and obtain ΔR_{th} = 1.41 °C/W. In this sense, a larger number of cell imprints per unit area is not only beneficial because more target cells can be bound, but it will also decrease the offset R_{th} value of the sensor setup prior to binding target cells from solution.

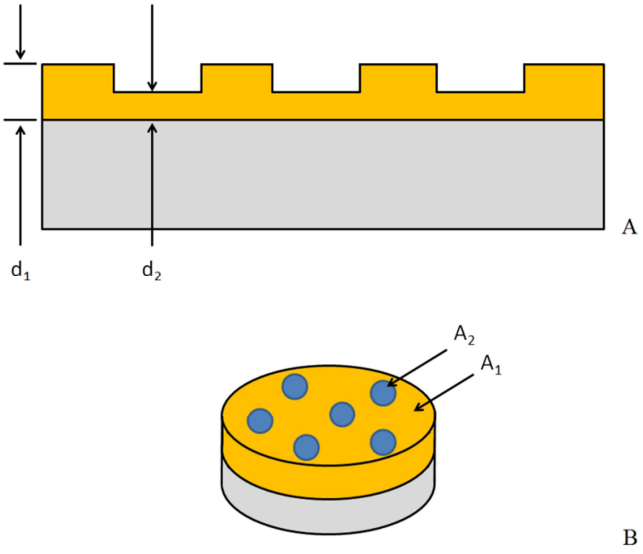

Figure 3.7: Illustration of a muffin-tin model for calculating the heat-transfer resistance of a cell-imprinted polymer layer in cross section (a) and perspective view (b). The non-imprinted region has a total area size A_1 and a layer thickness d_1. The imprints cover together an area A_2 and the remaining polymer thickness underneath the imprints is given by d_2.

3.3.3. Cross-selectivity test

To assess whether it is possible to distinguish between macrophages cells from different rodent species, SIPs imprinted for NR8383 cells and RAW cells were tested for cross selectivity. The time-dependence of the thermal resistance during these measurements is shown in **figure 3.8**.

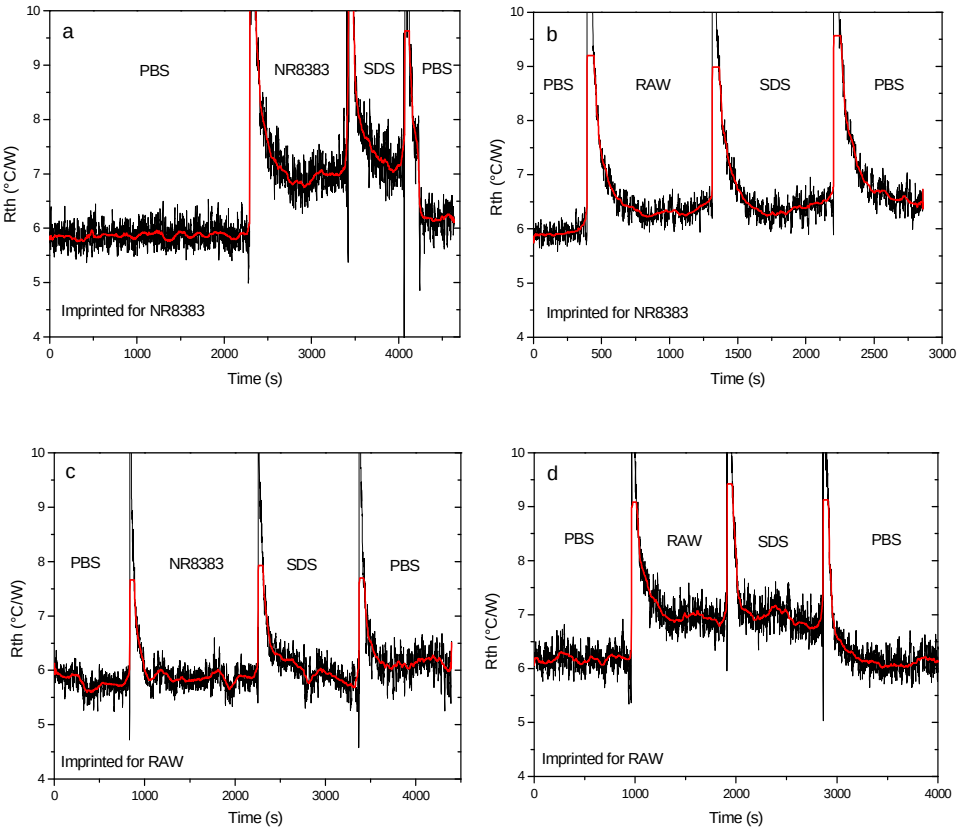

Figure 3.8: Macrophage detection in a cross-selectivity experiment. The set-up was used to selectively discriminate between rat- (NR8383) and mouse (RAW 264.7) macrophage cell lines. The measurements were performed as described in figure 3.3. (a) Time dependence of the thermal resistance for a SIP imprinted with NR8383 cells using NR8383 as target cells. (b) Time-dependent R_{th} response for the NR8383 SIP when exposed to RAW 264.7 cells. (c) Time-dependent R_{th} signal of a SIP imprinted for RAW 264.7 cells upon exposure to NR8383 cells. (d) Recognition of RAW 264.7 cells with a RAW 264.7-imprinted SIP layer.

The measurements summarized in figure 3.8 were performed analogous to the experiment described in Chapter 4.2.1. As described earlier, a typical increase of 1.2 °C/W is encountered upon addition of NR8383 cells to the liquid compartment above a NR8383 SIP-covered chip (figure 30a). Exposing an NR8383-imprinted layer to a RAW-cell suspension (figure 30b) shows no specific response, except for a minor signal drift from 5.9 to 6.2 °C/W. Also, when RAW-imprinted layers are exposed to a NR8383 suspension (figure 30c) cross-selectivity effects remain below the experimental resolution. However, the RAW-SIPs do bind RAW cells as seen in Figure 30d and the corresponding change of R_{th} (≈ 14%) is comparable to the recognition of NR8383 cells by NR8383-imprinted layers (figure 30a). The absolute and relative (calculated as the response in R_{th} divided by the baseline R_{th} value before addition of the cells, this number is multiplied by 100 to obtain a percentual response) R_{th} changes as compared to the starting conditions are summarized in **Table 3.1**.

Regarding the experiments with yeast-cells (**figure 3.9**), we can state that yeast cells bind exclusively to yeast imprints (figure 3.9a) and neither to NR8383- (figure 3.9b) nor to RAW imprints (figure 3.9c). *Vice versa*, these cell types show no sticking to yeast-imprinted layers as expected (figure 3.9d and 3.9e). All the data shown are included in Table 3.1. We note that the R_{th} change of 10% when binding yeast to yeast imprints is lower than in case of macrophages despite of the fact that the yeast imprints are especially numerous with more than 100,000 per cm^2 while the concentration of target cells was identical. We relate the moderate R_{th} increase to the small dimensions of these cells (5 µm), covering a smaller lateral area after binding, and being less extended along the heat-flow direction, thus corresponding to a less efficient thermal insulator.

Reference experiments with a non-imprinted PU layer gave for NR8383-, RAW as well as for yeast cells, an R_{th} change in the order of 1%, indicating that there is no relevant sticking effect of cells to non-imprinted (blank) polyurethane. This holds also when a blank layer is exposed to yeast cells. The data of these experiments are summarized and included in Table 3.1.

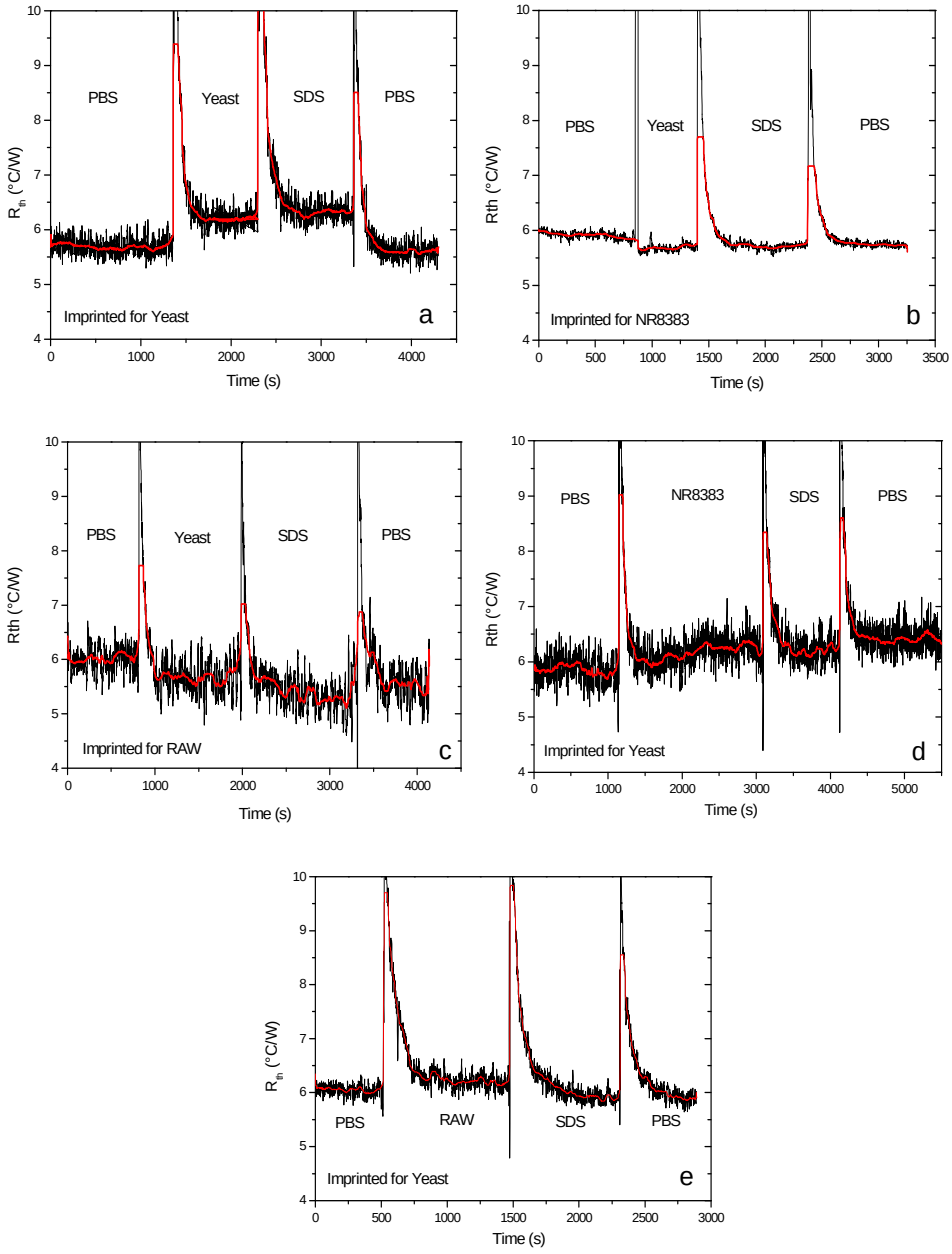

Figure 3.9: Time-dependent Rth data for an addition experiment with yeast cells on (a) a yeast SIP, (b) a NR8383 SIP and (c) a RAW SIP. In addition, Rth data for an addition experiment with (d) NR8383 and (e) RAW cells on a yeast SIP are shown.

Table 3.1: Absolute- and relative sensor response of NR8383-, RAW 264.7-, and yeast SIPs. The strongest response is encountered when template- and target are identical as highlighted on the diagonal of the matrix. As compared to these 'specific' responses, the cross reactions between non-complementary imprint- and cell types are insignificant. Response data for a blank polymer layer, corresponding to a zero-effect within error bars, are given for comparison (grey-shaded fields).

Target **Concentration**	NR8383 $1{\cdot}10^6 \pm 8{\cdot}10^4$ cells/ml		RAW 264.7 $1{\cdot}10^6 \pm 9{\cdot}10^4$ cells/ml		*S. cerevisiae* $1{\cdot}10^6 \pm 9{\cdot}10^4$ cells/ml	
	ΔRth (°C/W)	% response	ΔRth (°C/W)	% response	ΔRth (°C/W)	% response
Imprint: NR8383 7,900±440 cavities/cm^2	1.14 ± 0.2	19.5 ± 3.5	-0.18 ± 0,1	-2.8 ± 2	-0.18 ± 0.04	-3.1 ± 0.7
Imprint: RAW 264.7 21,650±8,760 cavities/cm^2	0.10 ± 0.2	1.79 ± 2,8	0.85 ± 0.2	13.9 ± 3.2	0.14 ± 0.2	2.4 ± 5.4
Imprint: *Sacch. Ceriv.* 183,220±54,230 cavities/cm^2	0.01 ± 0.2	0.19 ±3.1	0.14 ± 0.1	2.29 ± 2.1	0.55 ± 0,1	9.65 ± 2.6
Blank = non imprinted	0.04 ± 0.1	0.7 ± 2.3	0.05 ± 0.2	0.84 ± 2.8	0.14 ± 0.1	2.32 ± 2.0

The results in Table 3 clearly show that it is possible to discriminate between mouse and rat macrophage cells with little or no cross-selectivity observed. However, since these cells do not only differ in the distribution of functional groups on their membrane but also in size, a recognition experiment was also performed with silica beads and their corresponding imprints. The results of this experiment are shown in **figure 3.10**. The behavior of silica is different from that of the macrophages and yeast cells, used in previous experiments. Addition of silica beads leads to an increase in of the signal by 2.3 %, which falls within the noise of the system (3.3%). Furthermore, SDS rinsing removes the beads and the R_{th} value recovers instantly to the sensor baseline. Hence, we conclude that the recognition of cells involves indeed the formation of weak chemical bonds in addition to geometrical matching [71].

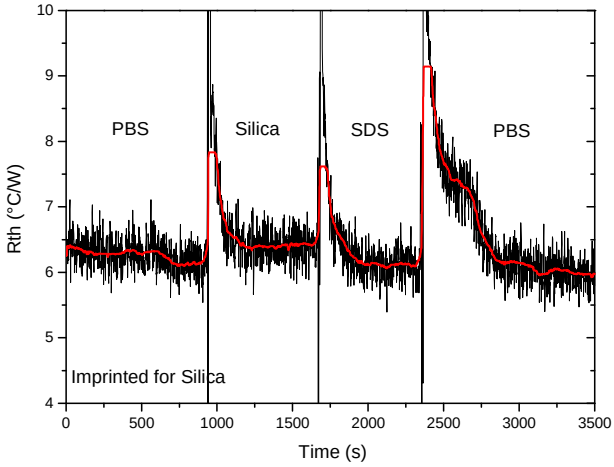

Figure 3.10: Time-dependent thermal resistance data obtained by an addition experiment using a SIP imprinted for silica beads. The experiment is conducted analogous to previously described experiments on biological cells.

3.3.4. Reusability test

An important parameter in the development of a biosensor is the ability to reuse the platform after a measurement is done. To investigate if this is possible for our set-up, a SIP imprinted for RAW 264.7 cells was exposed to two consecutive addition experiments with target cells. The results are shown in **figure 3.11**. In the first run of the addition experiment, the R_{th} stabilizes at 6.1 ± 0.2 °C/W after incubation in PBS. An increase in R_{th} is observed upon addition of RAW cells to the liquid compartment. The R_{th} finally stabilizes at 6.9 ± 0.2 °C/W, this increase in signal by 13.1 ± 4.2 % corresponds well with the values obtained in previous experiments, summarized in Table 3.1. After rinsing the flow cell with SDS and PBS, the signal returns to the baseline R_{th}. The consecutive addition run shows the same behaviour. Addition of the cells leads to a comparable increase in R_{th} (13.0 ± 3.7 %) and the signal returns back to baseline after flushing with SDS and PBS. These results indicate that the sensor surface can be regenerated and the microcavities are once more available for rebinding of the target cell after removal of bound cells from the surface.

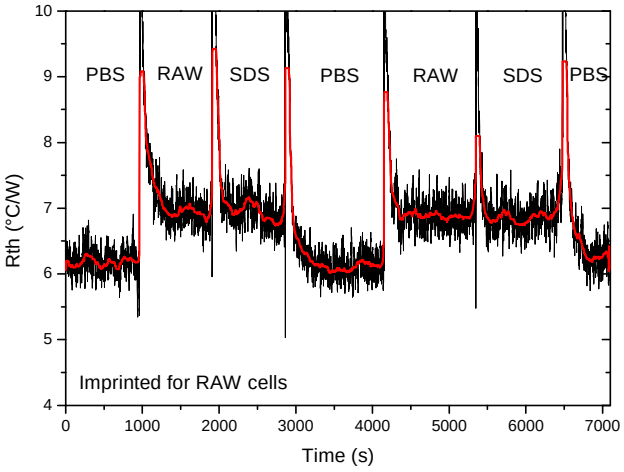

Figure 3.11: Repeatability experiment performed with a SIP imprinted for RAW 264.7 cells. After a first addition of target cells, the recognition signal turns back to the baseline by flushing the liquid compartment of the sensor setup with SDS- and PBS buffer. In a second run, the signal rises to the same level as during the first addition of cells. Flushing the liquid compartment with SDS and PBS returns the signal again back to baseline, proving that the sensor is reusable.

3.3.5. Sensitivity test: dose-response curve

These experiments clearly demonstrate that the sensor is able to detect cells in a specific, selective and reproducible manner. Another important parameter for a biosensor is its sensitivity. In order to determine the limit-of-detection of the sensor concept, the response of a SIP imprinted for NR8383 cells was analyzed under exposure to a dilution series of NR8383 cells in PBS buffer, see also chapter 4.2.5. The work flow during each addition run of the experiment was identical to the experiments described previously: the sensor was stabilized in PBS before manually injecting the cells into the flow cell of the device. Between each addition run the sensor surface is regenerated by flushing the flow cell with SDS solution and PBS buffer. The time dependence of T_1 and T_2 and the change of the heat-transfer resistance R_{th} are summarized in **figure 3.12**a and b respectively. These data clearly show that the response of the sensor can be quantified and that the sensor surface can be regenerated during at least six consecutive addition runs.

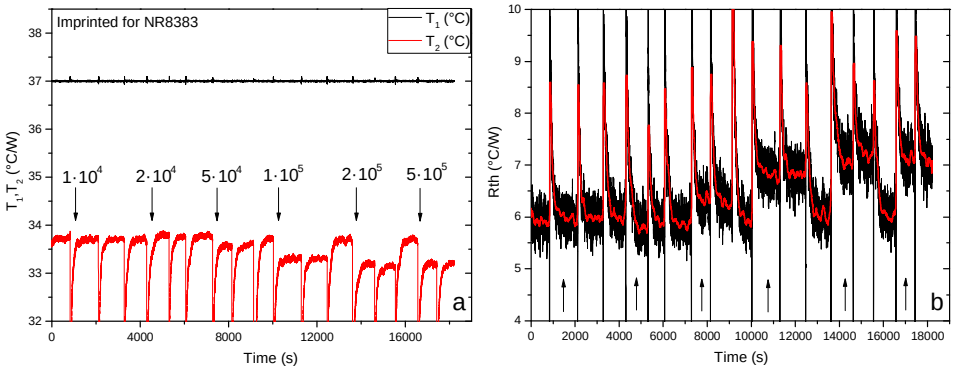

Figure 3.12: Dose-response experiment performed on a SIP imprinted with NR8383 cells. This experiment was done by exposing the SIP to an increasing concentration of target cells. (a) Time dependent temperature response. Each arrow indicates an addition of cells, the value above the arrows is the concentration added in cells/ml. (b) Stepwise increase of the heat-transfer resistance R_{th} as a function of time.

The results in figure 3.12 were used to construct the dose-response cure shown in **figure 3.13**. The error bars were taken from the standard deviations of the non-filtered data shown in figure 3.10b. The data shown clearly indicate that the sensor signal saturates at concentrations above 200,000 cells/ml.

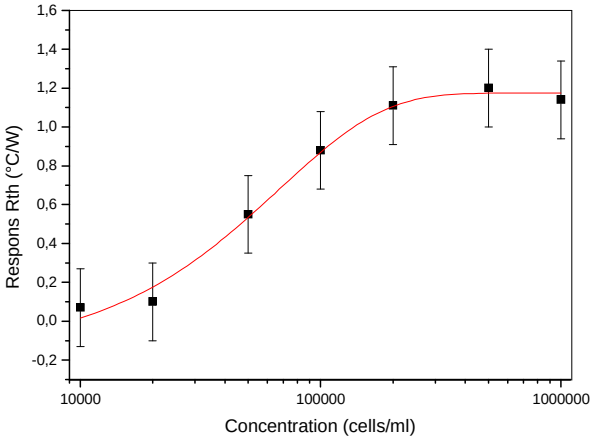

Figure 3.13: Dose-response curve: response in R_{th} as a function of the added target-cell concentration (logarithmic axis). An exponential fit is drawn trough the obtained data with an R^2-square value of 0.988 (red line).

The dose-response curve nicely follows an empirical, exponential fit function according to the formula:

$$\Delta R_{th}(c) = A - B \cdot \exp\{-c / C\}$$

Here, c is the concentration in cells per ml and the fit parameters have the numerical values A = 1.17 °C/W, B = 1.34 °C/W, and C = 67,500 cells/ml. The coefficient of determination R^2 = 0.988, indicating the excellent agreement with measured data. Assume that the accuracy in determining R_{th} changes is 0.2 °C/W (according to our conservative estimate for the error-bar widths), the first meaningful data are expected for concentrations around 30,000 cells/ml.

3.4. Conclusion

The sensor has been shown to be able to discriminate between three different cell types in a specific and selective manner due to the use of a synthetic receptor. Furthermore, it has been proven that the results can be quantified and the rebinding capacities of the sensor surface can be regenerated by flushing the set-up with SDS and PBS, making our sensor reusable. Experiments using silica beads indicate that a geometrical complementarity between target and receptor is insufficient but a match in chemical functionalities is also required to ensure reliable rebinding of the cell to the sensor surface.

As an explanation for the R_{th} increase upon binding of cells in the imprinted cavities, we propose the local blocking of heat transfer from the polyurethane layer to the liquid compartment: the total surface fraction covered with imprint-bound cells is below 10%, but the cell diameter of typically 10 – 20 µm exceeds the 1 µm thickness of the PU layers by a decade. Therefore, it is reasonable that the R_{th} change upon cell recognition (typically 1 °C/W) is similar to the R_{th} change observed when covering the blank aluminum with polyurethane (R_{th} change of 2 °C/W). We point out that the (reversible) R_{th} step upon cell recognition is persistent and not fading away over time. This is intrinsically different from calorimetric biosensors that are measuring the transient thermal energy associated with the binding of target entities by receptors [114].

In conclusion, the experiments conducted in this chapter provide an excellent proof-of-principle, indicating that the platform can indeed be used to selectively

detect and identify cells. However, although selective detection of human macrophages might be interesting in atherosclerosis research, the rodent macrophages used during these experiments differ in size and shape as well as in the distribution of chemical functionalities displayed on their membrane. Therefore, experiments using cells from the same species that are morphologically and functionally similar should be used to further assess the selectivity of the device. By using medically more relevant cell species an attempt is made to achieve a proof-of-application in the next chapter.

4. Identification and detection of human cancer cells in buffer: a proof-of-application

4.1. Introduction

The experiments conducted in the previous chapter indicate that our set-up is able to discriminate between widely similar mammalian cells. In this chapter, the selectivity of the sensor is tested further in order to achieve a proof-of-application. Therefore SIPs were imprinted with a breast cancer cell line (MCF-7 cells), an immortalized cell line of leukemic T lymphocytes (Jurkat cells) and peripheral blood mononuclear cells (PBMC's), a mixture of T- and B-lymphocytes, monocytes, and macrophages from a healthy test person. These SIPs were tested for cross-selectivity in order to assess whether our methodology is able to distinguish between healthy cells and tumor cells and between two different types of tumor cells.

It is well known, that the expression of proteins on the cell membrane of tumor cells differs from that of healthy cells [87]. For example, overexpression and aberrant glycosylation of the MUC1 protein is indicative for many types of tumors [89] as described in figure 1.19. MCF-7 breast cancer cells have shown a strong overexpression of the underglycosylated MUC1 [115]. In addition, Jurkat cells also overexpress this protein. However, the overexpression in Jurkat cells is less pronounced as compared to MCF-7 cells [116]. T-lymphocytes, B-lymphocytes and monocytes also express MUC1. However the expression level is lower in comparison to that in tumor cells and they display a normal glycosylation pattern [117-120].

Selective biosensor platforms for the identification of tumor cells could be very useful in handling cancer. Recently it was shown that tumor cells evade the primary tumor very early in the progression of the disease, even before clinical detection of the primary tumor itself [121]. Tumor cells invade adjacent structures, eventually reaching the lymphatic and blood circulation which makes them able to circulate the body as circulating tumor cells (CTC's). They are able to form micrometastatic deposits which may remain dormant for years [122]. In later phases of the disease they can form secondary tumors, a condition that is

known as metastasis, associated with poor prognosis for the patients [123, 124]. These characteristics make CTC's ideal targets for early detection of cancer. Over the last decades, numerous techniques have been developed for the detection of CTC's as a tool for cancer monitoring. These very sensitive and selective techniques often require labeling and require very expensive devices, operated by academically trained, specialized personnel [125]. Therefore, a low-cost, user-friendly and label-free detection platform for tumor cells might be a very interesting application in modern-day health care.

4.2. Materials & Methods

4.2.1. Cross-selectivity test

In order to investigate whether the set-up is able to distinguish between two types of cancer cells and between healthy cells and tumor cells, SIPs were created for three different cell types: MCF-7 and Jurkat cells in addition to healthy PBMC's. MCF-7 cells have an average diameter of 18 µm while Jurkat cells are smaller (12 µm) (**figure 4.1**). PBMC's on the other hand vary in diameter from 6 to 30 µm. Details about polyurethane synthesis, the imprint procedure and the cell culture protocol can be found in section 2.2. The SIPs were exposed to the three different cell types ($1\times10^6 \pm 2\times10^5$ cells/ml) in order to analyze cross-selectivity. The experiments were conducted analogous to the proof-of-concept experiments described in section 3 of the thesis. After stabilization of the signal in PBS, the SIP-coated sensor chips are exposed to manually injected cells in buffer solution. The sensor surface is regenerated by flushing the flow cell with SDS and PBS solution.

4.2.2. Enhancing the selectivity of the set-up

Based on the idea that a non-specific sensor response stems mainly from geometrical matching between cells and imprints rather than from chemical interactions, we developed a rinsing technique for selectivity enhancement. It was shown in section 3 that the mechanical friction arising from manually flushing the flow cell is insufficient to remove cells from their corresponding imprints. Incubation of the cells in SDS solutions will make the membrane of the cells permeable and renders them susceptible to removal by mechanical friction, provided by flushing the liquid compartment of the device with buffer solution.

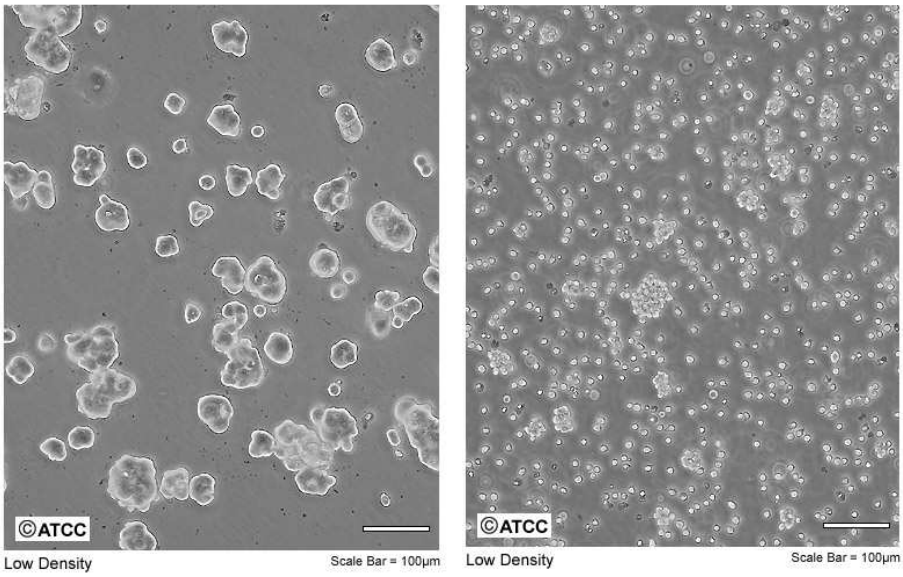

Figure 4.1: Microscopic image of MCF-7 (a) and Jurkat cells (b) (http://www.lgcstandards-atcc.org/).

However, if we could find a way to administer a more gentle form of mechanical friction, it might be possible to push out the more weakly bound analogue cells while leaving the more strongly bound target cells in place. The sensor setup was therefore connected to a computer-controlled flow system, allowing the medium inside the flow cell to be exchanged at defined moments at defined flow rates. The cell suspensions used during these experiments were injected into the flow cell at a rate of 2.5 ml/min during 72 seconds (a total volume of 3ml) after stabilization of the signal in PBS for 30 minutes until a stable plateau was reached. After stabilizing the signal, a first mild rinsing step was applied, flushing the flow cell with buffer solution at a rate of 0.25 ml/min during 12 minutes. The signal was allowed to stabilize again before a more stringent washing step was performed, flushing the flow cell at a rate of 2.5 ml/min during 72 seconds. These experiments were performed for every SIP described in Chapter 4.2.1, exposing each of the SIPs subsequently to cell suspensions containing each of the analogue cells and finally to a suspension containing the target cells.

4.3. Results

4.3.1. Differentiating between two types of cancer cells

In order to assess whether the concept allows distinguishing human cancer cells from each other SIPs were created for breast cancer cells (MCF-7 cells) and leukemic T-lymphocytes (Jurkat cells) and tested for cross-selectivity. **Figure 4.2** summarizes the recognition of the MCF-7 cells by MCF-7 imprints (figure 4.2a), the non-specific recognition of Jurkat cells by MCF-7 imprints (figure 4.2b), and the corresponding data on Jurkat imprints exposed to either MCF-7- or to Jurkat cells (figure 4.2c and 4.2d respectively).

The time-dependent R_{th} data show that the recognition of MCF-7 cells by MCF-7 imprints and the recognition of Jurkat cells by Jurkat imprints go along with a significant R_{th} increase by about 1.1 °C/W in both cases. However, there appears to be some modest cross-selectivity. Jurkat cells binding to MCF-7 imprints will lead to an increase in R_{th} by 0.33 °C/W while MCF-7 cells binding to Jurkat imprints will cause a rise in thermal resistance by 0.29 °C/W. The cross recognition between Jurkat and MCF-7 seems surprising but different types of cancer cells exhibit similar membrane properties and functional groups (glycolysation pattern) associated with *e.g.* the MUC1 membrane protein [115, 116]. As the rise in R_{th} caused by binding of the target is at least three times higher in comparison to the rise encountered when adding analogue cells, it can be concluded that the platform is indeed capable of distinguishing between two types of cancer cells.

Nevertheless, an improvement of the selectivity of the platform would be necessary since possible future medical applications arising from this prototype sensor, will aim at detecting trace amount of target cells in patient samples containing an overwhelming presence of competitor cells. Without this improvement the rise in thermal resistance caused by non-specific binding of the competitor cell might lead to a false positive result.

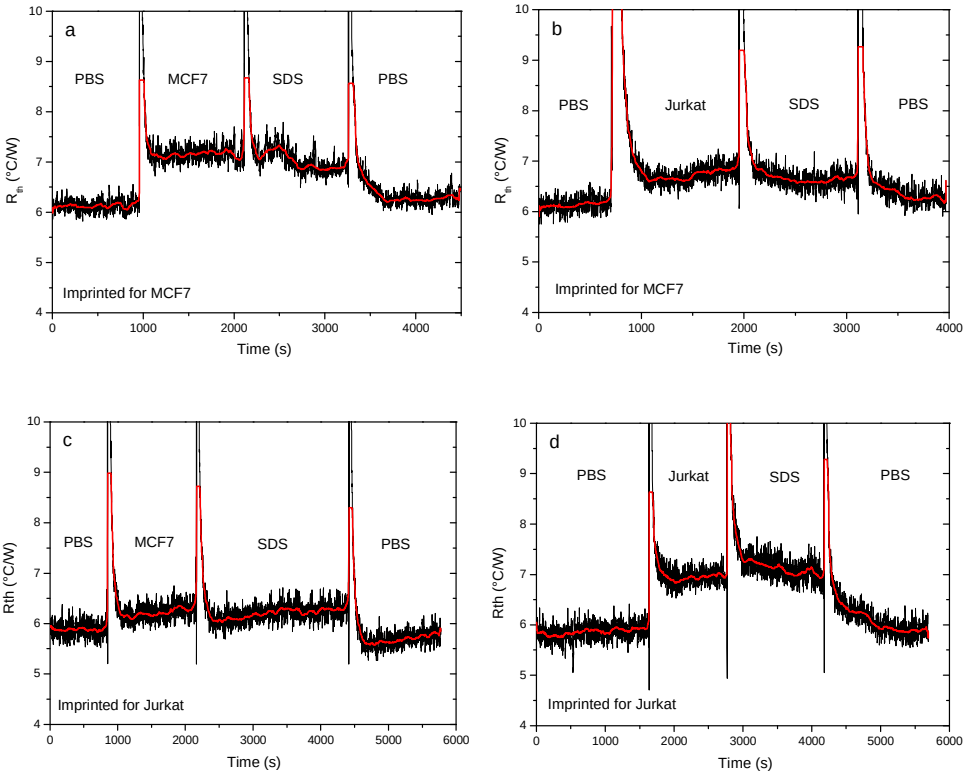

Figure 4.2: Time-dependent R_{th} data obtained from a cross-selectivity experiment aimed at discriminating between breast-cancer cells (MCF-7) and an immortalized line of leukemic T-lymphocytes (Jurkat cells). The response of a MCF-7 imprinted layer when exposed to a MCF-7 (a) and a Jurkat cell suspension. *Vice versa* the response of a Jurkat-imprinted SIP upon exposure to MCF-7 (c) and Jurkat cells (d) is shown

4.3.2. Differentiating between cancer cells and healthy cells

In order to assess whether it is possible to distinguish between healthy cells and cancer cells, a SIP was created for PBMC's and tested using all three cell types under study. In addition, the response of a MCF-7 and a Jurkat SIP to the PBMC's was analyzed (**figure 4.3**). The R_{th} date indicate that an increase in thermal resistance by 0.75 °C/W is encountered upon addition of PBMC's to the liquid compartment covering a PBMC imprinted sample (figure 4.3a). This increase is smaller in comparison to the increase encountered in a similar measurement exposing MCF-7- and Jurkat-imprinted samples to their target. This can be explained by the fact that PBMC's are a mixed cell population.

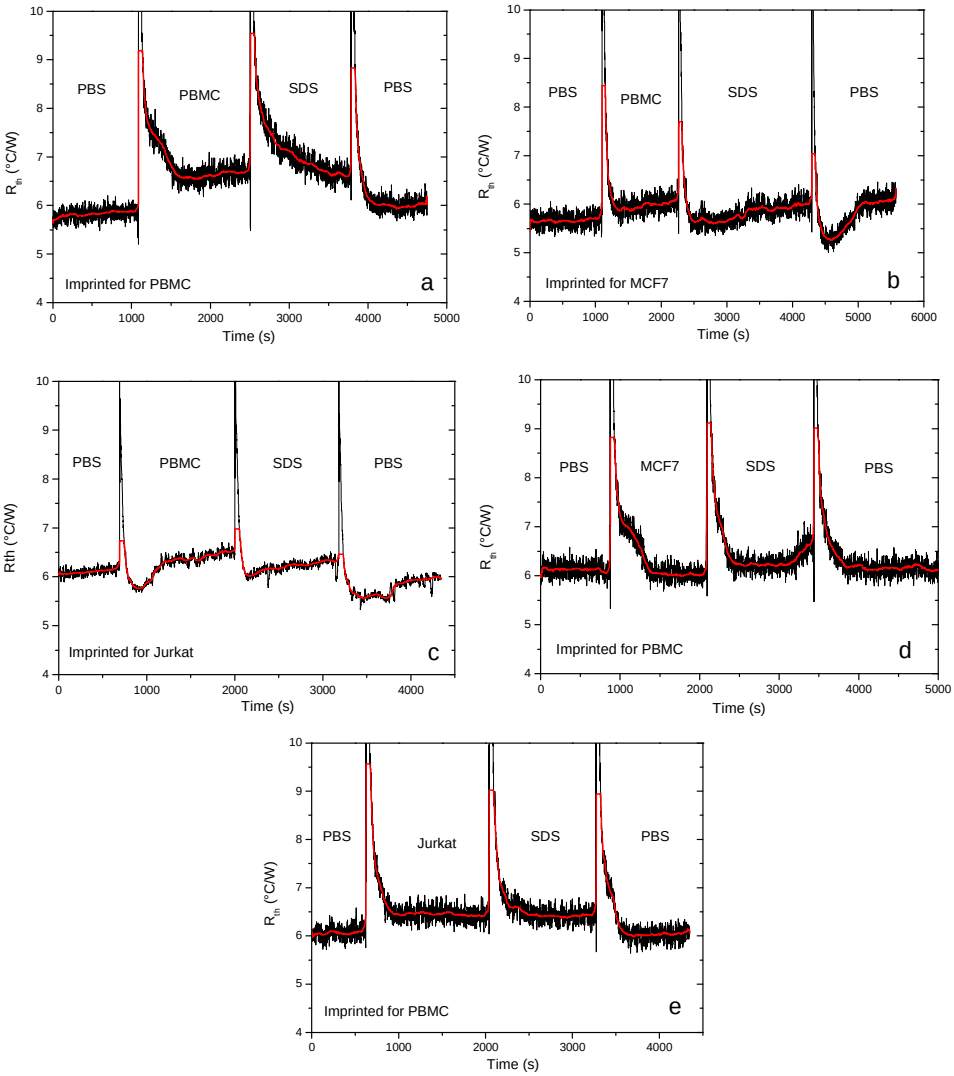

Figure 4.3: Time-dependence of R_{th} is shown for: PBMC cells in combination with a PBMC-imprinted SIP (a), a MCF-7 imprinted SIP (b), and a Jurkat SIP (c). Furthermore, the response of a PBMC-imprinted SIP for Jurkat cells (d) and MCF-7 cells (e) is shown.

There appears to be no cross-selectivity between MCF-7 and PBMC's as can be seen in figure 4.3b and figure 4.3d. Both cell types differ in origin and PBMC's do not display any cancer-related antigens on their surface. However, there is some cross-selectivity between Jurkat cells and PBMC's. An increase in the thermal resistance by 0.31 °C/W is encountered when exposing a Jurkat-imprinted SIP to PBMC's. *Vice versa*, Jurkat cells will increase the thermal resistance by

0.27 °C/W when they are added to the liquid compartment above a PBMC-imprinted SIP. This can be understood from the fact that Jurkat cells are an immortalized T-cell line while PBMC consists partly of healthy T-cells.

The results obtained in the experiments described in the last 2 sections are summarized in **Table 4.1**. Additionally, data obtained from experiments on NIP layers are also shown (grey areas in table 4.1) However, no apparent increase in thermal resistance is encountered upon exposing these blank polyurethane layers to cell suspensions. In general, the binding of target cells to their corresponding SIP results in an at least 3 times stronger rise of R_{th} as compared to the non-specific recognition of competitor cells. This way, the proposed method is able to distinguish between different cell types if we postulate that a sensor response by 5% or less is due to a non-specific effect. However, the amount of cancer cells is not known beforehand in blood samples and non-specific binding of PBMC may be dominant over specific cancer cell recognition. Therefore, we will aim now at a strategy to boost the selectivity ratio, allowing discriminating sharply between MCF-7, Jurkat, and PBMC.

Table 4.1: Data obtained with the human cancer-cell lines MCF-7 and Jurkat as well as PBMC's of a healthy volunteer. The sensor seems capable of discriminating between the different cell types but some significant cross-selectivity is observed.

Target **Concentration**	MCF-7 $1{\cdot}10^6 \pm 9{\cdot}10^4$ cells/ml		Jurkat $1{\cdot}10^6 \pm 7{\cdot}10^4$ cells/ml		PBMC $1{\cdot}10^6 \pm 1{\cdot}10^5$ cells/ml	
	ΔRth (°C/W)	% response	ΔRth (°C/W)	% response	ΔRth (°C/W)	% response
Imprint: MCF-7 24,840 ± 3,520 cavities/cm²	1.09 ± 0.1	18.0 ± 2.1	0.33 ± 0.1	5.0 ± 2.3	0.02 ± 0.1	0.4 ± 1.7
Imprint: Jurkat 22,550 ± 2,780 cavities/cm²	0.26 ± 0.1	4.4 ± 2.4	1.15 ± 0.2	19.7 ± 2.7	0.27 ± 0.1	4.4 ± 1.1
Imprint: PBMC 16,430 ± 2,950 cavities/cm²	-0.08 ± 0.1	-1.4 ± 1.7	0.31 ± 0.1	5.2 ± 2.3	0.75 ± 0.1	12.6 ± 2.1
Blank = non imprinted	0.05 ± 0.2	0.9 ± 3.0	0.08 ± 0.1	1.3 ±3.0	0.07 ± 0.1	1.2 ± 1.8

4.3.3. Enhancing selectivity: the flushing method

In order to enhance the selectivity of the device the device was connected to a pump-system allowing controlled medium exchange inside the flow cell rather than manually flushing the cell with a syringe. The experiments are performed as described in chapter 5.2.2 for the three cells types described in previous sections on SIPs imprinted for each cell type. The results are summarized in **figure 4.4**.

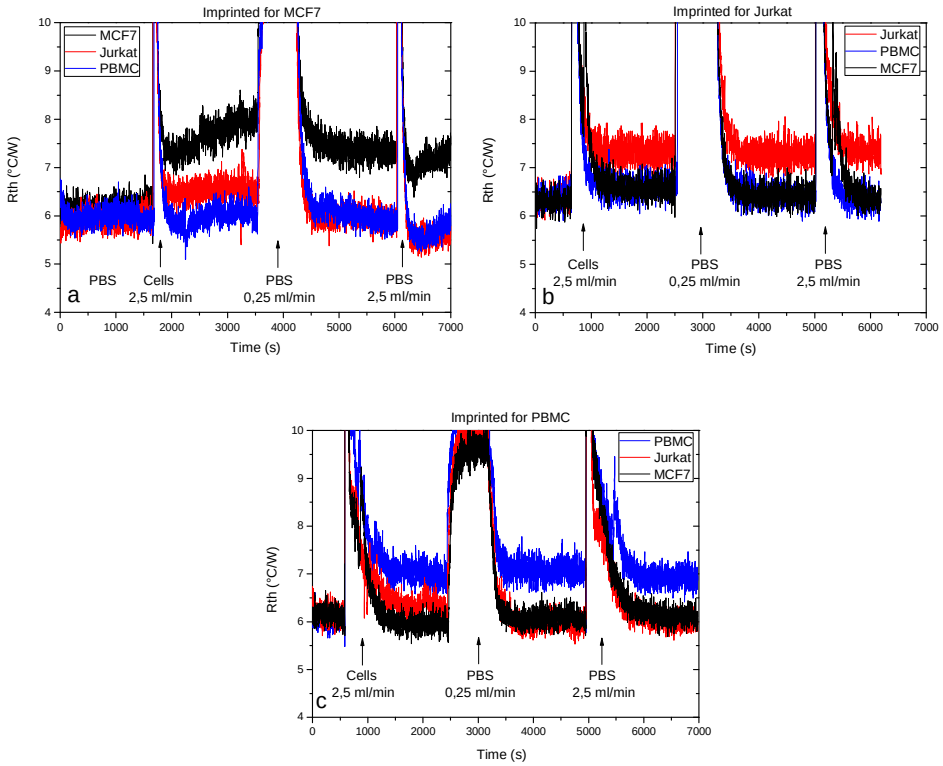

Figure 4.4: Enhancement of the selectivity by PBS rinsing using an automated medium exchange system. (a) Thermal response with an MCF-7 imprinted SIP towards MCF-7 cells (black line), Jurkat cells (red line), and PBMC (blue line). Mild rinsing with cell-free PBS was performed at a flow rate of 0.25 ml/min, stringent rinsing was done at 2.5 ml/min. (b) The same experiment was conducted on a Jurkat- and (c) PBMC-imprinted SIP. The color code and rinsing steps are identical with (a). All panels show that rinsing reestablishes the sensor baseline for cells that are non-complementary to the imprints; the signal is unaffected in all cases where cells and imprints are complementary (a, b, c).

Figure 4.4a summarizes the data obtained with a single MCF-7 SIP layer. When MCF-7 cells are introduced at a rate of 2.5 ml/min (3 ml in total, 72 seconds), R_{th} increases from 6.0 to 7.5 °C/W under static conditions. The flushed-in volume exceeds the initial PBS-filling of the liquid compartment by almost 30 times and R_{th} runs up to 8.0 °C/W, possibly due to sedimentation on top of the specific recognition. A mild rinsing step with cell-free PBS at a flow rate of 0.25 ml/min and total volume 3 ml (12 minutes) brings the R_{th} response back to 7.5°C/W and this remains stable even after stringent rinsing with the same PBS volume at a flow rate of 2.5 ml/min for 72 seconds.

Repeating this sequence with PBMC, the sensor baseline at 6.0 °C/W did not change over time. The same experiment with Jurkat cells gave a non-specific increase of 0.5 °C/W after introducing the Jurkat cell solution, while already the first rinsing re-established the baseline and there was no further change after stringent rinsing. This means that the shear forces exerted by the liquid flow are sufficient to break the non-specific sticking between cells and imprints in case that chemical complementarities are missing.

The analogous experiment with a Jurkat-imprinted SIP layer (figure 4..4b) showed a selective, permanent recognition of Jurkat cells while the non-specific response to MCF-cells and PBMC (+ 0.5 °C/W in both cases) vanished partially after mildly rinsing with PBS. However a further decrease in the non-specific response was encountered after the more stringent washing step, indicating that this second step was necessary in order to remove all analogue cells from the layer. The non-specific response of Jurkat cells to PBMC imprints (+ 0.4 °C/W) is cancelled out after the mild rinsing step as shown in figure 4.5c.

The results described in this section are condensed as bar charts in **figure 4.5**. After the second, 'stringent' rinsing step, the cross-response is in all cases smaller than the error bars defined by the noise level. At the same time, the R_{th} increase of SIPs, which have selectively rebound their template molecules, remains constant, demonstrating the efficiency of rinsing-based selectivity enhancement. This technical improvement is crucial in terms of the development of possible future applications for the detection of trace amounts of medically relevant cells in patient samples.

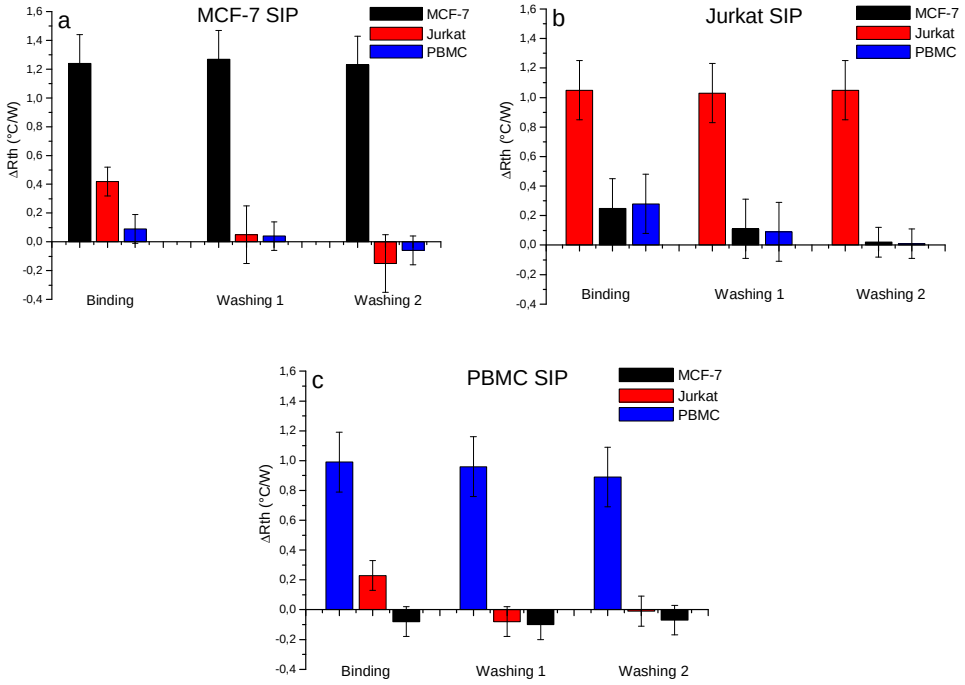

Figure 4.5: Bar-chart representation of the change of thermal resistance ΔR_{th} observed with three different types of SIPs upon exposure to MCF-7- (black), Jurkat- (red), and PBMC's (blue) during binding and the consecutive washing steps. The change in thermal resistance is shown for a MCF-7 (a), Jurkat (b) and PBMC SIP (c). Within error bars, the non-specific response is completely suppressed after the second washing step.

4.4. Conclusion

The results presented in this chapter constitute a proof for a possible future application of the proposed platform. The device is able to distinguish between disease-related cells (in this case tumor cells) and healthy blood cells (PBMC's) with minor cross-selectivity effects observed. This indicates that the device might be used in the future for the detection of CTC's or other disease-related cells in biological samples such as whole blood, blood plasma or spinal fluid. Furthermore, connecting the system to a syringe-driven pump system resulted in an improved selectivity of the set-up and allowed us to perform the measurements in a fully automated manner.

To benchmark the R_{th} based technique of cancer-cell detection with the state of the art, we mention recent reports describing the identification of circulating

tumor cells by image cytometry [126, 127]: according to this work, it is feasible to detect concentrations as low as 1 cell per ml after purification of blood samples and targeting the cells with fluorescently-labeled antibodies. The HTM technique presented here is a very first demonstration of the concept and not yet optimized towards ultralow detection limits. However, special benefits are the low-cost, label-free readout apparatus and cells are detected through their integral membrane properties, which do not need to be known in detail. Furthermore, the technique can be automated and digitalized, leaves the possibility for arraying and does not require an image analysis by an expert. Regarding other label-free techniques, MCF-7 cells were detected by amperometric- [128], magnetoelastic- [129], and microgravimetric sensors [130]. These concepts require cell concentrations in the range of 10^4 – 10^6 cells/ml in buffer while there is no information on the selectivity. The detection of Jurkat cells is documented by using antibodies as recognition elements and a photonic-crystal readout principle [131]. Typical numbers are $2{\cdot}10^5$ cells per assay (a factor ten higher in comparison to HTM) and the concept allowed to discriminate between two different Jurkat cell lines.

The final goal is selective detection of specific, disease-related cells in blood and their absolute concentration will generally be lower than the total cell count. The amount of cancer cells can first be increased by microfluidic approaches [100, 101]. Furthermore, the detection limit of our system (below $3{\times}10^4$ cells/ml) can be lowered by electronic-noise reduction, design modifications, and by increasing the number of cell imprints per unit area: a fourfold increase towards 100,000 MCF-7- or Jurkat imprints per cm^2 seems realistic. Finally, we observed that cells, which are only weakly and non-specifically bound are released from the SIP layer by rinsing while the true target cells remain sticking in the imprints. Surprisingly an increase in flow rate will not cause the target cells to be removed from the surface, rather the polyurethane surfaces seems to be damaged. This effect needs to be further examined in order to fully understand the interaction between target and imprint The flushing method opens up the possibility for a continuous, closed-loop operation with a steady flow. In this set-up cross-selectivity can be suppressed by the steady flow while the actual target cells become gradually enriched on the SIP-layer, even if their absolute concentration is low as compared to competitor cells.

5. The CHO cell experiment: exploring the selectivity limit of the methodology

5.1. Introduction

In previous chapters it was shown that the proposed biosensor platform is able to detect various types of mammalian cells in a specific, selective, fast and sensitive manner. Although these results were clearly promising in terms of possible future biomedical applications, it is interesting to explore just how far we can go. How selective is the proposed platform? How is the sensitivity of the device influenced when mixing the target cells of interest with a solution of competitor cells? Can we verify the results by benchmarking them with state-of-the-art optical techniques such as fluorescence microscopy? The answers to these questions will be given in this chapter.

The flushing method proposed in the previous chapter clearly resulted in an improved selectivity. To test the boundaries of this improved selectivity, it was assessed whether it was possible to distinguish between two cell types, differing in the expression of a single protein and between cell lines expressing different phenotypes of the same protein. Therefore, an experiment was conducted, based on a recently published article by Van Elssen *et al*. [132]. In this work, a modified Chinese hamster ovary cell line (CHO *ldlD*) was stably transfected with the coding sequence of MUC1. The CHO *ldlD* cells contain a defect making it impossible to obtain the necessary sugars for glycosylation of membrane proteins from their environment. The defect can be reversed by adding exogenous sources of monosaccharides such as galactose (Gal) and N-acetylgalactosamine (GalNAc) [132, 134].

MUC1 has five potential *O*-glycosylation sites, two serines and three threonines that are extensively glycosylated (**figure 5.1**). The enzyme N-acetylgalactosaminyltransferase (GalNAcTs) inititates O-linked glycosylation by attaching GalNAc to a serine or threonine resulting in the formation of the Tn antigen (step a). Sialyltransferase can catalyse the formation of a link between sialic acid and the GalNac moiety, forming the sialyl-Tn (STn) antigen (step b). Alternatively glycosylation can be elongated to core 3 and 4 antigens or core 1

structures can be formed by the addition of Gal to the GalNAc moiety, a reaction catalyzed by galactosyltransferase β3GalT, resulting in the formation of the T antigen (step c). The T antigen can become sialylated creating ST antigens by either linking sialic acid to the GalNAc, the Gal moiety or both, catalyzed by ST6GalNAc-I,II (step d), ST3Gal-I (step e) or both respectively.

It has been shown that cancer cells express the MUC1-associated antigens T (Gal/GalNAc) and Tn (GalNAc) as well as their sialylated counterparts (ST and STn) [135, 136]. The degree of glycosylation depends on the expression of tissue-specific glycosyltransferases [89], defects in the expression of these enzymes leads to defects in the glycosylation scheme, decreasing the degree of glycosylation in tumor-associated MUC1 glycoforms [90-93]. Therefore, the MUC1 protein is an excellent candidate for assessing the selectivity of the set up in terms of biomedical relevance.

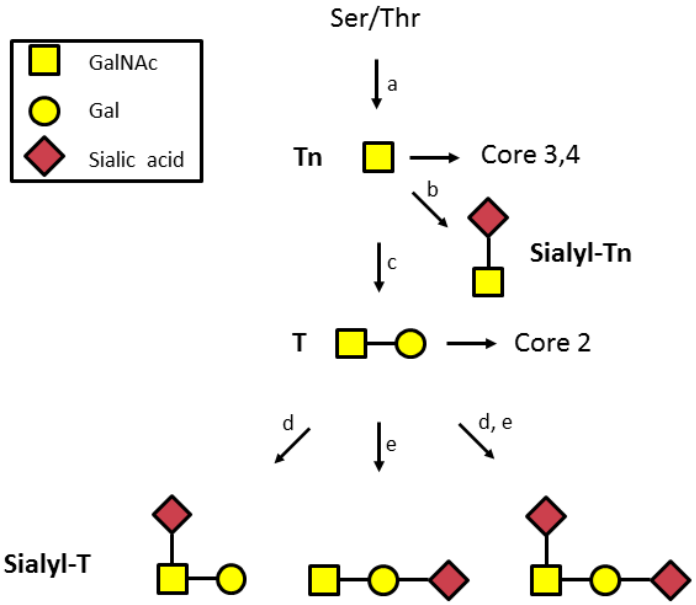

Figure 5.1: Schematic representation of the *O*-glycosylation mechanism leading to different glycoforms of MUC1. Formation of the Tn antigen (a), the STn antigen (b), the T antigen (c) and the ST antigen (d and e) are shown. Adapted from van Elssen *et al.* [132].

In addition, experiments were conducted analyzing the sensitivity of the device by diluting target cell suspensions in suspension containing an excess of analogue cells. Finally, target and analogue cells were differentially labeled with green and red fluorescent labels and the samples were analyzed by fluorescence microscopy an addition experiment, in order to verify the selectivity of the set-up and to attempt to quantify the binding characteristics of the rebinding process.

5.2. Materials & Methods

5.2.1. Cell culture protocol

Chinese Hamster Ovary (CHO) *ldlD* and CHO-*ldlD* cells stably transfected with MUC1. The cells were cultured in Dulbecco's Modified Eagles Medium/Nutrient F-12 Ham medium (DMEM/F12) supplemented with 3% FCS and 1% (P/S). Cells were passaged at a confluence of about 80% and MUC1 -transfected cell cultures were selected by addition of G418 disulphate salt. These cell lines are deficient in their UDP-galactose/UDP-acetylgalactosamine 4-epimerase enzyme, affecting both *N*-linked and *O*-linked glycosylation [133, 134], causing these cells to express a non-glycosylated isoform MUC1-F.

In order to restore the glycosylation, the CHO-*ldlD* MUC1 cells were incubated with 1 mM GalNAc, inducing them to express MUC1-Tn or with 1mM GalNAc and 0.1 mM Gal inducing them to express MUC1-T. Both antigens are associated with certain types of cancer [132, 134]. The appearance of the different cell lines is schematically represented in **figure 5.2**. Cell cultures were provided by the Maastricht University Medical Center (department of internal medicine, division of haematology). Cell culturing was performed at and in cooperation with the Biomedical Research Institute (BIOMED) of Hasselt University.). All chemicals used for cell culturing, selection and glycosylation were ordered at SIGMA-Aldrich N.V. (Diegem, Belgium). Prior to imprinting and thermal resistance measurements cells were washed six times in PBS. Cell counting to determine cell concentration in buffer medium was done by a haemocytometer (VWR International, Leuven, Belgium).

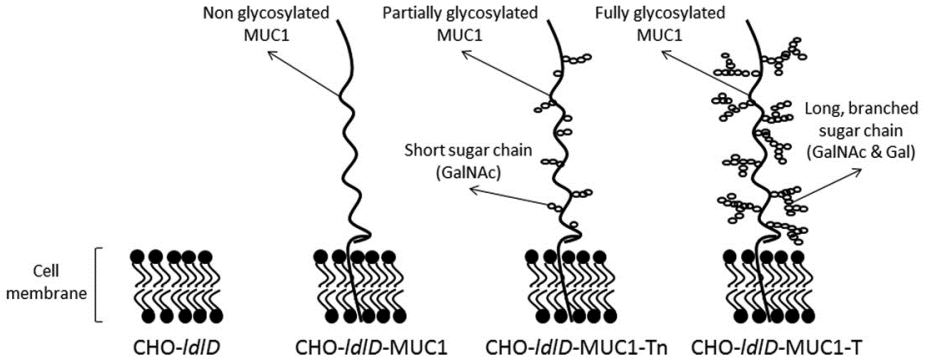

Figure 5.2: Schematic overview of the appearance of the different cell lines. Both CHO-*ldlD* and CHO-*ldlD*-MUC1 are shown as well as the two glycoforms of CHO-*ldlD*-MUC1: CHO-*ldlD*-MUC1-Tn (GalNAc glycosylation of MUC1) and CHO-*ldlD*-MUC1-T (GalNAc and Gal glcosylation of MUC1).

5.2.2. Optical characterization

In order to analyze the shape and size of the imprints made by the cells described in chapter 6.2.1, all SIPs under study were analyzed by optical microscopy. This analysis was performed with an Axiovert 40 inverted optical microscope (Carl Zeiss, Jena, Germany). In addition, the surface coverage of the polyurethane layers with cell imprints was determined on basis of the optical micrographs analyzed with the software package ImageJ 1.44P (National Institute of Health, Bethesda, USA). The method that was used for calculating the surface coverage is analogous to the one described in chapter 3.

5.2.3. Selectivity test experiment

The selectivity of the sensor set-up is further investigated in this experiment by imprinting samples with CHO*ldlD* cells and CHO*ldlD* cells transfected with MUC1-F (denoted CHO and CHO-MUC cells respectively). These samples were tested for cross-selectivity using the improved flushing method described in chapter 5. The cells were flushed in at a rate of 2.5 ml/min (total volume of 3 ml), after stabilization of the signal two PBS rinsing steps at rates of 0.25 and 2.5 ml/min both with a total volume of 3 ml were performed in order to remove any non-specifically bound cells from the SIP layer.

The selectivity of the device was analyzed further in depth by measuring the thermal resistance in an analogously performed experiment using samples imprinted for CHO cells expressing three different glycoforms of MUC1 denoted CHO-MUC1-F (no glycosylation), CHO-MUC1-Tn (GalNAc) and CHO-MUC1-T (Gal and GalNAc). All of the samples under study were exposed to all three cell types in order to assess cross-selectivity. New PID parameters (P=1, I=5 and D=0) were used in both experiments, in order to reduce the noise on the signal [137].

5.2.4. Analysis of a cross-selectivity experiment by fluorescence microscopy

In order to verify the selectivity of the proposed platform, samples were analyzed by fluorescence microscopy after a CHO/CHO-MUC selectivity experiment. In addition, this analysis might be used to quantify the number of cells that is actually retained by the SIP after ad addition experiment. In order to analyze a SIP sample with fluorescence microscopy after a cross-selectivity experiment, both cell types were fluorescently labeled prior to the heat-transfer measurements. CHO-MUC cells were labeled with DiI (SIGMA-Aldrich N.V., Diegem, Belgium) by incubating a cell suspension in PBS with 5 µM DiI solution for 30 minutes at 37 °C. CHO cells were incubated with 25 µM of calcein (Life Technologies Europe B.V., Gent, Belgium) for 30 minutes at room temperature. DiI is an orange-red carbocyanine dye that is inserted to the membrane of a cell after which it can diffuse laterally to stain the whole cell [138]. Calcein is a fluorescent dye that is transported into the cell where it chelates metal ions. It gets trapped inside the cell and after an intracellular esterase removes the quenching acetomethoxy group, it gives a strong green fluorescence [139]. The excitation and emission maxima of DiI and calcein are 549/565 and 495/515 nm respectively [138, 139] ensuring that no spectral overlap exist between both dyes. Addition experiments were performed using these labeled cells on samples imprinted for both cell types using the flushing method measuring scheme. The samples were analyzed after this experiment using a Nikon Ecplise 80i fluorescence microscope and NIS-elements BR software (Nikon Instruments Europe B.V., Amsterdam, The Netherlands). All images were made at 250 ms exposure time and a gain of 1. The fluorescence analysis was compared to the thermal resistance data. Prior to these measurements some background measurements were performed by drop-casting solutions of fluorescent-labeled

cells onto a blank aluminum substrate. This was done to proof that fluorescent labelling can indeed be performed successfully for both cell types. However, since DiI is incorporated into the membrane of the cells, it is possible that this will influence the rebinding of these cells to the SIP. Therefore an addition experiment was performed using DiI-labeled and non-labeled CHO-MUC cells in two consecutive exposure steps on a CHO-MUC-imprinted sample. In order to remove the target cells between both runs, the layer is flushed with SDS and PBS in between measurements.

5.2.5. Repeated exposure in a competitive assay

The sensitivity of the set-up was assessed in chapter 3 employing a dilution series of NR8383 cells in PBS. However, the sensitivity can be influenced by the presence of competitor cells, a parameter that is especially important when analyzing the presence/concentration of target cells in real biological samples. In biological samples derived from e.g. spinal fluid, blood plasma or whole blood, the concentration of disease-related cells is often massively overwhelmed by the presence of healthy blood cells such as erythrocytes, lymphocytes, macrophages or monocytes. Therefore, an experiment was performed analyzing the performance of a receptor layer imprinted for CHO-MUC cells when exposed to different concentrations of target cells in the presence of increasing amounts of analogue cells (CHO cells). This situation will assess the limit of sensitivity as target cells and analogue cells are very similar, both morphologically and functionally. In real patient samples the difference between target cells and competitor cells will be much bigger in most cases. For this experiment a CHO-MUC cell solution in PBS was diluted 2, 10, 20 and 100 times with a CHO cell suspension in PBS, the initial cell concentration of both solutions was identical (1×10^6 cells/ml). The sensitivity of the device was tested by exposing a CHO-MUC-imprinted sample to four consecutive addition runs for each of the solutions. In each run, 3 ml of cell solution was injected at a rate of 2.5 ml/min, after stabilization of the signal followed by a rinsing step flushing the flow cell with PBS at 0.25 ml/min during 12 minutes (achieving a total volume of 3 ml). Between each injection or flushing step the signal was allowed to stabilize.

5.3. Results & Discussion

5.3.1. Optical characterization of all SIPs under study

Polyurethane-coated aluminum substrates that were imprinted with CHO, CHO-MUCF, CHO-MUCT and CHO-MUCTn cells were characterized by means of optical microscopy. All samples were analyzed at 5 and 50 times magnification, the results are summarized in **figure 5.3**. These results clearly show that all cell types form spherical imprints with diameters around 20 µm that seem to be morphologically very similar. This is not surprising given the fact that these cells differ only in the expression of MUC1. The average surface concentration is determined by analyzing microscopic images obtained from three different samples for each SIP, analyzing five spots on each sample. The number of imprints in each image is determined by cell counting using ImageJ, and used for calculating the average surface coverage for each SIP. The results are summarized in **Table 5.1**. The surface coverage for all four SIPs seems to be identical (differences between coverage data fall within margins of error) and corresponds well to the values found for MCF-7 and Jurkat cells in chapter 4. Given the average diameter of the cells (20 µm) this means that about 10 % of the available surface area is imprinted.

Table 5.1: Average surface coverage for SIPs imprinted for CHO, CHO-MUCF, CHO-MUCT and CHO-MUCTn cells. All surface coverage values were obtained by analyzing optical microscopy images at 5x magnification (see figure 38) on five different spots on three samples for each SIP. The total number of imprints in each image was determined with ImageJ and these values were used to calculate the average number of imprints per cm^2 for each SIP.

Imprint	Coverage (imprints/cm^2)
CHO	22600 ± 800
CHO-MUCF	23800 ± 1500
CHO-MUCT	23300 ± 1500
CHO-MUCTn	23300 ± 1200

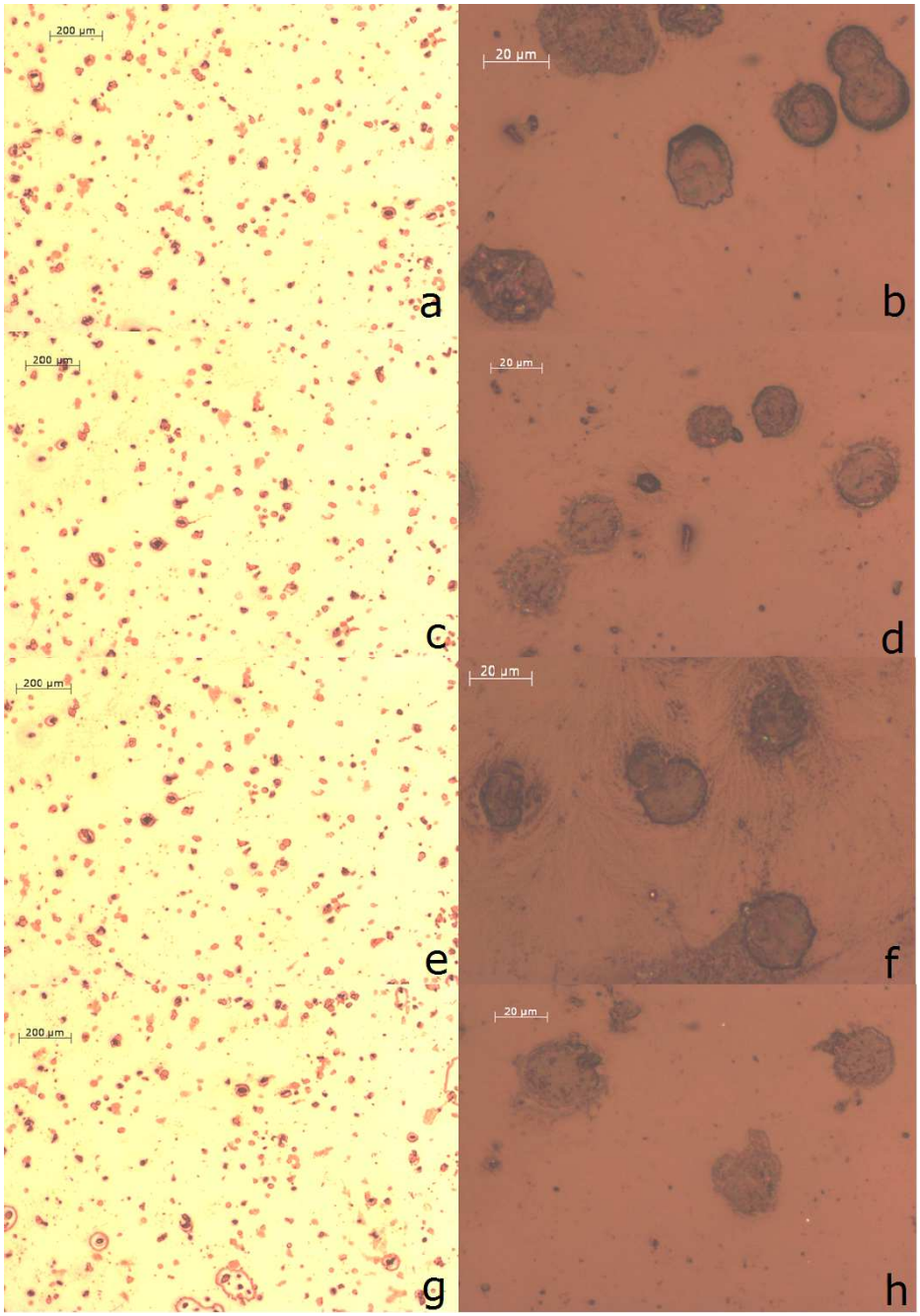

Figure 5.3: Optical microscopy images at 5x magnification (left) and 50x magnification (right) of a SIP imprinted for CHO (a, b), CHO-MUCF (c, d), CHO-MUCT (e, f) and CHO-MUCTn (g, h) cells. All samples show a wide similarity in the morphology and density of the imprints on their surface.

5.3.2. Distinguishing between cells differing in the expression of a single membrane protein

Samples imprinted with CHO and CHO-MUC cells were tested for cross-selectivity by exposing them consecutively to analogue and target cell suspensions. The resulting time-dependent thermal resistance data and the resultant box charts are shown in **figure 5.4**. Upon addition of the cells to the liquid compartment covering a SIP imprinted for CHO cells the thermal resistance rises by 1.0 ± 0.1 °C/W (see figure 5.4a and b). This increase in R_{th} is encountered for both target and analogue cells. Given the fact that both cell types are morphologically identical and also display a great functional similarity this finding is not surprising. The morphological fit between the CHO-MUC1 cells and the CHO imprints is aided by hydrogen bonds formed between functional groups within the microcavities of the SIP layer and complementary regions on the cell membrane where MUC1 expression is absent.

This theory is further confirmed by analyzing the effect of rinsing. The CHO cells remain bound to the imprints, resulting in a stable, increased thermal resistance, even after the two rinsing steps (red curve). However, CHO-MUC1 cells (black curve) that are less strongly bound to the surface due to incomplete hydrogen bonding will be removed by the mechanical friction provided by the rinsing steps, resulting in a drop in thermal resistance to the baseline value. The results obtained by performing the same experiment on a CHO-MUC1-imprinted sample (figure 40c and d), confirm these results. Addition of target (black curve) and analogue cells (red curve) will lead to a very high degree of cross selectivity, although the increase in R_{th} is slightly less pronounced for the analogue cells (0.8 ± 0.1 °C/W). After rinsing, CHO-MUC1 cells remain bound to the surface while the CHO cells are washed off. Combining the results of both experiments, it can be concluded that this set up is able to distinguish between two cell types differing solely in the expression of the MUC1 protein on their membrane. Furthermore, the improved PID parameters resulted in a two- to fourfold reduction of the noise levels in comparison to the measurements performed in previous sections, this in accordance with values found in literature for heat-transfer measurements with molecularly imprinted polymers [137].

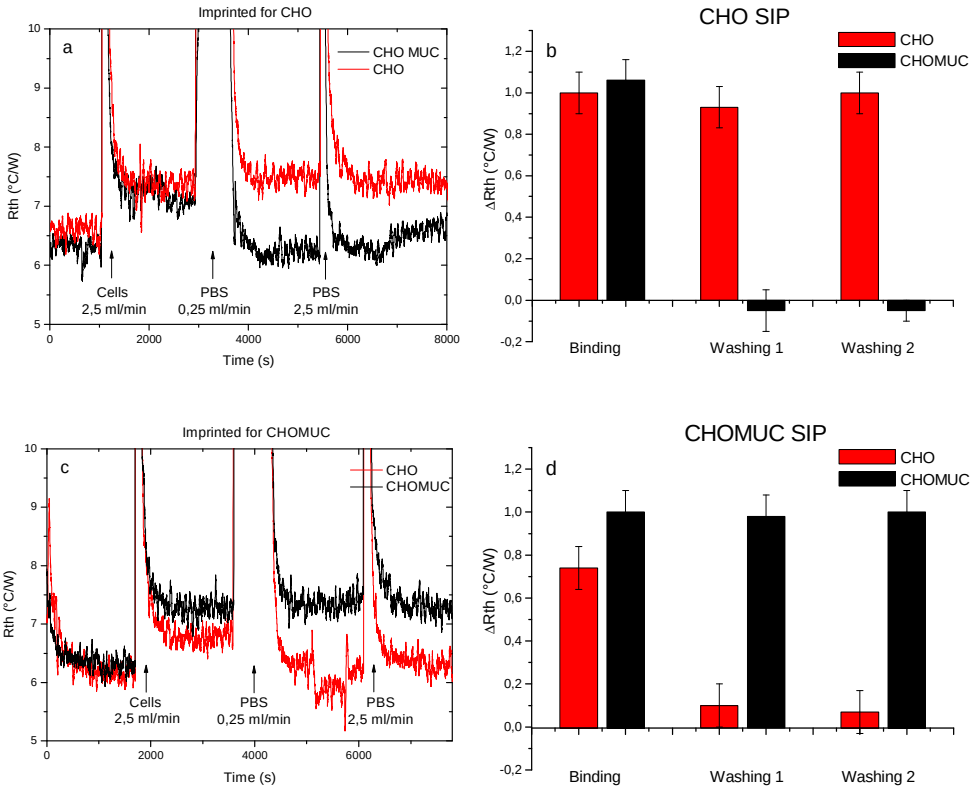

Figure 5.4: Timed-dependent R_{th} data for a CHO-imprinted SIP towards CHO cells (red line) and CHO-MUC cells (black line). Mild rinsing with cell-free PBS was performed at a flow rate of 0.25 ml/min, stringent rinsing was done at 2.5 ml/min (a). The same experiment was conducted on a CHO-MUC1-imprinted SIP (c). Bar charts summarizing the results are also shown (b, d). The color code and rinsing steps are identical to that in (a). All panels show that rinsing re-establishes the sensor baseline for analogue cells, while the signal is unaffected in both cases if cells and imprints are complementary (a, b, c, d).

5.3.3. Distinguishing between cells expressing different glycoforms of the same protein

In order to further assess the selectivity of the device, SIPs were synthetized for CHO cells displaying the MUC1-F (non-glycosylated), MUC1-Tn (GalNAc glycosylated) and MUC1-T (GalNAc and Gal glycosylated) glycoforms on their membrane. For reasons of simplicity these cells will be referred to as CHO-MUC1-F, CHO-MUC1-Tn and CHO-MUC1-T respectively. The thermal resistance was analyzed in an experiment similar to the one described above,

exposing each SIP consecutively to all three cell types, with the target cells being administered last in all cases. Between each run two PBS rinsing steps were performed as part of the flushing method scheme. The results are shown in **figure 5.5.** and clearly demonstrate that the set-up is able to distinguish between non-glycosylated and glycosylated isoforms.

Exposing a CHO-MUC1-F-imprinted SIP to target as well as analogue cells will result in an increase in thermal resistance (figure 5.5a). After two consecutive washing steps the glycosylated CHO-MUC1-T and CHO-MUC1-Tn cells are washed of the surface while the non-glycosylated CHO-MUC1-F (last addition step) remain bound to the imprinted polyurethane layer. The carbohydrate groups on the MUC1 protein of the analogue cells block certain epitopes on the surface of the protein leading to a less strong bound between these cells and the imprints on the surface, causing them to be washed away due to the mechanical friction provided by the rinsing steps. The absence of carbohydrate groups blocking certain antigens on the MUC1 protein will result in an increased number of hydrogen bonds formed between target and imprint, resulting in a stronger bond.

Vice versa the thermal resistance increases upon exposure of a CHO-MUC1-Tn- (figure 5.5b) and a CHO-MUC1-T-imprinted sample (figure 5.5c) to a CHO-MUC1-F cell solution (first addition step). The thermal resistance drops back to the baseline value after rinsing the flow cell with buffer, indicating that the CHO-MUC1-F cells get washed off the surface. The absence of sugar groups on the MUC1 protein of the CHO-MUC1-F cells leads to incomplete hydrogen bonding between these analogue cells and the imprints on the SIP, being imprinted for the glycosylated Tn and T isoforms. Therefore, it can be concluded that the sensor set-up is able to distinguish between cell types differing only in the absence/presence of sugar moieties on the MUC1 protein that they express on their surface. However, the sensor seems incapable of distinguishing between two cell types expressing MUC1 with different degrees of glycosylation. The results in figure 5.5b show that the thermal resistance does not return to baseline after two rinsing steps. This implies that the bond between the analogue cells and the SIP is too strong to remove these cells from the imprints by shear forces.

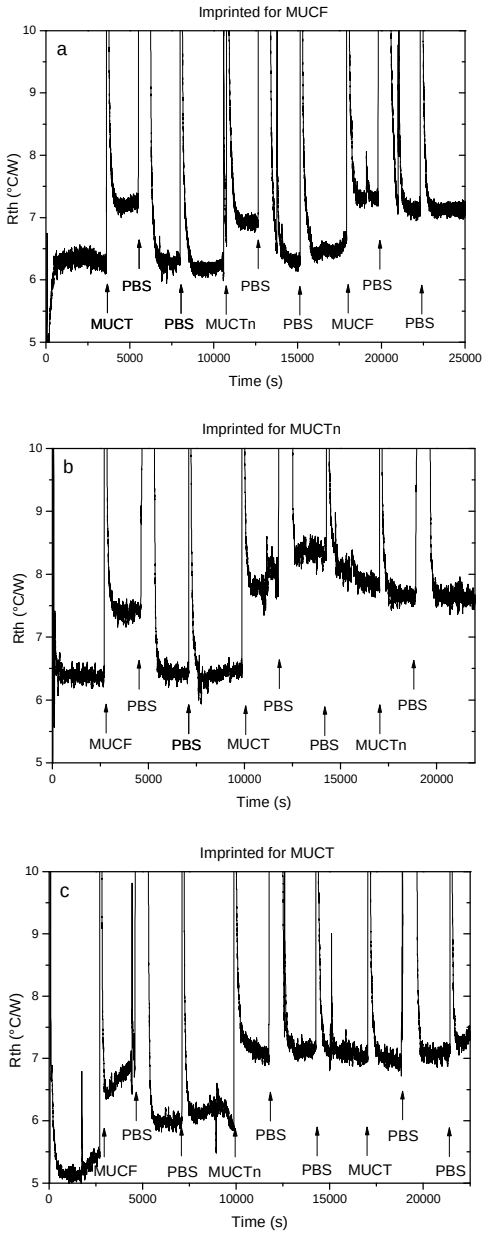

Figure 5.5: Timed-dependent R_{th} data for a CHO-MUC1-F-imprinted SIP exposed to CHO-MUC1-T-, CHO-MUC1-Tn- and CHO-MUC1-F cells consecutively (a). The same experiment was conducted on a CHO-MUC1-Tn- (b) and CHO-MUC1-T-imprinted SIP (c). The results indicate that the set-up is able to distinguish between cells based on the expression of non-glycosylated and glycosylated isoforms of MUC1 but is unable to distinguish between CHO-MUC1 cells expressing differentially glycosylated MUC isoforms.

Since the binding sites are still occupied by analogue cells, addition of a solution containing target cells will not cause an increase in R_{th}. The results obtained with a CHO-MUC1-T SIP (figure 5.5c), show a similar trend. Exposure to CHO-MUC1-Tn cells leads to an increase in R_{th}, which cannot be reversed by flushing the flow cell with PBS. Combining these results, it can be concluded that the presence/absence of galactose in addition to N-acetylgalactosamine moieties on the MUC1 protein only leads to a minor difference in the degree of hydrogen bonding to the imprints between analogue and target cells. Therefore, the mechanical friction provided by rinsing the flow cell with buffer is insufficient to remove the strongly bound analogue cells. This experiment clearly demonstrates that there is a limit to the remarkable selectivity of the proposed set-up. The results obtained in figure 5.4 and figure 5.5 are summarized in **Table 5.2**.

Table 6: Overview of cells retained on SIPs imprinted with either CHO, CHO-MUC1, CHO-MUC1-Tn and CHO-MUC1-T.

		SIP			
		CHO	CHO-MUC1	CHO-MUC1-Tn	CHO-MUC1-T
Cell solution	CHO	●	/	/	/
	CHO-MUC1	/	●	/	/
	CHO-MUC1-Tn	/	/	●	○
	CHO-MUC1-T	/	/	○	●

● Specific cell retention; ○ Non-specific cell retention; **/** No cell retention

5.3.4. Analysis of a cross-selectivity experiment by fluorescence microscopy

In order to verify the selectivity of the set-up and to quantify the number of cells retained by the SIP, samples were analyzed with fluorescence microscopy after a cross-selectivity experiment. To this extent, the cross-selectivity experiment described in chapter 5.3.1 was repeated with DiI-labeled CHO-MUC1 cells and calcein-labeled CHO cells. Prior to this experiment it was examined if it was possible to detect fluorescently labeled cells on a polyurethane-coated aluminum substrate. To this extent, a 50:50 mixture of calcein-labeled CHO and DiI-

labeled CHO-MUC1 cells was applied on a non-imprinted polyurethane sample, covered with a glass slip and the sample was analyzed by fluorescence microscopy. The resulting image is shown in **figure 5.6** and clearly indicates that both labels can be used to detect cells on a polyurethane-coated aluminum chip.

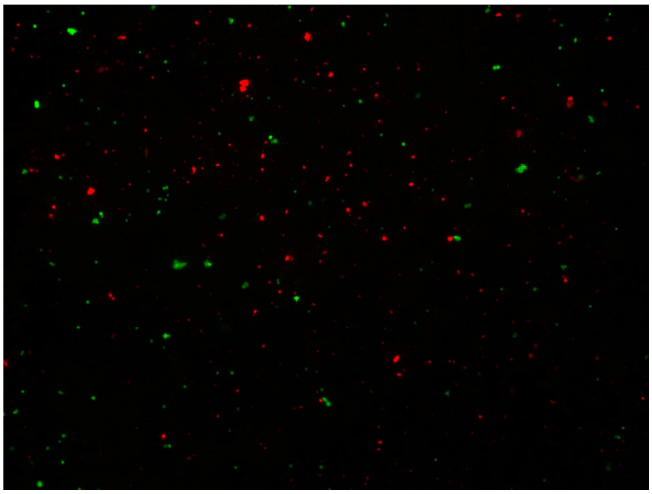

Figure 5.6: Fluorescence microscopy image (4 times magnification) showing a background experiment, performed by dropcasting a solution containing calcein-labeled CHO cells and DiI-labeled CHO-MUC1 cells in a 1:1 ratio onto an aluminum substrate covered by a non-imprinted polyurethane layer. Both cell types can be clearly visualized.

As described earlier, the DiI label is inserted into the membrane of the labeled cell and diffuses laterally in order to stain the rest of the cell. Since part of the label remains inside the cell membrane, it might be possible that it will have an adverse effect on the rebinding of labeled cells to a SIP that was imprinted for a non-labeled cell of the same cell type. Therefore, an experiment was conducted exposing a CHO-MUC1-imprinted SIP to DiI-labeled and non-labeled CHO-MUC1 cells in two consecutive runs. The method was performed by the so-called flushing method, described in section 4.3.3. Additionally the set up was flushed with SDS (at 2.5 ml/min with a total volume of 3 ml) and PBS (0.25 ml/min, total volume 3 ml) between each run, in order to remove any cells bound to the polyurethane layer. The result is shown in **figure 5.7**.

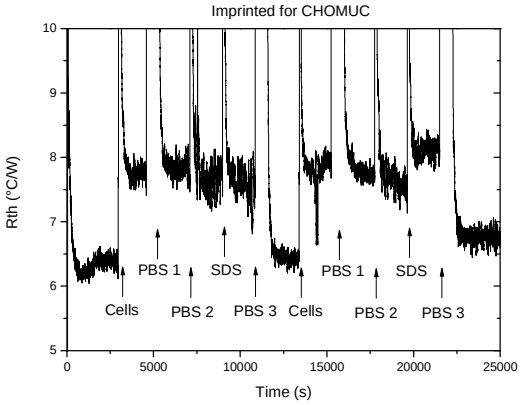

Figure 5.7: Time-dependent R_{th} data for an experiment exposing a SIP imprinted for CHO-MUC1 cells to DiI-labeled and non-labeled CHO-MUC1 cells in two consecutive addition runs. Between each run the flow cell is rinsed with PBS at rates of 0.25 ml/min (PBS 1) and 2.5 ml/min (PBS 2). Additionally the flow cell is rinsed with SDS and PBS solution (PBS 3) after both rinsing step, to ensure full removal of cells from the surface. In both runs the thermal resistance is increased similarly and does not return to the baseline value until the flow cell is fully rinsed with SDS and PBS.

The results in figure 5.7 indicate that the DiI label does not influence the rebinding of target cells to the SIP. In both runs, the R_{th} increases by 1.38 ± 0.10 °C/W upon addition of the cells and does not return to baseline after rinsing the cells with buffer, indicating complementarity between the cells and the imprint. Rinsing the flow cell with SDS and PBS returns the signal to the baseline value.

The time-dependent thermal resistance data obtained from a cross-selectivity experiment for DiI-labelled CHO-MUC1 and calcein-labelled CHO cells are shown in **figure 5.8**. The results provide visual proof that the proposed platform is capable of identifying and retaining CHO-MUC1 and CHO cells in a specific and selective manner. The fluorescence data (figure 5.8b and d) are in perfect agreement with the thermal resistance data (figure 5.8a and c). In both cases, the R_{th} data indicate that the analogous cells are washed off the surface by rinsing the flow cell with PBS while target cells remain bound to the SIP even after a washing step (see figure 5.8a and c). These results are in accordance with the results obtained in section 5.3.1.

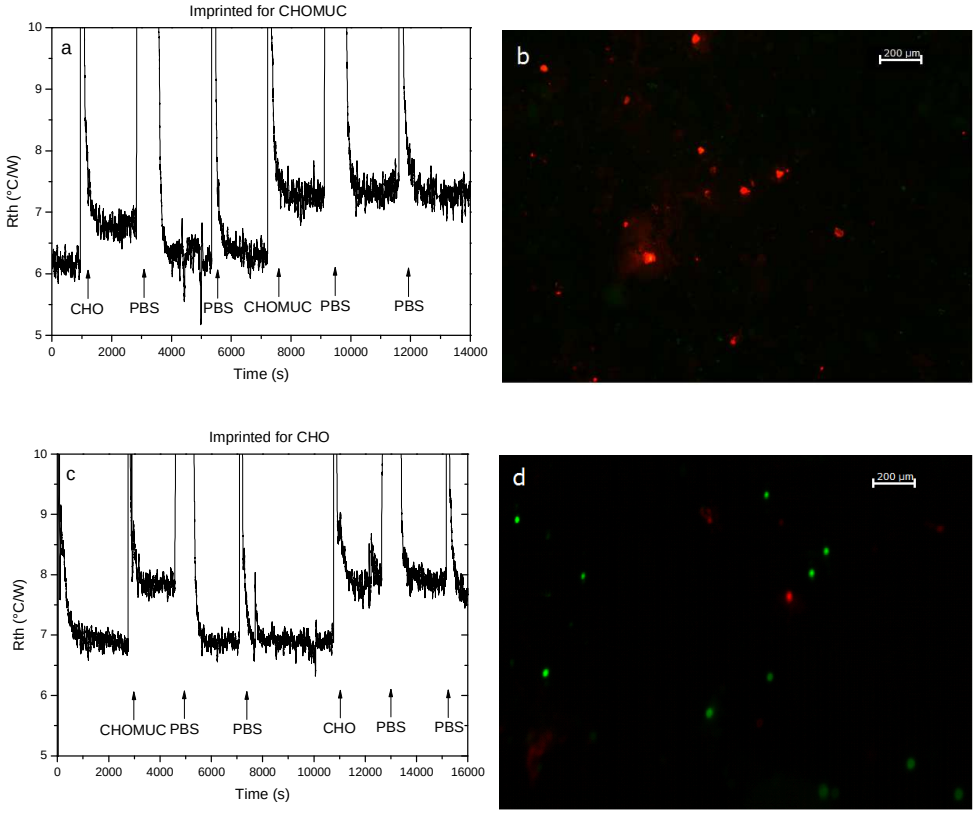

Figure 5.8: Time-dependent Rth data obtained by exposing a CHO-MUC SIP to calcein-labeled CHO cells and DiI-labeled CHO-MUC1 cells consecutively (a). The sample is analyzed after the R_{th} experiment by fluorescence microscopy, confirming that only the DiI-labelled CHO-MUC1 cells (red staining) remain bound to the layer (b). The experiment was repeated on a CHO-imprinted SIP both the R_{th} data (c) and the fluorescent analysis (d) are in line with the findings shown in (a). Both fluorescent images were made at 10x magnification.

The results obtained by HTM are confirmed by fluorescence microscopy analysis, showing only a red fluorescence signal associated with the DiI labelled-CHO-MUC1 cells after a cross-selectivity experiment performed on a CHO-MUC1 SIP (figure 5.8b). *Vice versa,* a sample imprinted for CHO cells that was used for the same experiment was analyzed by fluorescence microscopy. The image shown in figure 5.8d indicates that a large number off calcein labelled-CHO cells (green dots) are retained on the surface of the SIP, while only a couple of analogue cells are shown (red dots).

These results confirm that the SIP receptor is indeed very selective towards its target cell type and that HTM can be used to selectively detect cells in buffer. However, it is difficult to quantify the number of cells bound to the SIP from these images, since not all cells are stained to the same extent, some might not even be stained at all. Since the fluorescent images only show a fraction of the cells that are actually on the sample, it is impossible to quantify the number of target cells retained by the SIP by fluorescence microscopy alone.

5.3.5. Repeated exposure in a competitive assay

To assess the influence of the presence of competitor cells on the detection of target cells, a competitive assay was performed. In this experiment a SIP imprinted for CHO-MUC1 cells was exposed to a mixed cell solution (concentration 1×10^6 cells/ml) containing CHO-MUC1 cells as well as CHO cells in a ratio of 50:50, 10:90, 5:95 and 1:99. The SIPs were exposed four consecutive times to these mixed-population solutions and the flow cell was rinsed with 3 ml PBS buffer solution at a rate of 0.25 ml/min between each run. For each cell mixture the maximum possible change in heat transfer resistance (ΔR_{th}^{max}), which can be expected when the SIP has reached its maximum cell binding capacity, was calculated for each cell exposure cycle n as the difference between the average maximum R_{th} reached after each cell exposure and before PBS flushing ($<R_{th}^{n\_max}>$) and the average initial R_{th} before the first cell exposure cycle ($<R_{th}^{ini}>$): $\Delta R_{th}^{n\_max} = <R_{th}^{n\_max}> - <R_{th}^{ini}>$. The change in R_{th} obtained after each cell exposure cycle n (ΔR_{th}^{n}) was calculated as the difference between the average R_{th} reached at the end of each cell exposure cycle after flushing with PBS ($<R_{th}^{n}>$) and $<R_{th}^{ini}>$: $\Delta R_{th}^{n} = <R_{th}^{n}> - <R_{th}^{ini}>$. All above defined variables are visualized in **figure 5.9**. To normalize the change in R_{th}, the degree of saturation after each cell exposure cycle was calculated. This was defined as the size of the change in R_{th} after each cell exposure cycle in comparison to the maximum possible change in R_{th} in terms of percentage ($\%R_{th}^{n}$) and calculated as:

$$\%R_{th}^{n} = \frac{\Delta R_{th}^{n}}{\Delta R_{th}^{n\_max}} \times 100.$$

The time-dependent R_{th} data and the $\%R_{th}^{n}$, represented as bar charts are shown in **figure 5.10**. The blue line indicates the lower limit of detection, defined as three times the standard deviation on the $\%R_{th}^{n}$.

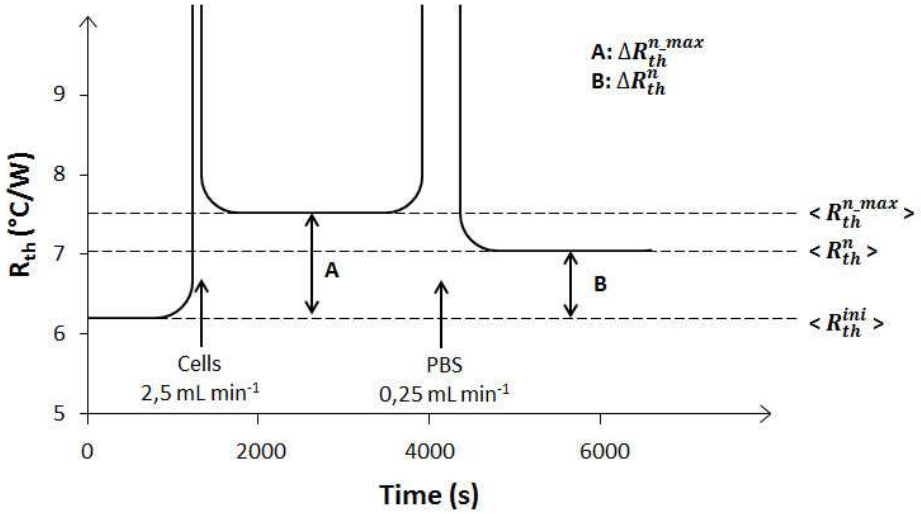

Figure 5.9: Schematic presentation of the time dependent R_{th} for one complete cell exposure cycle 'n'. The average maximum R_{th} reached after each cell exposure and before PBS flushing $<R_{th}^{n\_max}>$, the average initial R_{th} before the first cell exposure cycle $<R_{th}^{ini}>$, the maximum change in R_{th} obtained within each cell exposure cycle n ($\Delta R_{th}^{n\_max}$) and the change in R_{th} obtained after each cell exposure cycle n (ΔR_{th}^{n}) are indicated on the graph.

The results in figure 5.10a show that the thermal resistance at the interface increases by 1.42 ± 0.1 °C/W upon addition of the 50:50 cell mixture to the flow cell. After mildly rinsing the flow cell the R_{th} stabilizes at a value of 0.71 ± 0.1 °C/W above the baseline value of 6.21 ± 0.1 °C/W, indicating that about half of the available imprints was occupied by target cells. These results are in accordance to the findings obtained in figure 5.4, indicating that target and competitor cells are retained in the same manner upon addition of the mixture, due to their morphological and functional similarity. Upon flushing of the cells with PBS, competitor cells are removed from the surface, while the target cells remain bound to the SIP layer, explaining the decrease in R_{th} upon flushing. Repeating the exposure will result in a net increase in R_{th} after each exposure step. The signal saturates after the third exposure step and remains constant in

step four, indicating that all available binding sites are occupied by target cells after the third exposure step.

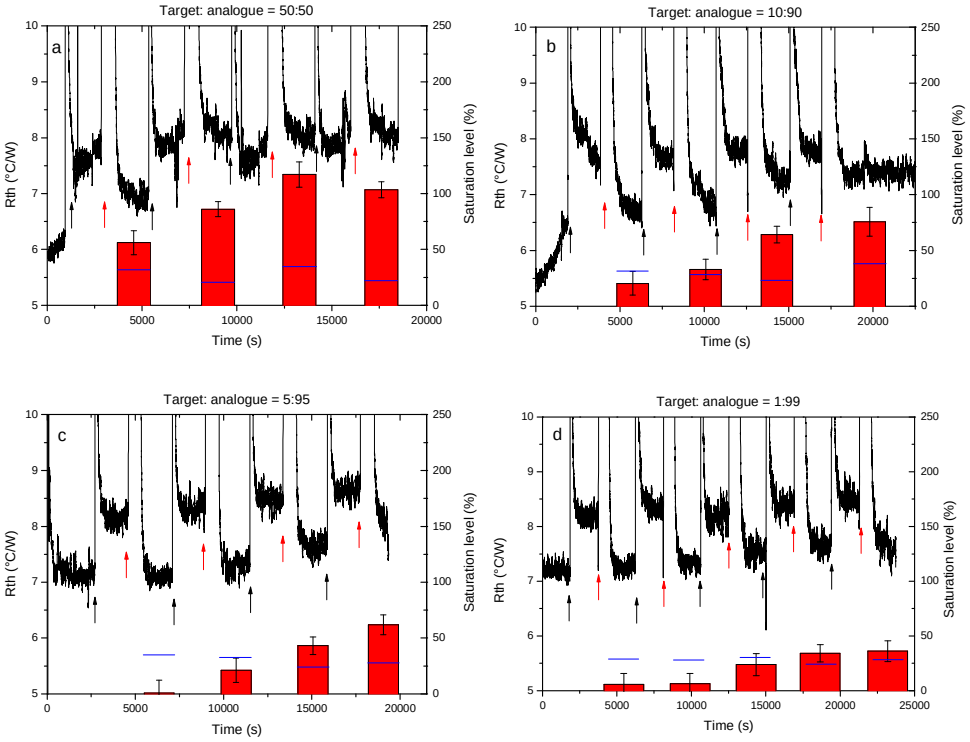

Figure 5.10: Time-dependent R_{th} data obtained by exposing a CHO-MUC1-imprinted sample four times to a 50:50 (a), 10:90 (b), 5:95 (c) and a 1/99 solution (d) of CHO-MUC1 and CHO cells respectively. After addition of the cells (black arrows), the flow cell is rinsed mildly with PBS buffer at a rate of 0.25 ml/min (red arrows). Box plots are shown, indicating the degree of saturation after each run, calculated as the ratio of the increase in R_{th} after and before flushing with PBS. In all cases, the R_{th} upon flushing increases gradually with each run (a, b, c, d). The blue lines indicate the threshold level of significance, defined by a signal-to-noise-ratio of 3.

Exposing the SIP to a 10:90 mixture of CHO-MUC1 and CHO cells, results in a more gradual increase in thermal resistance as can be obtained from the results in figure 5.9b. After the first exposure step, the increase in thermal resistance is too low to be considered significant as indicated by the blue line, representing the net increase in R_{th} at which a signal-to-noise-ratio of three is reached. After a second run, the threshold is reached. Increasing the number of exposure

steps, will increase the number of target cells retained on the surface of the SIP, which increases the thermal resistance signal further above the threshold.

The response in R_{th} develops even more gradually when exposing the SIP to a 5:95 mixture of CHO-MUC1 and CHO cells (figure 5.1c). After the first two exposure steps the increase in thermal resistance is too low to be detected by the set-up. Therefore, a third exposure step is required to reach the threshold. A further decrease in the concentration of target cells to 1:99 results in an insignificant rise in thermal resistance upon the first three exposure step. After the fourth consecutive exposure step, the R_{th} exceeds the threshold value. After an extra step, a minor increase in thermal resistance is observed, indicating that at very low concentrations the number of exposure steps needs to be increased.

Combining the results in this chapter, it can be concluded that the device can detect up to 1×10^4 cells/ml in the presence of an excess of competitor cells and the selectivity can be enhanced by increasing the number of exposure steps. However, further lowering the concentration of target cells will require an increased amount of addition runs, indicating that it would be more useful to develop a close-loop system. This way, analytes containing trace amounts of cells can gradually pass over the SIP layer, gradually increasing the number of cells retained on the surface of the SIP, thereby increasing the thermal resistance of the solid-liquid interface.

5.4. Conclusion

The results presented in this chapter demonstrate that the surface imprinting technique leads to the development of synthetic receptors displaying a remarkable selectivity. The proposed platform is able to distinguish between Chines Hamster Ovarian cell lines differing in the presence/absence of MUC1 expression. The results obtained during this experiment by the HTM are benchmarked by analyzing the sample after the experiment by fluorescence microscopy, clearly demonstrating that the conclusions that were drawn in the previous chapters are indeed correct.

In addition, the platform can also distinguish between cells expressing either non-glycosylated (displaying MUC1-F antigens) or glycosylated MUC1 (displaying either MUC1-T or MUC1-Tn antigens). The remarkable sensitivity of the SIP can

be explained by the fact that MUC1 is a fairly large protein. The core protein has an estimated mass of 125-225 kiloDalton (kDa) [140]. Furthermore, it is a well-known fact that glycosylation of the MUC1 protein increases the mass of the protein to 250-500 kDa [141]. Additionally, MUC1 protrudes up to 500 nm away from the cell membrane, much further than other membrane-spanning proteins such as syndecans and integrins [142]. These facts explain why our set-up is able to distinguish between cells based on the presence/absence of MUC1, being a large, protruding membrane protein. The sensitivity of the SIP towards presence/absence of carbohydrates on the surface of the MUC1 protein can be attributed to the increase in the number off functional groups available for imprinting and rebinding.

The results obtained from the competitive assay show that rebinding of cells to the SIP is indeed influenced by the presence of competitor cells. Given the fact that the amount of disease-related cells is vastly overwhelmed by the presence of healthy blood cells, this can be a problem. However, the situation analyzed in this case is a very artificial situation. In patient samples the morphological and functional difference between target and competitor cells will be much bigger. The difference between cancer cells and healthy cells for instance, is not solely based on the expression level or the glycosylation pattern of MUC1. However, the experiment with the repeated exposure runs revealed that the analogue cells are washed off by rinsing the flow cell with buffer, and that the thermal resistance will gradually increase between each exposure step due to the fact that more and more target cells will stick to the SIP layer. These results confirm that the development of a close-loop system where the SIPs are continuously exposed to solutions containing target cells could lead to a dramatic increase in sensitivity.

6. Conclusions and outlook

The results presented in this thesis suggest that surface imprinting of cells into polymer layers (creating whole-cell receptors) and the readout based on HTM form an ideal combination. The combination of both has the potential to evolve into a specific, low-cost diagnostic tool for the detection and follow-up of diseases going along with certain phenotypes of blood cells. Generally speaking, the assay can be performed in an automated way in a lab-on-chip device and one may also think of environmental applications such as the detection of pathogenic bacteria in drinking water. At the receptor side, the SIP layers are reusable many times and their selective binding capacity can be regenerated by washing with SDS- and buffer solutions. Furthermore, a simple improvement of the set-up, rinsing the flow cell with buffer after addition of the cells, resulted in a remarkable selectivity of the receptor. For a stable binding between cells and imprints, geometrical congruency alone is insufficient and also a complementarity of chemical functionalities is required. This way, the selective binding of cells can be achieved without using antibodies against certain cell-membrane groups, and this is a major benefit in terms of costs, reproducibility, and sensor-regeneration capacity.

At the side of the detection system, HTM requires only a minimum of instrumentation to monitor the temperature underneath and above the surface-imprinted polymer layer. Such a thermometric technique is widely insensitive to environmental and electronic disturbances. The HTM concept also allows for multiplexing towards sensor arrays consisting of chips with several regions imprinted with a variety of target cell types. Furthermore, cell recognition by SIPs is of course also possible with impedance spectroscopy and quartz-crystal microbalances [66, 71] but HTM does not rely on the electrical conductivity or piezoelectric properties of the platform material, any solid material can serve as a platform provided it does not inhibit the heat flow through the SIP layer. In this sense, HTM can also be combined with an impedimetric- or QCM readout in a single device because the transducing principles (here: heat flow) are mutually independent. In our experiments, aluminum was a first choice but other metals or oxides with good heat conductivity should perform similarly well. Note that

the cells had no direct contact with the aluminum chip due to the polyurethane interlayer.

In comparison to state-of-the-art techniques the proposed platform offers some enormous benefits. Our set-up is able to distinguish between various cell types in a fast, low-cost, user-friendly and label-free manner. In terms of sensitivity "golden standard" techniques based on flow cytometry outperform our set-up, as recent reports suggest that is possible to detect cells in concentrations as low as 1 cell per ml in the presence of an overwhelming amount of competitor cells [126, 127]. The experiments conducted on repeated exposure show that we are able to detect cells in the range of 10,000 cells per ml in presence of an excess of competitor cells in buffer. These measurements clearly show that by increasing the number of exposure steps, the sensitivity can be further increased.

As described earlier, patient samples can be purified in order to increase the ratio of target and competitor cells. In a first purifying step red blood cells can be removed from these samples by cell lysis [143]. This technique can be combined with microfluidic techniques to further increase the circulating tumor cell to healthy cell ratio of these samples [100, 101]. Recent reports have shown that is possible to lower the noise levels of our system by simply tuning the PID parameters [137]. The experiments described in section 5 of this thesis clearly illustrate that this has already led to a decrease of the noise level up to a factor 4, thereby lowering the detection limit of the system. It can be expected that further improvements made by electronic noise-reduction, filtering of the signal and careful redesigning of the sensor set up can decrease the detection limit of our set up to the order of 100 cells per ml or less.

In addition to these technical improvements of the HTM device, it is also possible to further optimize the imprinting procedure. It was shown by Kato *et al.* that it is possible to create dense microarrays of various adherent and non-adherent cell types on glass slides by functionalizing them with olyl polyethylene glycol (PEG) ether groups [144]. To this extent, they applied onto a glass surface bovine serum albumin (BSA) by non-specific adsorption, making the surface reactive. In a next step, these slides were incubated with biological anchoring membrane (BAM) groups, consisting out of three essential domains. The N-

hydroxysuccinimide (NHS) group makes the BAM chain extremely reactive and ensures binding of the chain to amino groups of BSA. A PEG chain is attached to this NHS group, ensuring appropriate spacing and orientation of the BAM chains as well as minimizing the steric hindrance between adjacent BAM chains. An olyl group will act as the anchor; these groups can be inserted into the membrane of the cells without reacting with proteins, sugars or metal ions in the membrane. Therefore, these BAM groups are perfectly suitable for increasing the amount of cells on the surface of the PDMS stamp used for imprinting, without changing any membrane functionalities of the cells. In a first series of experiments using this technique, we have obtained an increase in cell coverage on the surface of the stamp by a factor 10 as compared to the coverage on a non-treated stamp. However, the BAM groups were very reactive and the NHS group was hydrolyzed after a few days, rendering it useless for further experiments. In the future, appropriate storage will ensure that hydrolysis of the product will not occur again, and experiments on BAM anchoring will be continued. It can be expected that increasing the surface density of imprints on the surface of the SIP will increase the chance of cells binding to the surface, thereby increasing the sensitivity of the device.

The major progress that can be made towards improved selectivity of the set up lies in the development of a closed loop system. By continuously flowing biological samples at a steady rate over the SIP, it can be expected from the results obtained in this thesis that only target cells will bind to the layer. The thermal resistance will gradually increase in function of the number of target cells binding to the SIP layer. However, this will require some engineering since the set up in its present form cannot be used in closed loop modus. The flow cell has a height of 6 mm and therefore requires the cells to sediment to the surface of the chip under stopped-flow conditions. However, using standard microfluidic techniques in combination with PDMS grafting, it is possible to construct flow cells with heights below 100 µm [145], ensuring that cells will crawl over the surface of the SIP, thereby interacting with and binding to the microcavities. Since thermal equilibrium is necessary for measuring the R_{th} the flow has to be periodically interrupted during the actual measurement. Despite this drawback a close loop system will definitely have a positive influence on the sensitivity of the set-up, this opportunity will have to be examined in future research.

7. References

1. Turner, A.; Wilson, G. and Karube, I. In *Biosensors: Fundamentals and Applications*. Oxford University Press: Oxford **1987,** p. 770.

2. Schöning, M.J. and Poghossian, A. Bio FEDS (Field-effect Devices): state-of-the-art and new directions. *Electroanalysis*. **2006,** 18(19-20), 1893-1900.

3. Vermeeren, V.; Bijnens, N.; Wenmackers, S.; Daenen, M.; Haenen, K.; Williams, O.A.; Ameloot, M.; vandeVen, M.; Wagner, P. and Michiels, L. Towards a real-time, label-free diamond-based DNA sensor. *Langmuir.* **2007,** 23(26), 13193-13202.

4. van Grinsven, B.; Vanden Bon, N.; Grieten, L.; Murib, M.S.; Janssens, S.D.; Haenen, K.; Schneider, E.; Ingebrandt, S.; Schöning, M.J.; Vermeeren, V.; Ameloot, M.; Michiels, L.; Thoelen, R.; De Ceuninck, W. and Wagner, P. Rapid assessment of the stability of DNA duplexes by impedimetric real-time monitoring of chemically induced denaturation. *Lab Chip*. **2011,** 11(9), 1656-1663.

5. Ferreira, M.; Fiorito, P.A.; Oliveira, O.O.J. and Cordoba de Torresi, S.I. Enzyme-mediated amperometric biosensors prepared with the layer-by-layer (lbl) adsorption technique. *Biosens. Bioelecron.* **2004**, 19(12), 1611-1615.

6. Llopis, X.; Pumera, M.; Alegret, S. and Merkoçi, A. Lab-on-a-chip for ultrasensitive detection of carbofuran by enzymatic inhibition with replacement of enzyme using magnetic beads. *Lab Chip*. **2009**, 9, 213-218.

7. Yang, J.; Deng, S.; Lei, J.; Ju, H. and Gunasekaran, S. Electrochemical synthesis of reduced graphene sheet-AuPd alloy nanoparticle composites for enzymatic biosensing. *Biosens. Bioelectron*. **2011,** 29(1), 159-166.

8. Held, M.; Schumann, W.; Jahreis, K. and Schmidt, H.L. Microbial biosensor array with transport mutants of *Escherichia coli* K-12 for the simultaneous determination of mono- and disaccharides. *Biosens. Bioelectron*. **2002,** 17, 1089-1094.

9. Bohrn, U.; Stütz, E.; Fuchs, K.; Fleischer, M.; Schöning, M.J. and Wagner, P. Monitoring of irritant gas using a whole-cell-based sensor system. *Sensor. Actuat. B-Chem.* **2012**, 175, 208-217.

10. Bohrn, U.; Stütz, E.; Fleischer, M.; Schöning, M.J. and Wagner P. Using a cell-based gas biosensor for investigation of adverse effects of acetone vapors *in vitro*. *Biosens. Bioelectron.* **2013,** 40, 393-400.

11. Cooreman, P.; Thoelen, R.; Manca, J.; vandeVen, M.; Vermeeren, V.; Michiels, L.; Ameloot, M. and Wagner, P. Impedimetric immunosensors based on the conjugated polymer PPV. *Biosens. Bioelectron.* **2005,** 20(10), 2151-2156.

12. Vermeeren, V.; Grieten, L.; Vanden Bon, N.; Bijnens, N.; Wenmackers, S.; Janssens, S.D.; Haenen, K.; Wagner, P. and Michiels, L. Impedimetric, diamond-based immunosensor for the detection of C-reactive protein. *Sensor. Actuat. B-Chem.* **2011,** 157(1), 130-138.

13. Liu, G.; Khor, S.M.; Iyengar, S.G. and Gooding, J.J. Development of an electrochemical immunosensor for the detection of HbA1c in serum. *Analyst*. **2012**, 137, 829-832.

14. Lambert, P. and Bingley, P.J. What is type 1 diabetes? *Medicine*. **2002,** 30(1), 1-5.

15. Stafstrom, C.E. Persistent sodium current and its role in epilepsy. *Epilepsy Curr.* **2003,** 3(4), 148-149.

16. Tanenberg, R.J.; Newton, C.A. and Drake, A.J. Confirmation of hypoglycemia in the "dead-in-bed" syndrome, as captured by a retrospective continuous glucose monitoring system. *Endocr Pract.* **2010,** 16(2), 244-248.

17. Clark Jr., L.C.; Wolf, R.; Granger, D. and Taylor, Z. Continuous recording of blood oxygen tensions by polarography. *J. Appl. Physiol.* **1953,** 6(3), 189-193.

18. Clark Jr., L.C and Lyons, A. Electrode systems for continuous monitoring in cardiovascular surgery. *Ann. NY Acad. Sci.* **1962,** 102, 29.

19. Wilcox, A.J.; Baird, D.D. and Weinberg, C.R. Time of implantation of the conceptus and loss of pregnancy. *N. Engl. J. Med.* **1999,** 340 (23), 1796-1799.

20. Fan, X.G. and Zheng, Z.Q. A study of early pregnancy factor activity in preimplantation. *Am. J. Reprod. Immunol.* **1997,** 359-364.

21. Watson, J.D. and Crick, F.H.C. A structure for Deoxribose Nucleic Acid *Nature*, **1953,** 171, 737 – 738.

22. Barreiro, L.B.; Laval, G.; Quach, H.; Patin, E. and Quintana-Murci, L. Natural selection has driven population differentiation in modern humans. *Nat. Genet*. **2008,** 40, 340-345

23. Ingram, V.M. A Specific Chemical Difference between Globins of Normal and Sickle-cell Anemia Hemoglobins *Nature* **1956,** 178 (4537), 792-794.

24. Chang, J.C. and Kan, Y.W. Beta 0 thalassemia, a nonsense mutation in man. *Proc. Nat. Acad. Sci. USA.* **1979,** 76 (6), 2886-2889

25. Hamosh, A.; King, T.M.; Rosenstein B.J.; Corey, M. and Levison, H. Cystic fibrosis patients bearing both the common missense mutation Gly----Asp at codon 551 and the delta F508 mutation are clinically indistinguishable from delta F508 homozygotes, except for decreased risk of meconium ileus. *Am. J. Hum. Genet.* **1992,** 51 (2), 245-250.

26. Ng, J. and Liu, W.T. Miniaturized platforms for the detection of single-nucleotide polymorphisms. *Anal. Bioanal. Chem.* **2006,** 3, 427-434.

27. Tindall, E.A.; Petersen, D.C.; Woodbridge, P.; Shipany, K. and Hayes V.M. Assessing high-resolution melt curve analysis for accurate detection of gene variants in complex DNA fragments. *Hum. Mutat.* **2009,** 30, 876-883.

28. Fodde, R. and Losekoot, M. Mutation detection by denaturing gradient gel electrophoresis (DGGE). *Hum. Mutat.* **1994,** 3, 83-94.

29. Huang, C.; Stakenborg, T.; Cheng, Y.; Colle, F.; Steylaerts, T.; Jans, K.; Van Dorpe, P. and Lagae, L. Label-free genosensor based on immobilized DNA hairpins on gold surface. *Biosens. Bioelectron.* **2011,** 26(7), 3121-3126.

30. Tran, D.T.; Vermeeren, V.; Grieten, L.; Wenmackers, S.; Wagner, P.; Pollet, J.; Janssen, K.P.F.; Michiels, L. and Lammertyn J. Nanocrystalline diamond impedimetric aptasensor for the label-free detection of human IgE. *Biosens. Bioelectron.* **2011,** 26(6), 2987-2993

31. Baeumner, A.J.; Cohen, R.N.; Miksic, V. and Min J. RNA biosensor for the rapid detection of viable *Escherichia Coli* in drinking water. *Biosens. Bioelectron.* **2003,** 18(4), 405-413.

32. Janeway, C. *Immubobiology (5th ed.)* Garland Science: New York **2001**

33. Sesso, H.D.; Buring, J.E.; Rifaj, N.; Blake, G.J.; Gaziano J.M. and Ridker P.M. C-reactive protein and the risk of developing hypertension. *J. Am. Med. Assoc.* **2003,** 290, 2945-2951.

34. Yano, K. and Karube, I. Molecularly imprinted polymers for biosensor applications. *Trends Anal. Chem.* **1999,** 18, 199-204.

35. Kandimalla, V.B. and Ju, H. Molecular imprinting: a dynamic technique for diverse applications in analytical chemistry. *Anal. Bioanal. Chem.* **2004,** 380, 587-605.

36. Vincent, J.F.V.; Bogatyreva, O.A.; Bogatyrev, N.R.; Bowyer, A. and Pahl, A. Biomimetics: its practice and theory *J. R. Soc. Interface* **2006,** 3(9), 471-482.

37. www.velcro.com

38. Lafuma, A. and Quere, D. Superhydrophobic states. *Nature Mater.* **2003,** 2(7), 457-460.

39. Solga, A.; Cerman, Z.; Striffler, B.F.; Spaeth, M. and Barthlott, W. The dream of staying clean: Lotus and biomimetic surfaces. *Bioinspir. Biomim.* **2007,** 2, 1-9.

40. Haupt, K. and Mosbach K. Molecularly imprinted polymers and their use in biomimetic sensors. *Chem. Rev.* **2000,** 100, 2495-2504.

41. Piletsky, S.A. and Turner, A.P.F. Electrochemical sensors based on molecularly imprinted polymers. *Electroanal.* **2002,** 13, 317-323.

42. Alexander, C.; Andersson, H.S.; Andersson, L.I.; Ansell, R.J.; Kirsch, N.; Nichols, I.A.; O'Mahony, J. and Whitcombe, M.J. Molecular imprinting science and technology: A survey of the literature for the years up to and including 2003. *J. Mol. Recognit.* **2006,** 19, 106-180.

43. Owens, P.K.; Karlsson, L.; Lutz, E.S.M. and Andersson, L.I. Molecular imprinting for bio- and pharmaceutical analysis. *Trends Anal. Chem.* **1999,** 18, 146-154.

44. Vlatakis, G.; Andersson, L.I.; Müller, R. and Mosbach, K. Drug assay using antibody mimics made by molecular imprinting. *Nature* **1993,** 361, 645-647.

45. Yan, H. and Row, K.H. Characteristic and synthetic approach of molecularly imprinted polymer. *Int. J. Mol. Sci.* **2006,** 7, 155-178.

46. Cormack, P.A.G. and Elorza, A.Z. Molecularly imprinted polymers: synthesis and characterisation. *J. Chromatogr. B* **2004,** 804(1), 173-182.

47. Sellergen, B. and Allender, C.J. Molecularly imprinted polymers: a bridge to advanced drug delivery. *Adv. Drug Deliv. Rev.* **2005,** 57, 1733-1741.

48. Spivak, D.A. Optimization, evaluation, and characterization of molecularly imprinted polymers. *Adv. Drug Deliv. Rev.* **2005,** 57, 1779-1794.

49. Jahanzad, F.; Sajjadi, S.; Yianneskis, M. and Brooks, B.W. In-situ mass-suspension polymerisation. *Chem. Eng. Sci.* **2008,** 63(17), 4412-4417.

50. Benito-Peña, E.; Urraca, J.L.; Sellergen, B. and Moreno-Bondi, M.C. Solid-phase extraction of fluoroquinolones from aqueous samples using a water-compatible stochiometrically imprinted polymer. *J. Chromatogr. A*, **2008,** 1208, 62-70.

51. Alizadeh, T.; Zare, M.; Ganjali, M.R.; Norouzi, P. and Tavana, B. A new molecularly imprinted polymer (MIP)-based electrochemical sensor for monitoring 2, 4, 6-trinitrotoluene (TNT) in natural waters and soil samples. *Biosens. Bioelectron.* **2010,** 25(5), 1166-1172.

52. Sun, H.; Mo, Z.H.; Choy, J.T.S.; Zhu, D.R. and Fung, Y.S. Piezoelectric quartz crystal sensor for sensing taste-causing compounds in food. *Sensor. Actuat. B-Chem.* **2008,** 131(1), 148-158

53. Thoelen, R.; Vansweevelt, R.; Duchateau, J.; Horemans, F.; D'Haen J.; Lutsen, L.; Vanderzande, D.; Ameloot, M.; vandeVen, M.; Cleij, T.J. and Wagner, P. A MIP-based impedimetric sensor for the detection of low-MW molecules. *Biosens. Bioelectron.* **2008,** 23, 913-918.

54. Peeters, M.; Troost, F.J.; van Grinsven, B.; Horemans, F.; Alenus, J.; Murib, M.S.; Keszthelyi, D.; Ethirajan, A.; Thoelen, R.; Cleij, T.J. and Wagner, P. MIP-based biomimetic sensor for the electronic detection of serotonin in human blood plasma. *Sensor. Actuat. B-Chem.* **2012,** 171-172, 602-610.

55. Peeters, M.; Troost, F.J.; Mingels, R.H.G.; Welsch, T.; van Grinsven B.; Vranken, T.; Ingebrandt, S.; Thoelen, R.; Cleij, T.J. and Wagner P. Impedimetric detection of histamine inbowel fluids using synthetic receptors with pH-optimized binding characterstics. *Anal. Chem.* **2012,** 85, 1475-1483.

56. Alenus, J.; Galar, P.; Ethirajan, A.; Horemans, F.; Weustenraed, A.; Cleij, T.J. and Wagner P. Detection of L-nicotine with dissipation mode quartz crystal microbalance using molecular imprinted polymers. *Phys. Status Solidi A* **2012,** 209 (5), 905-910.

57. Alenus, J.; Ethirajan, A.; Horemans, F.; Weustenraed, A.; Csipai, P.; Gruber, J.; Peeters, M.; Cleij, T.J. and Wagner, P. Molecularly imprinted polymers as synthetic receptors for the QCM-D-based detection of L-nicotine in diluted saliva and urine samples. *Anal. Bioanal. Chem.* **2013,** 405(20):6479-87.

58. Peeters, M.; Csipai, P.; Geerets, B.; Weustenraed, A.; van Grinsven B.; Thoelen, R.; Gruber, J.; De Ceuninck, W.; Cleij, T.J.; Troost, F.J. and Patrick Wagner. Heat-transfer-based detection of L-nicotine, histamine and serotonin using molecularly imprinted polymers as biomimetic receptors. *Anal. Bioanal. Chem.* **2013,** 405(20):6453-60.

59. Bolisay, L.D.; Culver, J.N. and Kofinas, P. Molecularly Imprinted Polymers for Tobacco Mosaic Virus Recognition. *Biomater.* **2006,** 27(22), 4165-4168.

60. Ogiso, M.; Minoura, N.; Sinbo, T. and Shimizu, T. DNA detection system using molecularly imprinted polymer as the gel matrix in electrophoresis. *Biosens. Bioelectron.* **2007,** 22(9-10), 1974-1981.

61. Lu, C.H.; Zhang, Y.; Tang, S.F.; Fang, Z.B. and Yang, H.H. Sensing HIV-related protein using epitope-imprinted hydrophilic polymer-coated quartz crystal microbalance. *Biosens. Bioelectron.* **2012,** 31(1), 439-444.

62. Shi, H.; Tsai, W.B.; Garrison, M.D.; Ferrar, S. and Ratner, B.D. Template-imprinted nanostructured surfaces for protein recognition. *Nature* **1999,** 398, 593-597.

63. Hayden, O.; Lieberzeit, P.A.; Blaas, D. and Dickert, F.L. Artificial antibodies for bioanalyte detection-Sensing viruses and proteins. *Adv. Funct. Mater.* **2006,** 16, 1269-1278.

64. Alexander, C. and Vulfson, E.V. Spatially functionalized polymer surfaces produced via cell-mediated lithography. *Adv. Mater.* **1997,** 9, 751-755.

65. Cohen, T.; Starosvetsky, J.; Cheruti, U. and Armon, T. Whole cell imprinting in sol-gel thin films for bacterial recognition in liquids: macromolecular fingerprinting. *Int. J. Mol. Sci.* **2010,** 11, 1236-1252.

66. Qi, P.; Wan, Y. and Zhang, D. Impedimetric biosensor based on cell-mediated bioimprinted films for bacterial detection. *Biosens. Bioelectron.* **2013,** 39, 282-288.

67. Jenik, M.; Schirhagl, R.; Schirk, C.; Hayden, O.; Lieberzeit, P.; Blaas, D.; Guntram, P. and Dickert, F.L. Sensing Picornaviruses using molecular imprinting techniques on a quartz crystal microbalance. *Anal. Chem.* **2009,** 81, 5320-5326.

68. Jenik, M.; Seifner, A.; Lieberzeit, P.A. and Dickert, F.L. Pollen-imprinted polyurethanes for QCM allergen sensors. *Anal. Bioanal. Chem.* **2009,** 394, 523-528.

69. Hayden, O. and Dickert, F.L. Selective microorganism detection with cell surface imprinted polymers. *Adv. Mater.* **2001,** 13, 1480-1483.

70. DePorter, S.M.; Lui, I. and McNaughton, B.R. Programmed cell adhesion and growth on cell-imprinted polyacrylamide hydrogels. *Soft Matter* **2012,** 8, 10403-10408

71. Hayden, O.; Mann, K.J.; Krassnig, S. and Dickert, F.L. Biomimetic ABO blood-group typing. *Angew. Chem. Int. Ed.* **2006,** 45, 2626-2629.

72. Wulff, G. Molecular Imprinting in Cross-Linked Materials with the Aid of Molecular Templates: a Way towards Artificial Antibodies. *Angew. Chem. Int. Ed.* **1995,** 34, 1812-1832.

73. Davis, A.P. and Wareham, S. Carbohydrate recognition through noncovalent interatctions: a challenge for biomimetic and supramolecular chemistry. *Angew. Chem. Int. Ed.* **1999,** 38, 2978-2996.

74. Ferencik, M. In *Handbook of immunochemistry*, 1st ed.; Chapman & Hall: London, **1993**; p 22-49.

75. Schenkel-Brunner, H. In *Human blood groups, chemical and biochemical basis of antigen specificity*, 2nd ed.; Salvini-Plawen, A., ed.; Springer: Heidelberg, **2000**; p 54-90.

76. Mason, V.R. Sickle-cell anemia. *J. Am. Med. Assoc.* **1922**, 79, 1318-1320.

77. Kenny, M.W.; George, A.J. and Stuart, J. Platelet hyperactivity in sickle-cell disease: a consequence of hyposplenism. *J. Clin. Path.* **1980,** 33, 622-625.

78. Smith, W.R.; Penberthy, L.T.; Bovbjerg, V.E.; McClish, D.K.; Roberts, J.D.; Dahman, B.; Aisiku, I.P.; Levenson, J.L. and Roseff, S.D. Daily assessment of pain in adults with sickle cell disease. *Ann. Intern. Med.* **2008,** 148(2), 94-101.

79. Gladwin, M.T.; Sachdev, V.; Jison, M.L.; Shizukuda, Y.; Plehn, J.F.; Minter, K.; Brown, B.; Coles, W.A.; Nichols, J.S.; Ernst, I.; Hunter, L.A.; Blackwelder, W.C.; Schechter, A.N.; Rodgers, G.P.; Castro, O. and Ognibene, F.P. Pulmonary hypertension as a risk factor for death in patients with sickle cell disease. *N. Engl. J. Med.* **2004,** 350(9), 886-895.

80. Powars, D.R.; Elliott-Mills, D.D. and Chan, L. Chronic renal failure in sickle cell disease: risk factors, clinical course and mortality. *Ann. Intern. Med.* **1991,** 115(8), 614-620.

81. Adams, R.J.; Othene-Frempong, K. and Wang, W. Sickle cell and the brain. *Am. Soc. Hematol. Educ. Program* **2001,** 1, 31-46.

82. Kolodgie, F.D.; Narula, J.; Burke, A.P.; Haider, N. and Hiu-Lang, Y. Localization of apoptotic macrophages at the site of plaque rupture in sudden coronary death. *Am. J. Pathol.* **2000,** 157, 1259-1268.

83. Ley, K.; Miller, Y.I. and Hedrick, C.C. Monocyte and macrophage dynamics during atherogenesis. *Arterioscler. Thromb. Vasc. Biol.* **2011,** 37(7), 1506-1510.

84. Blanc-Brude, O.P.; Teissier, E.; Castier, Y.; Lesèche, G.; Bijnens, A.P.; Daemen, M.; Staels, B. and Tedgui A. IAP survivin regulates atherosclerotic macrophage survival. *Arterioscl. Throm. Vas.* **2007**, 27, 901-907.

85. Geny, Y.J. and Libby P. Progression of atheroma: a struggle between death and procreation. *Arterioscler. Thromb. Vasc. Biol.* **2002,** 22, 1370-1380.

86. Vogl, T.J.; Abolmaali, N.D.; Diebold, T.; Engelmann, K. and Ay, M. Techniques for the detection of coronary atherosclerosis: multi-detector row CT coronary angiography. *Radiology* **2002,** 223, 212-220.

87. Hollingsworth, M.A. and Swanson, B.J. Mucins in cancer: protection and control of the cell surface. *Nat. Rev. Canc.* **2004,** 4, 45-60.

88. Taylor-Papadimitriou, J.; Burchell, J.; Miles, D.W. and Dalziel, M. MUC1 and cancer. *Biochim. Biophys. Acta*, **1999,** 1455, 301.

89. Gendler, S.J. MUC1, the renaissance molecule. *J. Mammary Gland Biol.* **2001,** 6, 339-353.

90. Colomer, R.; Ruibal, A.; Genolla, J. and Salvador, L. Circulating CA 15-3 levels in the postsurgical follow-up of breast cancer patients in non-malignant diseases. *Br. J. Cancer* **1989,** 59, 283.

91. Van Leeuwen, E.B.; Cloosen, S.; Senden-Gijbers, B.L.; Agervirg Tarp, M.; Mandel, U.; Clausen, H.; Havenga, M.J.; Duffour, M.T.; Garcia-Vallejo, J.J.; Germeraad, W.T. and Bos, G.M. Expression of aberrantly glycosylated tumor mucin-1 on human DC after transduction with a fiber-modified adenoviral vector. *Cytotherapy* **2006,** 8, 24.

92. Van Elssen, C.H.M.J.; Frings, P.W.H.; Bot, F.J.; Van de Vijver, K.; Huls, M.B.; Meek, B.; Hupperets, P.; Germeraad, W.T.V. and Bos G.M.J. Expression of aberrantly glycosylated Mucin-1 in ovarian cancer. *Histopathology* **2010,** 57, 597.

93. Chandrasekaran, E.V.; Xue, J.; Neelamegham, S. and Matta, K.L. The pattern of glycosyl- and sulfotransferase activities in cancer cell lines: a predictor of individual cancer-associated distinct carbohydrate structures for the structural identification of signature glycans. *Carbohydr. Res.* **2006,** 341, 983.

94. Pinho, S.; Marcos, N.T.; Ferreira, B.; Carvalho, A.S.; Oliveira, M.J.; Santos-Silva, F.; Harduin-Lepers, A. and Reis, C.A Biological significance of cancer-associated sialyl-Tn antigen: modulation of malignant phenotype in gastric carcinoma cells. *Cancer Lett.* **2007,** 249, 157.

95. Zhao, Q.; Guo, X.; Nash, G.B.; Stone, P.C.; Hilkens, J.; Rhodes, J.M. and Yu, L.G. Circulating galectin-3 promotes metastasis by modifying MUC1 localization on cancer cell surface. *Cancer Res.* **2009,** 69, 6799.

96. Pochampalli, M.R.; el Bejjani, R.M. and Schroeder, J.A. MUC1 is a novel regulator of ErbB1 receptor trafficking. *Oncogene* **2007,** 26, 1693.

97. Wei, X.; Xu, H. and Kufe, D. Human MUC1 oncoprotein regulates p53-responsive gene transcription in the genotoxic stress response. *Cancer Cell* **2005,** 7, 167.

98. van de Wiel-van Kemenade, E.; Ligtenberg, M.J.; deBoer, A.J.; Buijs, F.; Vos, H.L.; Melief, C.J.; Hilkens, J. and Figdor, C.G. Episialin (MUC1) inhibits cytotoxic lymphocyte-target cell interaction. *J. Immunol.* **1993,** 151, 767.

99. Rahman, A.R.A.; Lo, C.M. and Bhansali, S. A MEMS micro-electrode array biosensor for impedance spectroscopy of human umbilical vein endothelial cells. *Sensor. Actuat. B-Chem.* **2006,** 118, 115-120.

100. Han, K.H.; Han, A. and Frazier, A.B. Microsystems for isolation and electrophysiological analysis of breast cancer cells from blood. *Biosens. Bioelectron.* **2006,** 21, 1907-1914

101. Chen, J.; Lib, J. and Sun, Y. Microfluidic approaches for cancer cell detection, characterization and separation. *Lab. Chip.* **2012,** 12, 1753-1767.

102. van Grinsven, B.; Vanden Bon, N.; Strauven, H.; Grieten, L.; Murib, M.S.; Monroy, K.L.; Janssens, S.D.; Haenen, K.; Schöning, M.J.; Vermeeren, V.; Ameloot, M.; Michiels, L.; Thoelen, R.; De Ceuninck, W. and Wagner, P. Heat-transfer resistance at solid-liquid interfaces: a tool for the detection of single-nucleotide polymorphisms in DNA. *ACS Nano* **2012,** 6, 2712-2721.

103. Lenz, M.; Striedl, G.; Fröhler, U. In *Thermal resistance, theory and practice, Special Subject Book January 2000: SMD Packages*, 1st ed; Infineon Technologies AG: Munich, **2000**; p 17.

104. Nakano, T.; Kikugawa, G. and Ohara, T. A molecular dynamics study on heat conduction characteristics in DPPC lipid bilayer. *J. Chem. Phys.* **2010,** 133, 154705.

105. Welsch, S.; Keppler, O.T.; Habermann, A.; Allespach, I. and Krijnse-Locker J. HIV-1 buds predominantly at the plasma membrane of primary human macrophages. *PLoS Pathog.* **2007,** 3(3), e36.

106. Lipman, M.C.; Johnson, M.A.; Bray, D.H. and Poulter, L.H. Changes to alveolar macrophage phenotype in HIV-infected individuals with normal CD4 counts and no respiratory-disease. *Thorax.* **1995,** 50(7), 777-781.

107. Rudnicka, D. and Schwartz, O. Intrusive HIV-1-infected cells. *Nat. Immunol.* **2009,** 10, 933-934.

108. Stix, G. Neurological insights. *Scientific American* **2007,** 297, 46-49.

109. Lin, E.Y.; Li, J.F.; Gnatovskiy, L.; Deng, Y.; Zhu, L.; Grzesik, D.A.; Qian, H.; Xue, X.N. and Pollard, J.W. Macrophages regulate the

angiogenic switch in a mouse model of breast cancer. *Cancer. Res.* **2006,** 66, 11238-11246.

110. Bingle, L.; Brown, N.J. and Lewis, C.E. The role of tumour-associated macrophages in tumour progression: implications for new anticancer therapies. *J. Pathol.* **2002,** 196, 254-265.

111. Edin, S.; Wikberg, M.L.; Dahlin, A.M.; Rutegard, J. and Oberg, A. The distribution of macrophages with a M1 or M2 phenotype in relation to prognosis and the molecular characteristics of colorectal cancer. *PLoS ONE* **2012,** 7(10), e47045.

112. Keblinski, P.; Phillpot, S.R.; Choi, S.U.S. and Eastman, J.A. Mechanisms of heat flow in suspensions of nano-sized particles (nanofluids). *Int. J. Heat Mass Trans.* **2002,** 45, 855-863.

113. Young, H.D. in *University physics*, 7th ed.; Addison, W., ed.; Reading, **1992.**

114. Lettau, K.; Warsinke, A.; Katterle, M.; Danielsson, B. and Scheller, F.W. A bifunctional molecularly imprinted polymer (MIP): analysis of binding and catalysis by a thermistor. *Angew. Chem. Int. Ed.* **2006,** 45, 6986-6990.

115. Zaretsky, J.Z.; Barnea, I.; Aylon, Y.; Gorivodsky, M.; Wreschner, D.H. and Keydar, I. MUC1 gene overexpressed in breast cancer: structure and transcriptional activity of the MUC1 promoter and role of estrogen receptor alpha in regulation of the MUC1 gene expression. *Mol. Cancer* **2006,** 5, 57.

116. Mukherjee, P.; Tinder, T.L.; Basu, G.D. and Gendler, S.J. MUC1 (CD227) interacts with Ick tyrosine kinase in Jurkat lymphoma cells and normal T cells. *J. Leukocyte Biol.* **2004,** 77, 90-99.

117. Agrawal, B.; Krantz, M.J.; Parker, J. and Longenecker, BM. Expression of MUC1 mucin on activated human T cells: implications for a role of MUC1 in normal immune regulation. *Cancer Res.* **1998,** 58, 4079-4081.

118. Chang, F.; Zhao, H.L.; Phillips, J. and Greenburg, G. The epithelial mucin, MUC1, is expressed on resting T lymphocytes and can function as a negative regulator of T cell activation *Cell. Immunol.* **2000,** 201, 83-88.

119. Treon, S.P.; Maimonis, P. and Bua, D. Elevated soluble MUC1 levels and decreased anti-MUC1 antibody levels in patients with multiple myeloma. *Blood.* **2000,** 96, 3147-3153.

120. Leong, C.F.; Raudhawati, O.; Cheong, S.K.; Sivagengei, K. and Noor Hamidah, H. Epithelial membrane antigen (EMA) of MUC1 expression in monocytes and monoblasts. *Pathology* **2004,** 35(5), 422-427.

121. Husemann, Y.; Geigl, J.B.; Schubert, F.; Musiani, P.; Meyer, M.; Burghart, E.; Forni, G.; Eils, R.; Fehm, T.; Riethmüller, G. and Klein, C.A. Systemic spread is an early step in breast cancer. *Cancer Cell* **2008,** 13, 59-68.

122. Meng, S.; Tripathy, D.; Frenkel, E.P.; Shete, S.; Naftalis, E.Z.; Huth, J.F.; Beitsch, P.D.; Leitch, M.; Hoover, S.; Euhus, D.; Haley, B.; Morrison, L.; Fleming, T.P.; Herlyn, D.; Terstappen, L.W.; Fehm, T.; Tucker, T.F.; Lane, N.; Wang, J. and Uhr, J.W. Circulating tumor cells in patients with breast cancer dormancy. *Clin. Cancer Res.* **2004,** 10, 8152-8162

123. Ghossein, R.A.; Scher, H.I.; Gerald, W.L.; Kelly, W.K.; Curley, T.; Amsterdam, A.; Zhang, Z.F. and Rosai, J. Detection of circulating tumor cells in patients with localized and metastatic prostatic carcinoma: clinical implications. *J. Clin. Oncol.* **1995,** 13, 1195-1200.

124. Coman, D.R.; deLong, R.P. and McCutcheon, M. Studies on the mechanisms of metastasis. The distribution of tumors in various organs in relation to the distribution of arterial emboli. *Cancer Res.* **1951,** 11, 648-651.

125. Gerges, N.; Rak, J. and Jabada, N. New technologies for the detection of circulating tumour cells. *Br. Med. Bull.* **2010,** 94, 49-64.

126. Scholtens, T.M.; Schreuder, F.; Ligthart, S.T.; Swennenhuis, J.F.; Tibbe, A.G.J.T.; Greve, J. and Terstappen, L.W.M.M. CellTracks TDI: an image cytometer for cell characterization. *Cytom. Part A* **2011,** 79A, 203-213.

127. Scholtens, T.M.; Schreuder, F.; Ligthart, S.T.; Swennenhuis, J.F.; Greve, J. and Terstappen, L.W. Automated identification of circulating tumor cells by image cytometry. *Cytom. Part A* **2012,** 81A, 138-148.

128. Zhao, J.; Yan, Y.; Zhu, L.; Li, X. and Li, G. An amperometric biosensor for the detection of hydrogen peroxide released from human breast cancer cells. *Biosens. Bioelectron.* **2013,** 41, 815-819.

129. Xiao, X.; Guoa, M.; Li, Q.; Cai, Q.; Yao, S. and Grimes, C.A. In-situ monitoring of breast cancer cell (MCF-7) growth and quantification of the cytotoxicity of anticancer drugs fluorouracil and cisplatin. *Biosens. Bioelectron.* **2008,** 24, 247-252.

130. Marx, K.A.; Zhou, T.; Montrone, A.; McIntosh, D. and Braunhut, S.J. Quartz crystal microbalance biosensor study of endothelial cells and their extracellular matrix following cell removal: evidence for transient cellular stress and viscoelastic changes during detachment and the elastic behavior of the pure matrix. *Anal. Biochem.* **2005,** 343, 23-34.

131. Lin, B.; Li, P. and Cunningham, B.T. A label-free biosensor-based cell attachment assay for characterization of cell surface molecules. *Sensor. Actuat. B-Chem.* **2006,** 114, 559-564.

132. Van Elssen, C.H.M.J.; Clausen, H.; Germeraad, W.T.V.; Bennet, E.P.; Menheere, P.P.; Bos, G.M.J. and Vanderlocht, J. Flow cytometry-based assay to evaluate human serum MUC1-Tn antibodies. *J. Immunol. Methods.* **2011,** 365, 87-94.

133. Krieger, M.; Brown, M.S. and Goldstein, J.L. Isolation of Chinese hamster cell mutants defective in the receptor-mediated endocytosis of low density lipoprotein. *J. Mol. Biol.* **1981,** 150, 167.

134. Kingsley, D.M.; Kozarsky, K.F.; Hobbie, L. and Krieger, M. Reversible defects in O-linked glycosylation and LDL receptor expression in a UDP-Gal/UDGalNAc 4-epimerase deficient mutant. *Cell* **1986,** 44, 749.

135. Brockhausen, I. Mucin-type O-glycans in human colon and breast cancer: glycodynamics and functions. *EMBO Rep.* **2006,** 7, 599.

136. Tarp, M.A.; Sorensen, A.L.; Mandel, U.; Paulsen, H.; Burchell, J.; Taylor-Papadimitriou, J. and Clausen, H. Identification of a novel cancerspecific immunodominant glycopeptide epitope in the MUC1 tandem repeat. *Glycobiology* **2007,** 17, 197.

137. Geerets, B.; Peeters, M.; van Grinsven, B.; Bers, K.; de Ceuninck, W. and Wagner P. Optimizing the thermal read-out technique for MIP-based biomimetic sensors: towards nanomolar detection limits. *Sensors*, **2013,** 13, 9148-9159.

138. Johnson, I. and Spence, M.T.Z. in *Molecular probes handbook, a guide to fluorescent probes and labeling technologies*, 11th ed; Life Technologies, Invitrogen: Carlsbed, California, **2010**; chapter 14.4.

139. Patel, H.; Clemens, T. and Heerklotz, H. Characterizing vesicle leakage by fluorescence lifetime measurements. *Soft Matter*, **2009,** 5, 2849-2851.

140. Gendler, S.J. and Spicer, A.P. Epithelial mucin genes. *Annu. Rev. Physiol.* **1995,** 57, 607-634.

141. Lagow, E.; DeSouza, M.M. and Carson, D.D. Mammalian reproductive tract mucins. *Hum. Reprod. Update.* **1999,** 5, 280-292.

142. Brayman, M.; Thathiah, A. and Carson, D.D. MUC1: a multifunctional cell surface component of reproductive tissue epithelia. *Reprod. Biol. Endocrinol.* **2004,** 2, 4.

143. Yang, L.; Lang, J.C.; Balasubramanian, P.; Jatana, K.R.; Schuller, D.; Agrawal, A.; Zborowski, M. and Chalmers, J.J. Optimization of an enrichment process for circulating tumor cells from the blood of head and neck cancer patients through depletion of normal cells. *Biotechnol. Bioengin.* **2009,** 102 (2), 5.

144. Kato, K.; Umezawa, K.; Funeriu, D.P.; Miyakel, M.; Miyake, J. and Naganume, T. Immobilized cluster of nonadherent cells on a oleyl poly(ethylene glycol) ether-modified surface. *BioTechniques* **2003,** 35, 1014-1021.

145. Whitesides, G.M. The origins and the future of microfluidics *Nature* **2006,** 442, 368-373.

8. Scientific publications & patents

Publications

1. K.L.J. Monroy, A. Kick, **K. Eersels**, B. van Grinsven, P. Wagner, M. Mertig *Pys. Stat. Sol. A***, 2013**, 210 (5), 918-925.

2. M.S., Murib, B. van Grinsven, L. Grieten, S.D. Janssens, V. Vermeeren, **K. Eersels**, J. Broeders, M. Ameloot, L. Michiels, W. De Ceuninck, K. Haenen, M.J. Schöning, P. Wagner. *Phys. Stat. Sol. A,* **2013**, 210 (5), 911-917.

3. **K. Eersels***, B. van Grinsven*, A. Ethirajan, S. Timmermans, K.L.J. Monroy, J.F.J Bogie, S. Punniyakoti, T. Vandenryt, J.J.A. Hendriks, T.J. Cleij, M.J.A.P. Daemen, V. Somers, W. De Ceuninck, P. Wagner. *ACS Appl. Mater. Interfaces*, **2013**, 5 (15), 7258–7267.

4. K. Bers*, **K. Eersels***, B. van Grinsven, J.F.J. Bogie, E. Bouwmans, C. Puettmann, S. Barth, J.J.A. Hendriks, G. Bos, W. Germeraad, W. De Ceuninck, P. Wagner. *Langmuir* **2013** (submitted).

* both authors contributed equally

Patents

1. **Kasper Eersels**, Marloes Peeters, Anitha Ethirajan, Bart van Grinsven, Ward De Ceuninck and Patrick Wagner. Heat-transfer resistance based analysis of bioparticles. European patent application: **EP13157264.6** (patent filed 28 February 2013).

9. Oral & Poster presentations

Oral presentations

1. "Characterization of macrophage-imprinted polyurethane layers."

   K. Eersels, S. Timmermans, J. Hendriks, A. Ethirajan, M.J.A.P. Daemen, T.J. Cleij, P. Wagner.

   20th July 2011: Engineering of Functional Interfaces, Johannes Kepler University, Linz, Austria.

2. "Structural imprinting of polyurethane layers for the development of a atherosclerosis risk assessment biosensor."

   K. Eersels, S. Timmermans, J. Bogie, J. Hendriks, P. Stinissen, A. Ethirajan, M.J.A.P. Daemen, T.J. Cleij, P. Wagner.

   16th July 2012: Engineering of Functional Interfaces, University of Applied Sciences, Kaiserslautern, Germany.

3. "Biosensors @ Uhasselt."

   K. Eersels, B. van Grinsven, A. Ethirajan, S. Timmermans, K.L. Jiménez Monroy, T. Vandenryt, J.J.A. Hendriks, T.J. Cleij, M.J.A.P. Daemen, V. Somers, W. De Ceuninck, and P. Wagner.

   7th March 2013: TedXUhasseltSalon, Hasselt University, Belgium.

4. "Surface imprinted polymers (SIPs) and the heat-transfer method (HTM): a marriage parfait for the selective detection of mammalian cells."

   K. Eersels, B. van Grinsven, A. Ethirajan, S. Timmermans, K.L. Jiménez Monroy, T. Vandenryt, J.J.A. Hendriks, T.J. Cleij, M.J.A.P. Daemen, V. Somers, W. De Ceuninck, and P. Wagner.

   8th July 2013: Engineering of Functional Interfaces, Hasselt University, Belgium.

5. "A novel biosensor platform for the detection of human cells."

   K. Eersels, B. van Grinsven, A. Ethirajan, S. Timmermans, K.L. Jiménez Monroy, T. Vandenryt, J.J.A. Hendriks, T.J. Cleij, M.J.A.P. Daemen, V. Somers, W. De Ceuninck, and P. Wagner.

   16th August 2013: 5th Graduate Student Symposium on Molecular Imprinting, Belfast, United Kingdom.

Poster presentations

1. "Structural imprinting of polymers for the microgravimetric detection of monocytes."

   K. Eersels, S. Timmermans, J. Hendriks, A. Ethirajan, M.J.A.P. Daemen, T.J. Cleij, P. Wagner.

   07th April 2011, Biomedica 2011, Eindhoven, The Netherlands.

2. "Surface imprinting of polymers for the microgravimetric detection of macrophages."

   K. Eersels, S. Timmermans, J. Hendriks, A. Ethirajan, M. Daemen, T. Cleij, P. Wagner.

   25th April 2011, Belgian Physical Society, General Scientific Meeting, Namur, Belgium.

3. "Structural imprinting for NR8383 cells, RAW 264.7 cells and Saccharomyces Cerevisiae: potential for atherosclerosis screening?"

   K. Eersels, S. Timmermans, J. Bogie, J. Hendriks, P. Stinissen, A. Ethirajan, M.J.A.P. Daemen, T.J. Cleij, P. Wagner.

   18th April 2012, Biomedica 2012, Liège, Belgium.

4. "Structural imprinting for mammalian macrophages: potential for atherosclerosis screening?"

K. Eersels, S. Timmermans, J. Bogie, J. Hendriks, P. Stinissen, A. Ethirajan, M.J.A.P. Daemen, T.J. Cleij, P. Wagner.

25th April 2012, Nanosense symposium 2012, Diepenbeek, Belgium.

5. "Structural imprintin of polyurethane layers with mammalian macrophages for the development of an atherosclerosis biomimetic sensor."

   K. Eersels, S. Timmermans, J. Bogie, J. Hendriks, P. Stinissen, A. Ethirajan, M.J.A.P. Daemen, T.J. Cleij, P. Wagner.

   30th May 2012, Belgian Physical Society, General Scientific Meeting, Brussels, Belgium.

6. "The heat-transfer method (HTM): a novel readout platform for the selective detection of mammalian cells by surface imprinted polymers."

   K. Eersels, B. van Grinsven, A. Ethirajan, S. Timmermans, K.L. Jiménez Monroy, T. Vandenryt, J.J.A. Hendriks, T.J. Cleij, M.J.A.P. Daemen, V. Somers, W. De Ceuninck, and P. Wagner.

   22th May 2013, Belgian Physical Society, General Scientific Meeting, Louvain-La-Neuve, Belgium.

7. "The heat-transfer method (HTM): a novel readout platform for the selective detection of macrophages and cancer cells."

   K. Eersels, B. van Grinsven, A. Ethirajan, S. Timmermans, K.L. Jiménez Monroy, T. Vandenryt, J.J.A. Hendriks, T.J. Cleij, M.J.A.P. Daemen, V. Somers, W. De Ceuninck, and P. Wagner.

   19th June 2013, Biomedica 2013, Aachen, Germany.

10. Appendix 1: List of abbreviations

- AA = Acryl amide
- AFM = Atomic force microscopy
- AIDS = Auto-immune deficiency syndrome
- BAM = Biological anchoring molecule
- BSA = Bovine serum albumin
- CHO = Chinese Hamster Ovarian
- CRP = C-reactive protein
- CTC = Circulating tumor cell
- CVD = Cardiovascular disease
- DMEM/F12 = Dulbecco's modified eagles medium/ Nutrient F-12 Ham medium
- DNA = Deoxyribonucleic acid
- EGDM = Ethylene glycol dimethacrylate
- EPF = Early pregnancy factor
- FACS = Fluorescence-activated cell sorting
- FCS = Fetal Calf Serum
- Gal = Galactose
- GalNAc = N-acetyl galactosamine
- hCG = human Chorionic gonadotropine
- HIV = Human immunodeficiency virus

Appendix 1: List of abbreviations

- HTM = Heat-transfer method
- MAA = Methacrylic acid
- MIP = Molecularly imprinted polymer
- MUC1 = Mucine1 protein
- NCD = Nano-crystalline diamond
- NHS = N-hydroxysuccinimide
- NIP = Non-imprinted polymer
- PBMC = Peripheral blood mononuclear cell
- PBS = Phosphate-buffered saline
- PDMS = Polydimethylsiloxane
- PEG = Poly ethylene glycol
- PID = Proportional-integral-derivative
- PU = Polyurethane
- QCM = Quartz crystal microbalance
- RNA = Ribonucleic acid
- RPMI = Roswell Park Memorial Institute medium
- R_{th} = Thermal resistance
- SDS = Sodium dodecyl sulphate
- SEM = Scanning electron microscope
- SIP = Surface-imprinted polymer
- SNP = Single-nucleotide polymorphism
- THF = Tetrahydrofuran

11. Appendix 2: List of figures

Appendix 2: List of figures

12. Appendix 3: List of tables